CT-839-SS1
DOV: 7015

Centro de Investigación y de Estudios Avanzados
del Instituto Politécnico Nacional
Unidad Guadalajara

Control activo de vehículos

Tesis que presenta:

Riccardo Cespi

para obtener el grado de:

Maestro en Ciencias

en la especialidad de:

Ingeniería Eléctrica

Directores de Tesis

Dr. Bernardino Castillo Toledo
Dr. Stefano Di Gennaro

CINVESTAV del IPN Unidad Guadalajara, Guadalajara, Jalisco, Agosto de 2014.

CLASIF.. CT 007940
ADQUIS.. CT-859-551
FECHA: 19-06-2015
PROCED.. DDO: 2015
$

Control activo de vehículos

Tesis de Maestría en Ciencias
Ingeniería Eléctrica

Por:

Riccardo Cespi -

Ingeniero en Control Automático
Corso di Laurea in INGEGNERIA INFORMATICA E AUTOMATICA
2007-2012

Becario de Conacyt, expediente no. 486289/280985

Directores de Tesis

Dr. Bernardino Castillo Toledo
Dr. Stefano Di Gennaro

CINVESTAV del IPN Unidad Guadalajara, Agosto de 2014.

Centro de Investigación y de Estudios Avanzados

del Instituto Politécnico Nacional

Unidad Guadalajara

Active Control of Ground Vehicles

A thesis presented by:
Riccardo Cespi

to obtain the degree of:
Master in Science

in the subject of:
Electrical Engineering

Thesis Advisors:
Dr. Bernardino Castillo-Toledo
Dr. Stefano Di Gennaro

CINVESTAV del IPN Unidad Guadalajara,Guadalajara, Jalisco, August 2006

Active Control of Ground Vehicles

Master of Science Thesis
In Electrical Engineering

By:
Riccardo Cespi
Engineer in Automatic Control
Università degli Studi de L'Aquila 2007-2012

Scholarship granted by CONACYT, No. 486289

Thesis Advisors:
Dr. Bernardino Castillo-Toledo
Dr. Stefano Di Gennaro

CINVESTAV del IPN Unidad Guadalajara, August, 2006.

Dedication

A mio padre Faliero, a mia madre Preziosa e a mio fratello Raoul che sono sempre stati pronti ad appoggiarmi. Formiamo un grande famiglia.

Ai miei direttori di tesi Bernardino Castillo-Toledo e Stefano Di Gennaro che sono una ispirazione per me. Riconosco la grande pazienza e umanità con cui mi hanno cresciuto dal punto di vista tecnico-scientifico.

Al mio amico e professore Cuauhtemoc Acosta-Lua che mi ha aiutato ad identificare, isolare e risolvere le problematiche presentatesi durante il corso del mio lavoro di ricerca.

A Fátima Roxana Ramos Guerrero.

Al CONACYT per il costante appoggio economico.

Resumen

En esta tesis se presentan diferentes argumentos relativos al problema de control activo de automóviles.

El objectivo principal de este trabajo es el desarollo de un controlor dinámico capaz de garantizar la estabilidad del vehículo en caso de pérdida de adherencia.

En primer lugar, se presenta un controlador basado en un observador no lineal de la velocidad lateral y la velocidad angular de yaw, para vehículos que poseen una dinámica de rotación no despreciable.

A partir de estos resultados, se preresenta un controlador dinámico que estima la velocidad lateral, la posición de rotación y la velocidad de alabeo.

Se muestra que el controlador dinámico garantiza la convergencia exponencial de las estimaciones. Esta técnica se basa en medidas de aceleracion longitudinal y lateral, velocidad longitudinal, velocidad de guiñada y ángulo del volante, medidas generalmente disponibles en vehículos modernos.

Finalmente, se propone una técnica de estimación del coeficiente de fricción entre llanta y asfalto basado en medidas de deformación de la llanta del vehículo.

Adicionalmente, se presenta un simulador de autovehículos, llamado CarSim, que ha sido usado para estudiar el desempeño de los controladores presentados.

Abstract

In this thesis different topics pertaining to the active control of ground vehicles are presented.

The overall goal of this study is the development of an electronic control able to ensure safe conditions in case of vehicle stability loss.

First, a nonlinear observed-based controller for lateral and yaw velocity is proposed, for vehicles in which the roll dynamics can not be neglected.

Then a dynamic controller which estimates the lateral velocity, the roll position and the roll velocity is presented.

The nonlinear controller ensures exponential convergence of the estimations. This technique is based on measurements of the longitudinal and lateral accelerations, longitudinal velocity, yaw rate and steer angle, usually available in modern vehicles.

In the end, the estimation of tyre-road friction coefficient based on tyre carcass deflection is discussed.

A car simulator, namely CarSim, has been used to check the performance of the proposed controllers.

Contents

List of Symbols

Symbol	Description
a_x	Longitudinal Acceleration
a_y	Lateral Acceleration
v_x	Longitudinal Velocity
v_y	Lateral Velocity
ω_z	Yaw Position
α_x	Roll Position
ω_x	Roll Rate
$F_{x,f}$	Longitudinal Force at Front Axis
$F_{y,f}$	Lateral Force at Front Axis
$F_{x,r}$	Longitudinal Force at Rear Axis
$F_{y,r}$	Lateral Force at Rear Axis
M_z	Rear Torque Vectoring
δ_c	Active Front Steering
μ_x	Longitudinal Friction Coefficient
μ_y	Lateral Friction Coefficient
m	Vehicle Mass
m_s	Vehicle Sprung Mass
l_f	Frontal Axis Length
l_r	Rear Axis Length
J_x	Roll Inertia
J_z	Yaw Inertia
h	Center of Gravity Height
k_x	Roll Stiffness
b_x	Roll Damping

Syllogism	Extended Name
DLC	Double Lane Change
AFS	Active Front Steering
RTV	Rear Torque Vectoring
CG	Center of Gravity
KF	Kalman Filter
ISO	International Organization for Standardization
SUV	Sport Utility Vehicle
ATI	Automotive Training Institute

Chapter 1

Introduction

In this chapter general concepts are described in order to develop the thesis. Objectives, structure and different correlate works are presented.

1.1 Preliminaries

The elimination of the mechanical link between actuator and device allows greater flexibility in the control of the device itself. In automotive, this principle has led to various subsystems which are controlled "by–wire", such as steer–by–wire, brake–by–wire, *et cetera*, and more in general to vehicle chassis active control systems, developed to enhanced vehicle stability and handling performance in critical situations. This technology allows a simpler design of active controllers for automobiles [1], [2], [3], [4], [5], [6], [7]. Examples include yaw stability control systems [8], [9], roll stability control systems [10], and integrated vehicle dynamic control systems [11], [12], [13], [14]. These active devices modify the vehicle dynamics imposing forces or moments to the vehicle, see e.g. [15], [16], [17], [18]. In the next future, the active systems will possibly use more sensors than those actually available onboard, such as the so–called intelligent or smart tires [19], [20], magnetic sensors [21], etc., allowing precise and distributed measurements from the environment, especially of the tire–road friction [22]. These new sensors will increase the performance of the control action, the vehicle stability, and the safety and comfort of the driver.

In this work we consider three aspects, commonly encountered when designing an active control

1. The increased number of sensors/elaborators/ actuators leads to problems due to the limited power available on a vehicle. This is particularly important for controllers which are designed as stand–alone. Saturations can occur more easily for stand–alone controllers than for integrated ones.

2. Usual actuators used for active attitude control are Active Front Steering (AFS) and Rear Torque Vectoring (RTV). The control action is commonly determined on the basis of approximated models, simple enough to obtain an implementable controller but accurate enough to capture the main aspects of the physics of the problem. Normally, such models consider only the lateral and yaw dynamics, assuming the other dynamics as (bounded) disturbances acting on the system. As an example the roll dynamics are usually neglected. However, in some cases, these perturbative dynamics could be easily considered without complicating excessively the control law. This is the very case of the roll dynamics, which is especially important to consider for particular types of tall vehicles, with no active devices on the suspensions. In these cases, the action of these dynamics may become important, and lead to instability.

3. Another difficulty faced in this work is the fact that some of the state variables, necessary to implement such control strategies, are usually not measured, due to sensor cost and space occupancy in the vehicle. For instance, the lateral velocity is rarely measured. Therefore, in order to obtain a satisfactory control performance, these state variables have to be determined from other measurements, such as longitudinal and lateral acceleration, longitudinal velocity, yaw rate and steer angle.

With this discussion in mind, and aiming at designing a control less prone to saturation, in this work we consider an integrated control with AFS and RTV as controls. The roll dynamics of the vehicle are considered in the model and in the controller design to obtain a more effective control action. Finally, the controller dynamics are designed to reconstruct the unmeasured variables, such as the lateral velocity and the roll position/velocity. Hence, this dynamic controller uses only the information available from the sensors normally available on modern vehicles, i.e. longitudinal and lateral accelerations, longitudinal velocity and yaw rate. The controller guarantees the exponential convergence of the estimation variables to the real ones, as well as the exponential tracking of (bounded) references for lateral velocity and yaw angular velocity. A significant advantage of the proposed controller is the fact that it embeds an observer relying on the kinematic model of the vehicle. Therefore, it is robust with respect variations of various parameters, one of them being the tire–road friction coefficient. This last is one of the most important parameter, whose estimation may be difficult in the case of sudden variations due to change of road conditions.

Earlier works on observers for the estimation of the lateral velocity, without roll angular velocity, are mainly based on linear techniques as in [11], [12], or quasilinear techniques as in [23], [24]. A nonlinear observer linearizing the error dynamics is proposed in [25] and [26], while a similar observer is presented in [27]. Linear and nonlinear observers using the sliding mode techniques are considered in [34] and [35]. Other observers are based on the Extended Kalman Filter (EKF). These observers are used for estimating vehicle velocity and tire forces [36], without the explicit use of friction models. An EKF based on a tire–road

friction model which includes estimation of the adhesion coefficient and road inclination angle is suggested in [37]. In [38], the use of an EKF based on a nonlinear tire–road friction model is considered, which also includes estimation of cornering stiffness. The strategy proposed in [39] combines dynamic and kinematic models of the vehicle with numerical band–limited integration of the equations to provide a side–slip estimate. In [40], the side–slip angle is estimated along with the yaw rate, with an approach similar to the one hereinafter considered, but without yaw rate measurements. In [41], a sliding mode observer is used for the estimation of the (longitudinal and lateral) velocity, along with a Kalman Filter for estimating the side–slip angle.

As far as active control of a vehicle is concerned, in [42] an active angle control of the front wheel is proposed, using a model reference method based on a linear observer. In [43] a yaw stabilizing algorithm is presented, combining AFS with a low level control of the longitudinal wheel slip, and an adaptive law that estimates the maximal tire–road friction parameter for each wheel. In [2] AFS and RTV are combined in an integrated controller to guarantee vehicle stability, making use of an adaptive feedback. In [44] a robust control algorithm of sliding mode control is designed, showing that the vehicle's handling and stability can be improved via four wheel active steering control. Model predictive control is used in [45], to obtain an integrated control for AFS and yaw moment. With the same technique, in [46] differential braking and AFS are used for tracking desired references. Finally, in [47], the problem of vehicle yaw control is addressed using a rear active differential, to minimize the yaw–rate error and body slip–angle error. In [50], an automatic steering feedback/feedforward controller for trajectory tracking in unmanned vehicles is proposed. The feedback relies on a fuzzy controller, with rules and parameters of the membership functions optimized by genetic algorithms. The feedforward controller is designed to assist the controller when the vehicle is engaged in a curved section of trajectory. In [51], a driver–assistance system is presented, based on the combination of an automatic road departure avoidance system and the driver's steering input. An H_∞ controller ensures the robustness with respect the main uncertainties. In [52], an integration of AFS and electronic stability control is proposed. A supervisor determines the target yaw rate and velocity, while a control determines the optimal yaw rate and the longitudinal force. In [53], a robust sliding–mode learning control is presented, facing uncertainties in the system parameters and an unknown disturbance due to the tire–road interaction. In [54] a variable stiffness and damping suspension system, using a magneto–rheological damper, is used for improving lateral stability.

The main difference of the present work with the aforementioned works is that in none of them the influence of the roll dynamics on the yaw and lateral dynamics is considered. In [48], [49], the roll dynamics are taken into account, to design an integrated control managing possible actuator saturations, but at the expenses of considering a further control action, i.e. semi–active suspensions. On the contrary, in the present work passive suspensions are considered, and the focus is instead on the design of a controller that enhances the control

performance, avoiding possible instability due to saturation linked to these roll dynamics.

1.2 Objectives

The objectives of this thesis are the following:

- Comparison of the proposed mathematical model with respect to the mathematical model used by the simulator CarSim.
- Analysis of the observer stability using a Lyapunov candidate function.
- Design of the reference system.
- Development of the tracking control laws.
- CarSim implementation of the observer–based controller.
- Study of the dynamic controller: proof and CarSim implementation.
- Analysis of relation between the tyre lateral deflection and tyre lateral force.
- Identification of the tyre-road friction coefficient.

1.3 Thesis Structure

This thesis is composed as follows:

In Chapter 2 a brief theory background is recalled including mathematic topics as observers design and non-linear stability theory. Theory vehicle dynamic is also reviewed.

In Chapter 3 a nonlinear observer-based controller is presented with special attention to the observer asymptotic stability. Then a reference system is designed to provide vehicle safety conditions. The tracking control lows are described and some simulations conclude the chapter.

In Chapter 4 a dynamic controller is developed. Two standard maneuver are used to show the good performance and behavior of the dynamic controller.

In Chapter 5 the relation between lateral tyre deflection and lateral tyre force is studied. This technique is based on new results as in "The Apollo" project which includes in-wheel tyre optical sensors for many vehicle states estimation.

In Chapter 6 the configuration of the car simulator CarSim is explained.

Finally, in Chapter 7 some conclusions are presented and future works are proposed.

Chapter 2

Vehicle Dynamic

In this chapter, physical concepts about the vehicle dynamics and a brief analysis of the mathematic model are presented.

2.1 Introduction

In order to design a controller, a good representative model of the system is needed. A vehicle mathematical model, which is appropriate for both acceleration and deceleration, is described in this section. This model will be used for design of control laws and computer simulations. Although the model considered here is relatively simple, it retains the essential dynamics of the system.

2.2 Vehicle Dynamic

The dynamics of a ground vehicle can be described by the so–called bicycle model [55], [56]

$$\begin{aligned} m(\dot{v}_x - v_y\omega_z) &= ma_x - m_s h\omega_z\dot{\alpha}_x \\ m(\dot{v}_y + v_x\omega_z) &= ma_y + m_s h\ddot{\alpha}_x \\ J_z\dot{\omega}_z &= \mu_y(F_{y,f}l_f - F_{y,r}l_r) + J_{zx}\ddot{\alpha}_x + M_z \end{aligned} \tag{2.1}$$

where m, J_z are the total vehicle mass and inertia with respect to the perpendicular axis, l_f, l_r are the distances from the vehicle center of gravity ($C.G.$) to the front and rear tires, a_x, a_y are the longitudinal and lateral accelerations, v_x, v_y are the longitudinal and lateral velocities of the $C.G.$, ω_z is the yaw rate, α_x is the roll angle, m_s is the so–called sprung mass, h is the distance between the center of gravity and the roll axis, and J_{xz} is the inertia

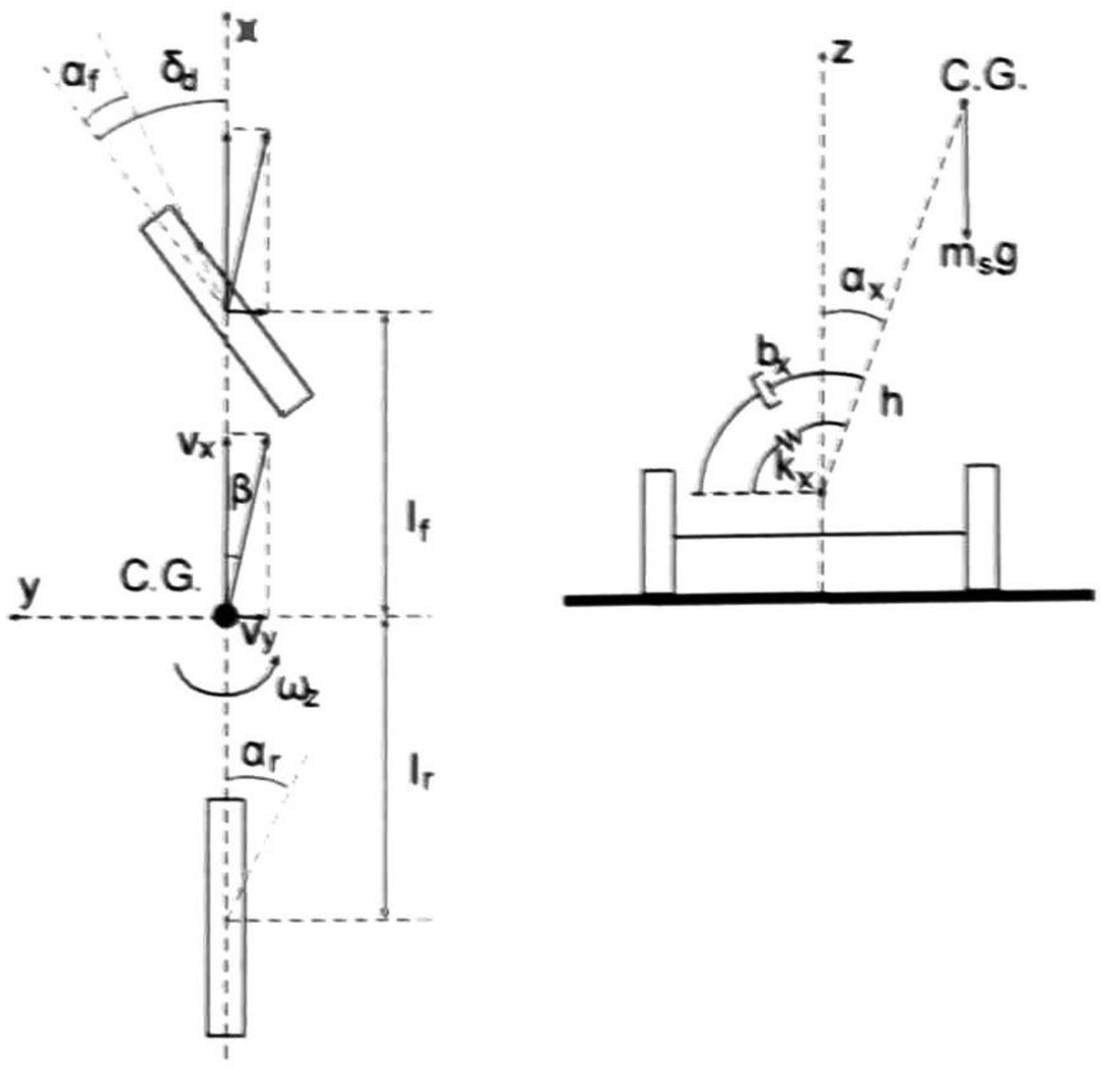

Figure 2.1: Linear bicycle model with roll angle

product with respect to the longitudinal and yaw axes (see Figure 2.1). Moreover, $F_{y,f}$, $F_{y,r}$ are the lateral forces of the front and rear tires, which depend on the slip angles

$$\alpha_f = \delta_d + \delta_c - \frac{v_y + l_f\omega_z}{v_x}, \quad \alpha_r = -\frac{v_y - l_r\omega_z}{v_x}$$

with δ_d the wheel angle, and δ_c AFS angle. We will not consider a specific tire model (see for instance [59], [60] and reference therein). Finally, μ_y is the lateral tire–road friction coefficient, and M_z is the RTV yaw moment.

In (2.1), the vehicle roll acceleration can be expressed as follows [57], [56], [58]

$$\begin{aligned} J_x\ddot{\alpha}_x = &-b_x\dot{\alpha}_x - k_x\alpha_x + m_s g h \sin\alpha_x \\ &+ m_s h(\dot{v}_y + \omega_z v_x)\cos\alpha_x + J_{xz}\dot{\omega}_z \end{aligned} \tag{2.2}$$

where $J_x = J_x^G + m_s h^2$ is the vehicle moment of inertia with respect to the longitudinal axis, J_x^G is the vehicle moment of inertia with respect to the longitudinal axis passing for the $C.G.$, g is the weight acceleration, and b_x, k_x are the suspension roll damping and stiffness.

Considering small angles α_x, and considering that $J_{xz} \simeq 0$, from (2.1) and (2.2), we obtain

the system dynamics

$$\begin{aligned}
\dot{v}_x &= v_y\omega_z + a_x - \frac{m_s}{m}h\omega_z\omega_x \\
\dot{v}_y &= -v_x\omega_z + \frac{J_x}{J_{x,e}}a_y - \frac{k_{x,e}}{J_{x,s}}\alpha_x - \frac{b_x}{J_{x,s}}\omega_x \\
\dot{\omega}_z &= \frac{\mu_y}{J_z}(F_{y,f}l_f - F_{y,r}l_r) + \frac{1}{J_z}M_z \\
\dot{\alpha}_x &= \omega_x \\
\dot{\omega}_x &= -\frac{k_{x,e}}{J_{x,e}}\alpha_x - \frac{b_x}{J_{x,e}}\omega_x + \frac{m_s}{J_{x,e}}ha_y
\end{aligned} \tag{2.3}$$

with

$$J_{x,e} = J_x - \frac{m_s^2}{m}h^2, \quad J_{x,s} = \frac{mJ_{x,e}}{m_s h}, \quad k_{x,e} = k_x - m_s gh.$$

This model describes the vehicle dynamics under the following assumptions

1. Pitch dynamic is neglected.

2. The system is rigid.

3. The suspension is passive.

Note that the longitudinal and lateral accelerations a_x, a_y in (2.3), which can be expressed in terms of the front/rear longitudinal and lateral tire forces

$$a_x = \frac{\mu_x}{m}(F_{x,f} + F_{x,r}), \qquad a_y = \frac{\mu_y}{m}(F_{y,f} + F_{y,r})$$

are measured by accelerometers, usually present aboard of a modern automobile. Here, $F_{x,f}$, $F_{x,r}$ are the front/rear tire longitudinal forces, and μ_x is the longitudinal tire–road friction coefficient.

The control problem is the following: given bounded reference signals $v_{y,r}(t)$, $\omega_{z,r}(t)$, with bounded references, for the lateral and angular velocities, the *control problem* is to determine a *dynamic* controller such that $\lim_{t\to\infty}(v_y(t) - v_{y,r}(t)) = 0$ and $\lim_{t\to\infty}(\omega_z(t) - \omega_{z,r}(t)) = 0$. This controller is dynamic since it does not relies on the measurements of the whole state of the system (2.3), given by the state variables v_x, v_y, ω_z, α_x, ω_x. In particular, in this work it is supposed that the state variables v_y, α_x, ω_x are not measured, and the controller needs to reconstruct them by means of appropriate dynamics.

2.3 Analysis of the Mathematic Model

The mathematic model (2.3) can be expressed in the state space form as follows:

$$\begin{aligned}
\dot{x}_1 &= 0 \\
\dot{x}_2 &= -x_1 x_3 + f_1(x_1, x_2, x_3, u_1) - c_2 x_4 - c_3 x_5 \\
\dot{x}_3 &= f_2(x_1, x_2, x_3, u_1) + f_3(x_1, x_2, x_3) + u_2 \\
\dot{x}_4 &= x_5 \\
\dot{x}_5 &= -c_4 x_4 - c_5 x_5 + f_3(x_1, x_2, x_3, u_1) \\
\\
y_1 &= x_2 \\
y_2 &= x_3
\end{aligned} \tag{2.4}$$

where it has been considered that the longitudinal velocity v_x is constant which allows to suppose $\dot{v}_x = 0$.

The reader can appreciate that the mathematic model (2.4) has a vector relative degree equal to one with respect to the outputs. Then there is a zero dynamic composed by three equations.

Let us consider a reference system which generates the reference variables $x_{2,ref}$ and $x_{3,ref}$.

By applying the feedback linearization to the two control laws u_1, u_2 one gets:

$$\begin{aligned}
\dot{x}_1 &= 0 \\
\dot{x}_2 &= \dot{x}_{2,ref} - k1(x_2 - x_{2,ref}) \\
\dot{x}_3 &= \dot{x}_{3,ref} - k2(x_3 - x_{3,ref}) \\
\dot{x}_4 &= x_5 \\
\dot{x}_5 &= -\alpha_1 x_4 - \alpha_2 x_5 + \alpha_3 \dot{x}_{2,ref} + \alpha_4 x_1 x_{3,ref}
\end{aligned} \tag{2.5}$$

with $\alpha_1, \alpha_2, \alpha_3, \alpha_4 > 0$.

Since x_1 is constant, $\dot{x}_{2,ref}$ and $x_{3,ref}$ are bounded signals, one can conclude that the system has a stable zero dynamic.

Chapter 3

Observer-Based Controller

In this chapter a nonlinear observer is presented and a reference system is proposed in order to obtain an observer-based controller for lateral velocity and yaw rate.

3.1 Observer Design

In this section it is supposed that a_x, a_y, ω_z, v_x are measurable. This is an acceptable hypothesis in modern vehicles, usually equipped with the necessary sensors. The proposed nonlinear observer relies on a copy of the plant (2.3)

$$\begin{aligned}
\dot{\hat{v}}_x &= \hat{v}_y\omega_z + a_x - \frac{m_s}{m}h\omega_z\hat{\omega}_x + k_{o1}(v_x - \hat{v}_x) \\
\dot{\hat{v}}_y &= -\hat{v}_x\omega_z + \frac{J_x}{J_{x,e}}a_y - \frac{k_{x,e}}{J_{x,s}}\hat{\alpha}_x - \frac{b_x}{J_{x,s}}\hat{\omega}_x \\
&\qquad + (k_{o2} - \omega_z)(v_x - \hat{v}_x) \\
\dot{\hat{\alpha}}_x &= \hat{\omega}_x + k_{o3}(v_x - \hat{v}_x) \\
\dot{\hat{\omega}}_x &= -\frac{k_{x,e}}{J_{x,e}}\hat{\alpha}_x - \frac{b_x}{J_{x,e}}\hat{\omega}_x + \frac{m_s}{J_{x,e}}ha_y + k_{o4}(v_x - \hat{v}_x)
\end{aligned} \tag{3.1}$$

where $k_{o1}, \cdots, k_{o4}$ are the observer gains, to be determined. Using (2.3), (3.1), the dynamics of the estimation errors

$$\begin{aligned}
e_{v_x} &= v_x - \hat{v}_x \\
e_{v_y} &= v_y - \hat{v}_y \\
e_{\alpha_x} &= \alpha_x - \hat{\alpha}_x \\
e_{\omega_x} &= \omega_x - \hat{\omega}_x
\end{aligned} \tag{3.2}$$

can be easily calculated

$$\begin{aligned}
\dot{e}_{v_x} &= -k_{o1}e_{v_x} + \omega_z e_{v_y} - \frac{m_s}{m}h\omega_z e_{\omega_x} \\
\dot{e}_{v_y} &= -k_{o2}e_{v_x} - \frac{1}{J_{x,s}}(k_{x,e}e_{\alpha_x} + b_x e_{\omega_x}) \\
\dot{e}_{\alpha_x} &= -k_{o3}e_{v_x} + e_{\omega_x} \\
\dot{e}_{\omega_x} &= -k_{o4}e_{v_x} - \frac{1}{J_{x,e}}(k_{x,e}e_{\alpha_x} + b_x e_{\omega_x})
\end{aligned} \tag{3.3}$$

where $J_{x,s} = m_e J_x/(m_s h)$. Equations (3.3) are linear and time varying due to the term ω_z. In the following it will be shown how to determine the gains $k_{o1}, \cdots, k_{o4}$ in (3.1) so that the exponential convergence of the estimation errors is ensured, to this end, let us consider the following:.

Assumption 1 *The yaw angular velocity ω_z remains bounded for all $t \geq t_0$, i.e. $|\omega_z| \leq \omega_{z,\max}$.* ◇

This assumption is physically reasonable, since the vehicle is a finite energy system, and thus the maximal yaw angular velocity remains bounded. In what follows, we derive an observer that, for $|\omega_z| > 0$ and under Assumption 1, will ensure the exponential convergence to zero of the estimation errors. Note that during a maneuver ω_z may pass through zero, but cannot be identically zero in a finite interval of time except when the lateral forces are zero, namely when the vehicle is proceeding straight. When ω_z is identically zero, an observability loss appears as explained in [68].

3.2 Non-linear Time-Varying Observer Stability Proof

The design of the observer gains $k_{o1}, \cdots, k_{o4}$ in (3.1) is done using the following Lyapunov candidate

$$\begin{aligned}
V_o(t,e) &= V_{o,1}(t, e_{v_x}, e_{v_y}) + V_{o,2}(e_{\alpha_x}, e_{\omega_x}); \\
V_{o,1}(t,e) &= \frac{1}{2}(\gamma_1 e_{v_x}^2 + e_{v_y}^2) - \kappa_1 \mathcal{S}_{\omega_z} e_{v_x} e_{v_y}; \\
V_{o,2}(e_{\alpha_x}, e_{\omega_x}) &= \frac{1}{2}\begin{pmatrix} e_{\alpha_x} \\ e_{\omega_x} \end{pmatrix}^T P_2 \begin{pmatrix} e_{\alpha_x} \\ e_{\omega_x} \end{pmatrix}
\end{aligned}$$

with $e = \left(e_{v_x}, e_{v_y}, e_{\alpha_x}, e_{\omega_x}\right)^T$, $\gamma_1 > \kappa_1^2 > 0$, $\kappa_1 \neq 0$ constant, $P_2 = P_2^T > 0$, and $\mathcal{S}_{\omega_z} = \text{sign}(\omega_z)$ the classical sign function defined as:

$$\text{sign}(\omega_z) = \begin{cases} 1 & \text{if } \omega_z > 0 \\ 0 & \text{if } \omega_z = 0 \\ -1 & \text{if } \omega_z < 0. \end{cases}$$

To this aim, deriving the Lyapunov candidate along the dynamics (3.3), one works out

$$\begin{aligned}\dot{V}_o(t,e) = \gamma_1 e_{v_x}\Big(&- k_{o1}e_{v_x} + \omega_z e_{v_y} - \frac{m_s}{m}h\omega_z e_{\omega_x}\Big)\\ &+ e_{v_y}\Big(- k_{o2}e_{v_x} - \frac{k_{x,e}}{J_{x,s}}e_{\alpha_x} - \frac{b_x}{J_{x,s}}e_{\omega_x}\Big)\\ &- \kappa_1 \mathcal{S}_{\omega_z} e_{v_x}\Big(- k_{o2}e_{v_x} - \frac{k_{x,e}}{J_{x,s}}e_{\alpha_x} - \frac{b_x}{J_{x,s}}e_{\omega_x}\Big)\\ &- \kappa_1 \mathcal{S}_{\omega_z} e_{v_y}\Big(- k_{o1}e_{v_x} + \omega_z e_{v_y} - \frac{m_s}{m}h\omega_z e_{\omega_x}\Big)\\ &- 2\kappa_1 \delta_{_D}(\omega_z)\dot{\omega}_z e_{v_x}e_{v_y}\\ &+ \begin{pmatrix} e_{\alpha_x}\\ e_{\omega_x}\end{pmatrix}^T P_2 A_2 \begin{pmatrix} e_{\alpha_x}\\ e_{\omega_x}\end{pmatrix} - \begin{pmatrix} e_{\alpha_x}\\ e_{\omega_x}\end{pmatrix}^T P_2 \begin{pmatrix} k_{o3}\\ k_{o4}\end{pmatrix} e_{v_x}\end{aligned}$$

where the derivative of $\mathcal{S}_{\omega_z}$ is given by

$$\frac{d}{dt}\mathcal{S}_{\omega_z} = 2\delta_{_D}(\omega_z)\dot{\omega}_z$$

with $\delta_{_D}(\omega_z)$ the Dirac distribution, and

$$A_2 = \begin{pmatrix} 0 & 1\\ -\dfrac{k_{x,e}}{J_{x,e}} & -\dfrac{b_x}{J_{x,e}}\end{pmatrix}$$

For $|\omega_z| > 0$ and under Assumption 1, $\delta_{_D}(\omega_z) = 0$ and

$$\begin{aligned}\dot{V}_o(t,e) = &-\Big(k_{o1}\gamma_1 - \kappa_1 k_{o2}\mathcal{S}_{\omega_z}\Big)e_{v_x}^2 - \kappa_1|\omega_z|e_{v_y}^2\\ &- \left\| \begin{matrix} e_{\alpha_x}\\ e_{\omega_x}\end{matrix}\right\|_{Q_2}^2 + \Big(\gamma_1\omega_z - k_{o2} + \kappa_1 k_{o1}\mathcal{S}_{\omega_z}\Big)e_{v_x}e_{v_y}\\ &+ \Big(\kappa_1\frac{k_{x,e}}{J_{x,s}}\mathcal{S}_{\omega_z} - p_{21}k_{o3} - p_{22}k_{o4}\Big)e_{v_x}e_{\alpha_x}\\ &+ \Big(- \gamma_1\frac{m_s}{m}h\omega_z + \kappa_1\frac{b_x}{J_{x,s}}\mathcal{S}_{\omega_z}\\ &\qquad - p_{22}k_{o3} - p_{23}k_{o4}\Big)e_{v_x}e_{\omega_x}\\ &- \frac{k_{x,e}}{J_{x,s}}e_{v_y}e_{\alpha_x} + \Big(\kappa_1\frac{m_s}{m}h|\omega_z| - \frac{b_x}{J_{x,s}}\Big)e_{v_y}e_{\omega_x}\end{aligned}$$

can be easily calculated

$$\begin{aligned}
\dot{e}_{v_x} &= -k_{o1}e_{v_x} + \omega_z e_{v_y} - \frac{m_s}{m}h\omega_z e_{\omega_x} \\
\dot{e}_{v_y} &= -k_{o2}e_{v_x} - \frac{1}{J_{x,s}}(k_{x,e}e_{\alpha_x} + b_x e_{\omega_x}) \\
\dot{e}_{\alpha_x} &= -k_{o3}e_{v_x} + e_{\omega_x} \\
\dot{e}_{\omega_x} &= -k_{o4}e_{v_x} - \frac{1}{J_{x,e}}(k_{x,e}e_{\alpha_x} + b_x e_{\omega_x})
\end{aligned} \tag{3.3}$$

where $J_{x,s} = m_e J_x/(m_s h)$. Equations (3.3) are linear and time varying due to the term ω_z. In the following it will be shown how to determine the gains $k_{o1}, \cdots, k_{o4}$ in (3.1) so that the exponential convergence of the estimation errors is ensured, to this end, let us consider the following:.

Assumption 1 *The yaw angular velocity ω_z remains bounded for all $t \geq t_0$, i.e. $|\omega_z| \leq \omega_{z,\max}$.* ◇

This assumption is physically reasonable, since the vehicle is a finite energy system, and thus the maximal yaw angular velocity remains bounded. In what follows, we derive an observer that, for $|\omega_z| > 0$ and under Assumption 1, will ensure the exponential convergence to zero of the estimation errors. Note that during a maneuver ω_z may pass through zero, but cannot be identically zero in a finite interval of time except when the lateral forces are zero, namely when the vehicle is proceeding straight. When ω_z is identically zero, an observability loss appears as explained in [68].

3.2 Non-linear Time-Varying Observer Stability Proof

The design of the observer gains $k_{o1}, \cdots, k_{o4}$ in (3.1) is done using the following Lyapunov candidate

$$\begin{aligned}
V_o(t,e) &= V_{o,1}(t, e_{v_x}, e_{v_y}) + V_{o,2}(e_{\alpha_x}, e_{\omega_x}); \\
V_{o,1}(t,e) &= \frac{1}{2}(\gamma_1 e_{v_x}^2 + e_{v_y}^2) - \kappa_1 \mathcal{S}_{\omega_z} e_{v_x} e_{v_y}; \\
V_{o,2}(e_{\alpha_x}, e_{\omega_x}) &= \frac{1}{2}\begin{pmatrix} e_{\alpha_x} \\ e_{\omega_x} \end{pmatrix}^T P_2 \begin{pmatrix} e_{\alpha_x} \\ e_{\omega_x} \end{pmatrix}
\end{aligned}$$

with $e = \left(e_{v_x}, e_{v_y}, e_{\alpha_x}, e_{\omega_x}\right)^T$, $\gamma_1 > \kappa_1^2 > 0$, $\kappa_1 \neq 0$ constant, $P_2 = P_2^T > 0$, and $\mathcal{S}_{\omega_z} = \text{sign}(\omega_z)$ the classical sign function defined as:

$$\text{sign}(\omega_z) = \begin{cases} 1 & \text{if } \omega_z > 0 \\ 0 & \text{if } \omega_z = 0 \\ -1 & \text{if } \omega_z < 0. \end{cases}$$

To this aim, deriving the Lyapunov candidate along the dynamics (3.3), one works out

$$\begin{aligned}
\dot{V}_o(t,e) = {} & \gamma_1 e_{v_x}\Big(- k_{o1}e_{v_x} + \omega_z e_{v_y} - \frac{m_s}{m}h\omega_z e_{\omega_x}\Big) \\
& + e_{v_y}\Big(- k_{o2}e_{v_x} - \frac{k_{x,e}}{J_{x,s}}e_{\alpha_x} - \frac{b_x}{J_{x,s}}e_{\omega_x}\Big) \\
& - \kappa_1 \mathcal{S}_{\omega_z} e_{v_x}\Big(- k_{o2}e_{v_x} - \frac{k_{x,e}}{J_{x,s}}e_{\alpha_x} - \frac{b_x}{J_{x,s}}e_{\omega_x}\Big) \\
& - \kappa_1 \mathcal{S}_{\omega_z} e_{v_y}\Big(- k_{o1}e_{v_x} + \omega_z e_{v_y} - \frac{m_s}{m}h\omega_z e_{\omega_x}\Big) \\
& - 2\kappa_1 \delta_{_D}(\omega_z)\dot{\omega}_z e_{v_x}e_{v_y} \\
& + \begin{pmatrix} e_{\alpha_x} \\ e_{\omega_x} \end{pmatrix}^T P_2 A_2 \begin{pmatrix} e_{\alpha_x} \\ e_{\omega_x} \end{pmatrix} - \begin{pmatrix} e_{\alpha_x} \\ e_{\omega_x} \end{pmatrix}^T P_2 \begin{pmatrix} k_{o3} \\ k_{o4} \end{pmatrix} e_{v_x}
\end{aligned}$$

where the derivative of $\mathcal{S}_{\omega_z}$ is given by

$$\frac{d}{dt}\mathcal{S}_{\omega_z} = 2\delta_{_D}(\omega_z)\dot{\omega}_z$$

with $\delta_{_D}(\omega_z)$ the Dirac distribution, and

$$A_2 = \begin{pmatrix} 0 & 1 \\ -\dfrac{k_{x,e}}{J_{x,e}} & -\dfrac{b_x}{J_{x,e}} \end{pmatrix}$$

For $|\omega_z| > 0$ and under Assumption 1, $\delta_{_D}(\omega_z) = 0$ and

$$\begin{aligned}
\dot{V}_o(t,e) = {} & -\Big(k_{o1}\gamma_1 - \kappa_1 k_{o2}\mathcal{S}_{\omega_z}\Big)e_{v_x}^2 - \kappa_1|\omega_z|e_{v_y}^2 \\
& - \left\| \begin{matrix} e_{\alpha_x} \\ e_{\omega_x} \end{matrix} \right\|_{Q_2}^2 + \Big(\gamma_1\omega_z - k_{o2} + \kappa_1 k_{o1}\mathcal{S}_{\omega_z}\Big)e_{v_x}e_{v_y} \\
& + \Big(\kappa_1\frac{k_{x,e}}{J_{x,s}}\mathcal{S}_{\omega_z} - p_{21}k_{o3} - p_{22}k_{o4}\Big)e_{v_x}e_{\alpha_x} \\
& + \Big(- \gamma_1\frac{m_s}{m}h\omega_z + \kappa_1\frac{b_x}{J_{x,s}}\mathcal{S}_{\omega_z} \\
& \qquad - p_{22}k_{o3} - p_{23}k_{o4}\Big)e_{v_x}e_{\omega_x} \\
& - \frac{k_{x,e}}{J_{x,s}}e_{v_y}e_{\alpha_x} + \Big(\kappa_1\frac{m_s}{m}h|\omega_z| - \frac{b_x}{J_{x,s}}\Big)e_{v_y}e_{\omega_x}
\end{aligned}$$

where

$$P_2 = P_2^T = \begin{pmatrix} p_{21} & p_{22} \\ p_{22} & p_{23} \end{pmatrix} > 0$$

has been determined as solution of the Lyapunov equation

$$P_2 A_2 + A_2^T P_2 = -Q_2, \qquad Q_2 = Q_2^T > 0.$$

This expression can be simplified choosing the observer gains $k_{o1}, \cdots, k_{o4}$ such that

$$\begin{pmatrix} k_{o1} \\ k_{o2} \end{pmatrix} = \frac{1}{\gamma_1 - \kappa_1^2} \begin{pmatrix} \frac{1}{2}\kappa_1 \omega_{z,\max} + \kappa_1 \gamma_1 |\omega_z| \\ \frac{1}{2}\kappa_1^2 \omega_{z,\max} \mathcal{S}_{\omega_z} + \gamma_1^2 \omega_z \end{pmatrix}$$
$$\begin{pmatrix} k_{o3} \\ k_{o4} \end{pmatrix} = P_2^{-1} \begin{pmatrix} \kappa_1 \frac{k_{x,e}}{J_{x,s}} \mathcal{S}_{\omega_z} \\ -\gamma_1 \frac{m_s}{m} h \omega_z + \kappa_1 \frac{b_x}{J_{x,s}} \mathcal{S}_{\omega_z} \end{pmatrix} \tag{3.4}$$

so obtaining

$$\dot{V}_o(t,e) = -\frac{1}{2}\kappa_1 \omega_{z,\max} e_{v_x}^2 - \kappa_1 |\omega_z| e_{v_y}^2 - \left\| \begin{matrix} e_{\alpha_x} \\ e_{\omega_x} \end{matrix} \right\|_{Q_2}^2$$
$$- \frac{k_{x,e}}{J_{x,s}} e_{v_y} e_{\alpha_x} + \left(\kappa_1 \frac{m_s}{m} h |\omega_z| - \frac{b_x}{J_{x,s}} \right) e_{v_y} e_{\omega_x}$$

Choosing

$$Q_2 = \begin{pmatrix} \lambda_1 & 0 \\ 0 & \lambda_2 \end{pmatrix} \tag{3.5}$$

$\lambda_1, \lambda_2 > 0$ one gets

$$\dot{V}_o(t,e) \leq -\frac{1}{2}\kappa_1 \omega_{z,\max} e_{v_x}^2 - \kappa_1 \omega_{z,\max} e_{v_y}^2 - \lambda_1 e_{\alpha_x}^2 - \lambda_2 e_{\omega_x}^2$$
$$+ \frac{k_{x,e}}{J_{x,s}} e_{v_y} e_{\alpha_x} + \left(\kappa_1 \frac{m_s}{m} h |\omega_z| - \frac{b_x}{J_{x,s}} \right) e_{v_y} e_{\omega_x}$$

where it has been considered that $|\omega_z| \leq \omega_{z,\min}$ (Assumption 1).

The cross terms can be eliminated using the following inequalities

$$\pm \alpha_1 e_{v_y} e_{\alpha_x} \leq \frac{\alpha_1}{\mu_1} e_{v_y}^2 + \alpha_1 \mu_1 e_{\alpha_x}^2$$
$$\pm \alpha_2 e_{v_y} e_{\omega_x} \leq \frac{|\alpha_2|}{\mu_2} e_{v_y}^2 + |\alpha_2| \mu_2 e_{\omega_x}^2$$
$$\leq \frac{\alpha_{2,\max}}{\mu_2} e_{v_y}^2 + \alpha_{2,\max} \mu_2 e_{\omega_x}^2$$

thanks to Assumption 1, where $\mu_1, \mu_2 > 0$ are weighting terms, and

$$\alpha_1 = \frac{k_{x,e}}{J_{x,s}} > 0, \qquad \alpha_2 = \kappa_1 \frac{m_s}{m} h|\omega_z| - \frac{b_x}{J_{x,s}}.$$

Hence,

$$\begin{aligned}\dot{V}_o(t,e) \leq & -\frac{1}{2}\kappa_1 \omega_{z,\max} e_{v_x}^2 \\ & - \left(\kappa_1 \omega_{z,\max} - \frac{\alpha_1}{\mu_1} - \frac{\alpha_{2,\max}}{\mu_2}\right) e_{v_y}^2 \\ & - (\lambda_1 - \alpha_1 \mu_1) e_{\alpha_x}^2 - (\lambda_2 - \alpha_{2,\max}\mu_2) e_{\omega_x}^2.\end{aligned}$$

Setting

$$\begin{aligned}\kappa_1 &= \frac{1}{\omega_{z,\max}}\left(2\lambda_o + \frac{\alpha_1}{\mu_1} + \frac{\alpha_{2,\max}}{\mu_2}\right) \\ \lambda_1 &= \lambda_o + \alpha_1 \mu_1 \\ \lambda_2 &= \lambda_o + \alpha_{2,\max}\mu_2\end{aligned} \tag{3.6}$$

$\lambda_o > 0$, where $\mu_1, \mu_2 > 0$ can be chosen in order to ensure better performance, and κ_1 does not depend on time, one finally gets

$$\dot{V}_o(t,e) \leq -\lambda_o(e_{v_x}^2 + e_{v_y}^2 + e_{\alpha_x}^2 + e_{\omega_x}^2) < 0.$$

Hence, the error system in (3.3) has the origin exponentially stable, and the estimation errors (3.2) tend exponentially to zero, with a time constant $\tau = 1/\lambda_o$. We can conclude with the following.

Theorem 1 *Under Assumption 1, when $|\omega_z| > 0$ the observer (3.1), with the gains (3.4), (3.6), ensures the global exponential convergence to zero of the estimation errors (3.2), with a time constant $\tau = 1/\lambda_o$, for a $\lambda_o > 0$ fixed by the designer.* ◇

3.3 Design of an Active Controller

The control inputs are the AFS angle δ_c and the RTV yaw moment M_z. The former can be computed inverting, in some feasible region, the function $F_{y,f}$, as explained in [2].

This allows considering as control input the difference

$$\Delta_c = F_{y,f} - F_{y,f,d}, \qquad F_{y,f,d} = F_{y,f}(\alpha_{f,d})$$

$$\alpha_{f,d} = \delta_d - \frac{v_y + l_f \omega_z}{v_x}$$

instead of δ_c. Therefore, the equations used to determine the control law are obtained from (2.3)

$$\begin{aligned}\dot{v}_y &= -v_x\omega_z + \frac{1}{m_e}\Big[\mu_y(F_{y,f,d} + F_{y,r}) \\ &\quad - \frac{m_s}{J_x}h(k_{x,e}\alpha_x + b_x\omega_x) + \mu_y\Delta_c\Big] \qquad (3.7)\\ \dot{\omega}_z &= \frac{\mu_y}{J_z}(F_{y,f,d}l_f - F_{y,r}l_r) + \frac{\mu_y l_f}{J_z}\Delta_c + \frac{1}{J_z}M_z.\end{aligned}$$

Considering as Lyapunov candidate

$$V_s = \frac{1}{2}(\omega_z - \omega_{z,r})^2 + \frac{1}{2}(v_y - v_{y,r})^2$$

the control is obtained imposing that the time derivative along the dynamics (3.7) is equal to

$$\begin{aligned}\dot{V}_s &= (v_y - v_{y,r})\Big[- v_x\omega_z + \frac{\mu_y}{m_e}(F_{y,f,d} + F_{y,r}) \\ &\quad - \frac{m_s}{m_e J_x}h(k_{x,e}\alpha_x + b_x\omega_x) + \frac{\mu_y}{m_e}\Delta_c - \dot{v}_{y,r}\Big] \\ &\quad + (\omega_z - \omega_{z,r})\Big[\frac{\mu_y}{J_z}(F_{y,f,d}l_f - F_{y,r}l_r) + \frac{\mu_y l_f}{J_z}\Delta_c \\ &\quad + \frac{1}{J_z}M_z - \dot{\omega}_{z,r}\Big] \\ &= -k_{s1}(v_y - v_{y,r})^2 - k_{s2}(\omega_z - \omega_{z,r})^2\end{aligned}$$

$k_{s1}, k_{s2} > 0$, $m_e = m - m_s^2h^2/J_x$. Therefore, for $\mu_y > 0$, one gets the control

$$\begin{aligned}\Delta_c &= -k_{s1}\frac{m_e}{\mu_y}(v_y - v_{y,r}) + \frac{m_e}{\mu_y}\dot{v}_{y,r} + \frac{m_e}{\mu_y}v_x\omega_z \\ &\quad - F_{y,f,d} - F_{y,r} + \frac{m_s}{\mu_y J_x}h(k_{x,e}\alpha_x + b_x\omega_x) \\ M_z &= -k_{s2}J_z(\omega_z - \omega_{z,r}) + J_z\dot{\omega}_{z,r} - \mu_y(F_{y,f,d}l_f - F_{y,r}l_r) \\ &\quad - \mu_y l_f\Delta_c\end{aligned}$$

ensuring the exponential convergence of the tracking errors $\omega_z - \omega_{z,r}, v_y - v_{y,r}$ to zero.

Since v_y, α_x, ω_x are not measured, the first step will be the design of an observer to estimate these variables. The applied control is hence obtained considering the estimates $\hat{v}_y$,

$\hat{\alpha}_x$, $\hat{\omega}_x$

$$\begin{aligned}\hat{\Delta}_c = &-k_{s1}\frac{m_e}{\mu_y}(\hat{v}_y - v_{y,r}) + \frac{m_e}{\mu_y}\dot{v}_{y,r} + \frac{m_e}{\mu_y}v_x\omega_z \\ &- \hat{F}_{y,f,d} - \hat{F}_{y,r} + \frac{m_s}{\mu_y J_x}h(k_{x,e}\hat{\alpha}_x + b_x\hat{\omega}_x) \\ \hat{M}_z = &-k_{s2}J_z(\omega_z - \omega_{z,r}) + J_z\dot{\omega}_{z,r} - \mu_y(\hat{F}_{y,f,d}l_f - \hat{F}_{y,r}l_r) \\ &- \mu_y l_f\hat{\Delta}_c\end{aligned} \tag{3.8}$$

where

$$\hat{F}_{y,f,d} = D_{f,y}\sin\left(C_{f,y}\arctan B_{f,y}\hat{\alpha}_{f,d}\right)$$
$$\hat{F}_{y,r} = D_{r,y}\sin\left(C_{r,y}\arctan B_{r,y}\hat{\alpha}_r\right)$$

with $\hat{\alpha}_{f,d} = \delta_d - (\hat{v}_y + l_f\omega_z)/v_x$, $\hat{\alpha}_r = -(\hat{v}_y - l_r\omega_z)/v_x$.

3.4 Simulation Results

In this section the behavior of the proposed nonlinear controller is shown for an interesting case, when the vehicle performs a double lane maneuver. The driver performs a step steer of 100° at $t = 1$ s, and a step steer of $-100°$ at $t = 2$ s, and with $\delta_d = 0$ at $t = 3$ s. During the imposed maneuver, the tire–road friction coefficient is supposed to vary from $\mu_y = 0.9$ (dry surface) to $\mu_y = 0.5$ (wet surface) at $t = 2.2$ s.

The initial longitudinal velocity is $v_x(0) = 28$ m/s (about 100 km/h). The initial values of the observer variables are

$$\hat{v}_x(0) = v_x, \quad \hat{v}_y(0) = 0, \quad \hat{\alpha}_x(0) = 0, \quad \hat{\omega}_x(0) = 0$$

and the nominal vehicle parameters, used in the observer (3.1) and in the controller (3.8), are given in Table 3.1.

To show that the proposed controller is robust with respect to parameter variations, we have considered the parameters given in Table 3.2 for the vehicle dynamics (2.3).

There are various ways to generate the references $v_{y,r}(t)$, $\omega_{z,r}(t)$. The results presented in the previous sections require that $v_{y,r}(t)$, $\omega_{z,r}(t)$ and their derivatives are bounded signals, but no further constraints are necessary. For the sake of concreteness, we generate them as the signals generated by a copy of the model (2.3) without the roll dynamics (ideal "decoupled" behavior)

$$\begin{aligned}\dot{v}_{y,r} &= -v_x\omega_{z,r} + \frac{\mu_r}{m}\Big(F_{y,f,r}(\alpha_{f,r}) + F_{y,r,r}(\alpha_{r,r})\Big) \\ \dot{\omega}_{z,r} &= \frac{\mu_r}{J_z}\Big(F_{y,f,r}(\alpha_{f,r})l_f - F_{y,r,r}(\alpha_{r,r})l_r\Big)\end{aligned} \tag{3.9}$$

Variable	*Value*	*Unit*
m_0	1862	kg
$m_{s,0}$	1592	kg
h_0	0.63	m
$J_{z,0}$	2488	$kg\ m^2$
$b_{x,0}$	10000	$Nm\ rad/s$
$k_{x,0}$	114000	$Nm\ rad$
$J_{x,0}$	614	$kg\ m^2$

Table 3.1: Nominal parameters used in the observer and controller

Variable	*Value*	*Unit*
m	1800	kg
m_s	1550	kg
h	0.63	m
J_z	2400	$kg\ m^2$
b_x	10000	$Nm\ rad/s$
k_x	114000	$Nm\ rad$
J_x	600	$kg\ m^2$
l_f	1.18	m
l_r	1.77	m

Table 3.2: Real parameters used in the observer and controller

with $\alpha_{f,r} = \delta_d - (v_{y,r} + l_f\omega_{z,r})/v_x$, $\alpha_{r,r} = -(v_{y,r} - l_r\omega_{z,r})/v_x$, and μ_r the tyre–road friction coefficient used in the reference generator. The reference system (3.9) includes also some "modified (ideal) tire functions" $F_{y,f,r}$, $F_{y,r,r}$.

In Figures 3.1, and 3.2 the behavior of the controlled vehicle is show when in the controller (3.8) and in the observer (3.1) the terms relative to the roll dynamics are not considered. This behavior is compared with that when the roll is considered. It is clear the improvement of the results, which are more evident in vehicles with high center of gravity, such as SUVs, as considered in this simulations.

The obtained results are shown in Figures 3.3 – 3.9, with $k_{s1} = 50$, $k_{s2} = 50$ in (3.8), and $k_{o1}, \cdots, k_{o4}$ in (3.1) set considering $\gamma_1 = 100$, $\kappa_1 = 9$ in (3.4), and $\lambda_1 = 1$, $\lambda_2 = 1000$ in (3.5). Notice the good tracking performance of both the observer and the controller. Moreover, this observer–based controller shows good performances with respect to system parameter variations. In particular, it is robust with respect variations of the tire–road friction coefficient, since the performance does not depend relevantly on this crucial parameter.

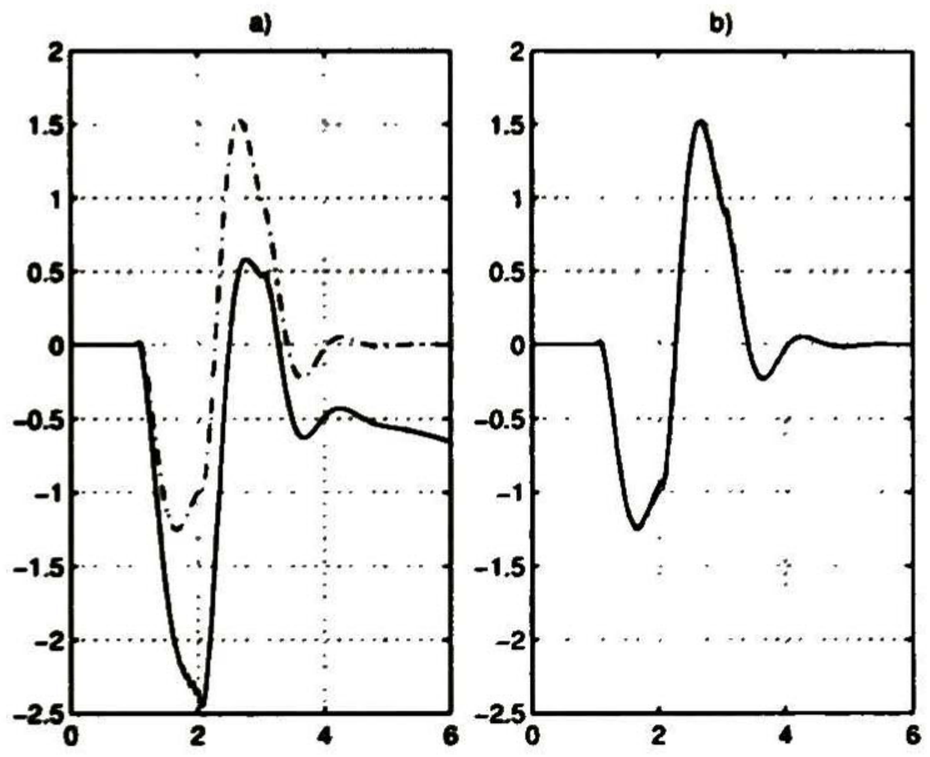

Figure 3.1: Lateral velocity v_y (solid), estimation $\hat{v}_y$ (gray), and reference $v_{y,r}$ (dot-line) [m/s vs s]. a) Case in which the terms due to the roll dynamics are neglected in the controller (3.8) and in the observer (3.1); b) Case in which the terms due to the roll dynamics are considered in the controller (3.8) and in the observer (3.1).

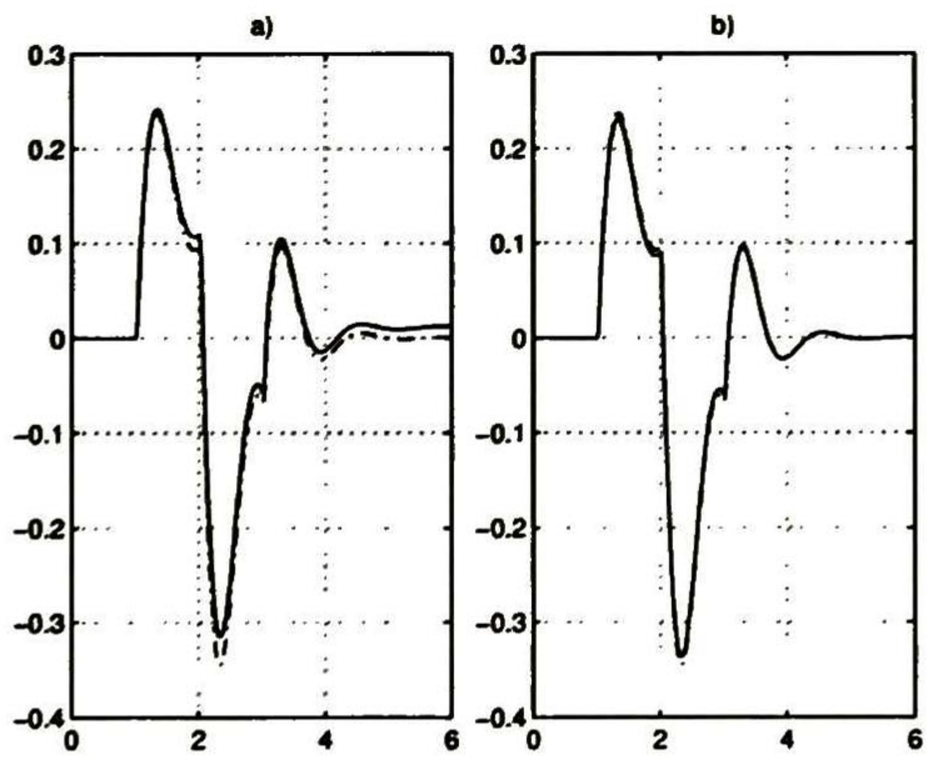

Figure 3.2: Yaw angular velocity ω_z (solid) and reference $\omega_{z,r}$ (dot–line) [rad/s vs s]. a) Case in which the terms due to the roll dynamics are neglected in the controller (3.8) and in the observer (3.1); b) Case in which the terms due to the roll dynamics are considered in the controller (3.8) and in the observer (3.1).

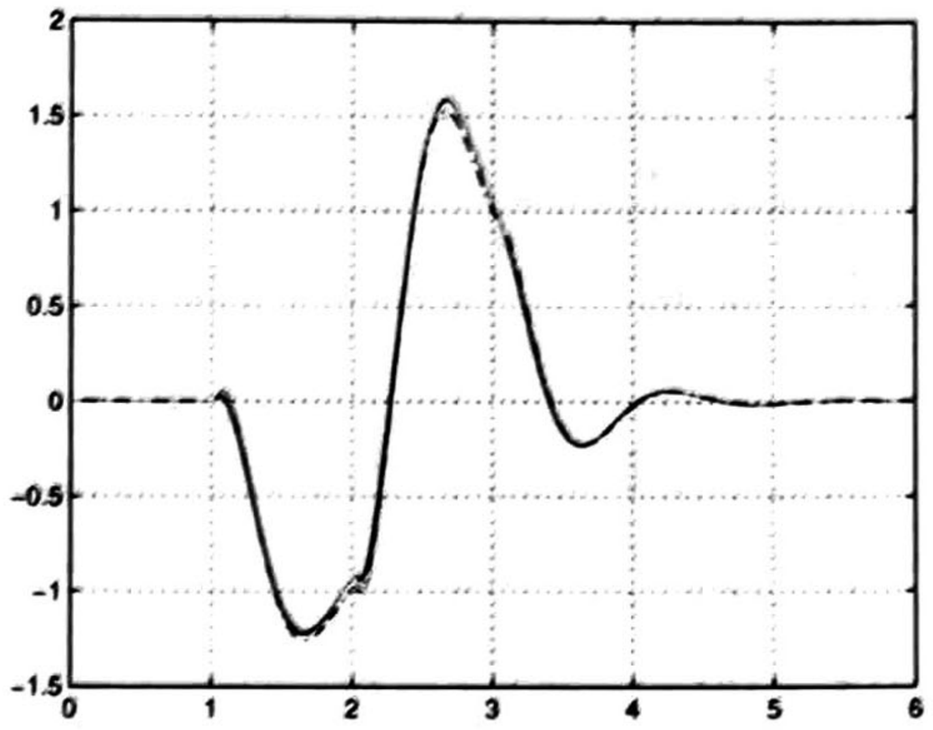

Figure 3.3: Lateral velocity v_y (solid), estimation $\hat{v}_y$ (gray), and reference $v_{y,r}$ (dot–line) [m/s vs s].

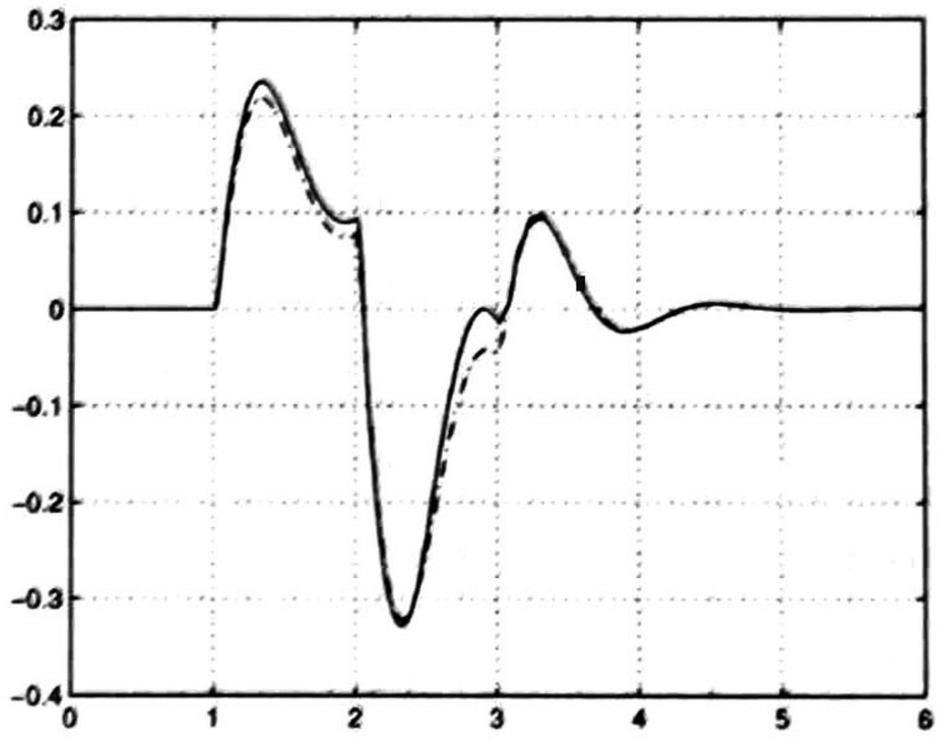

Figure 3.4: Yaw angular velocity ω_z (solid) and reference $\omega_{z,r}$ (dot–line) [rad/s vs s].

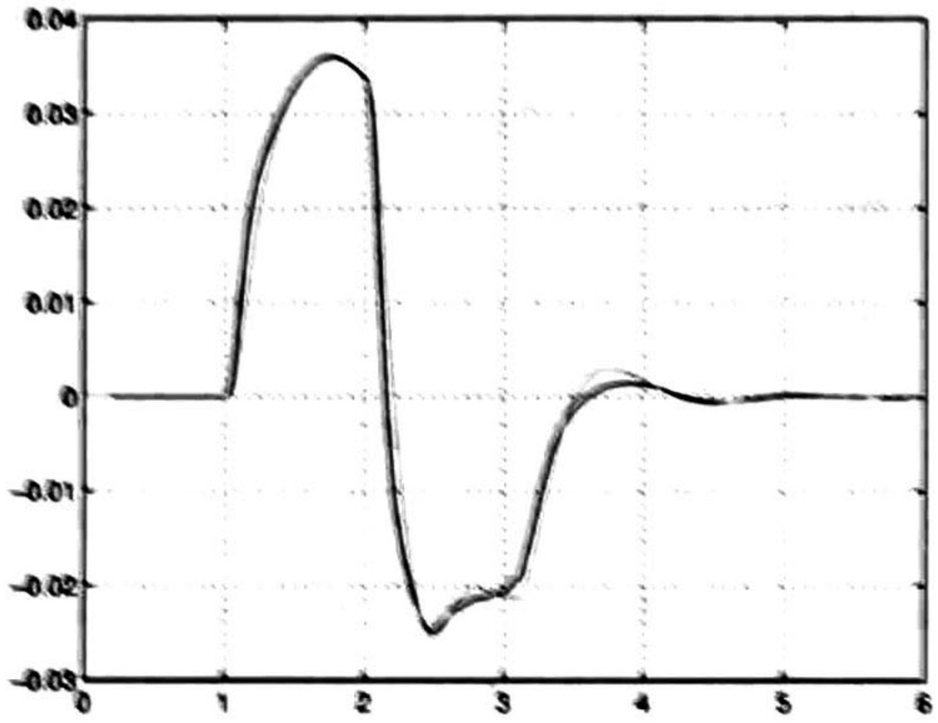

Figure 3.5: Roll angle α_x (solid) and estimation $\hat{\alpha}_x$ (gray) [deg vs s].

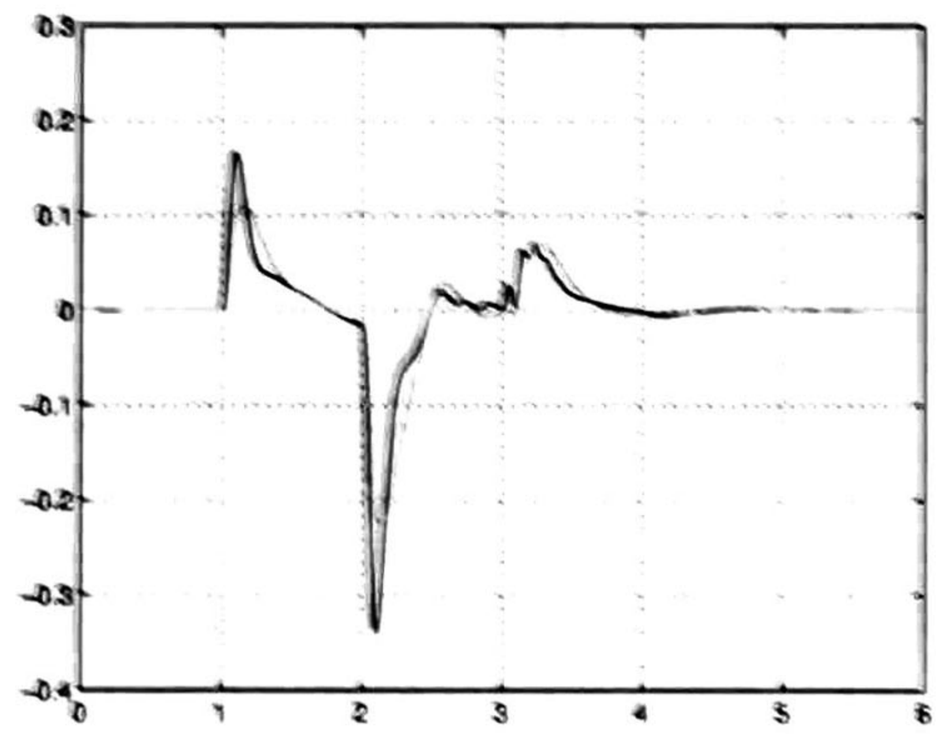

Figure 3.6: Roll velocity ω_x (solid) and estimation $\hat{\omega}_x$ (gray) [deg/s vs s].

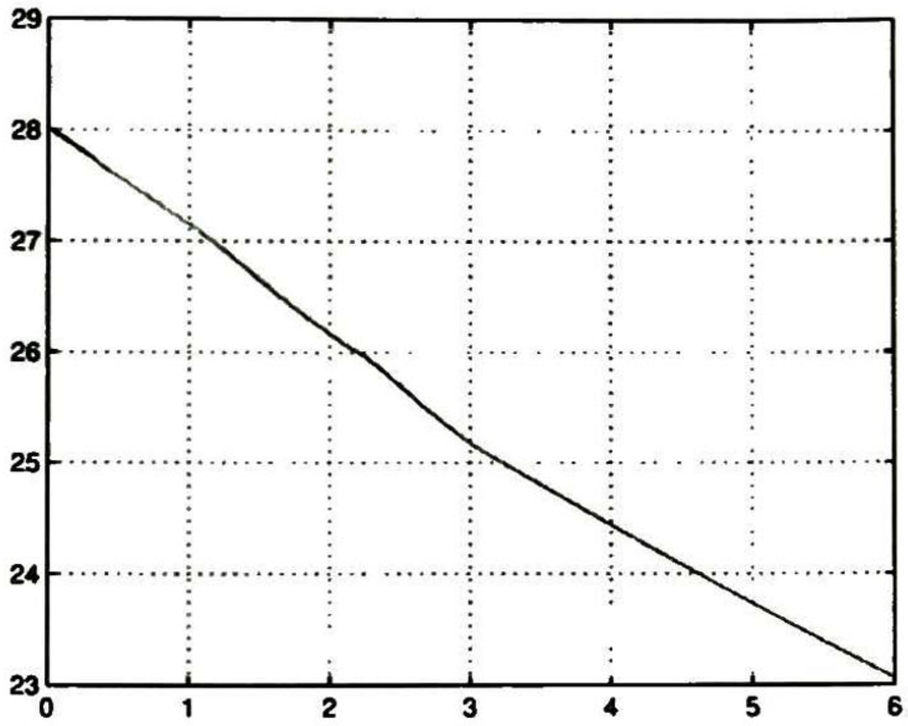

Figure 3.7: Longitudinal velocity v_x (solid) and estimation $\hat{v}_x$ (gray) [m/s vs s].

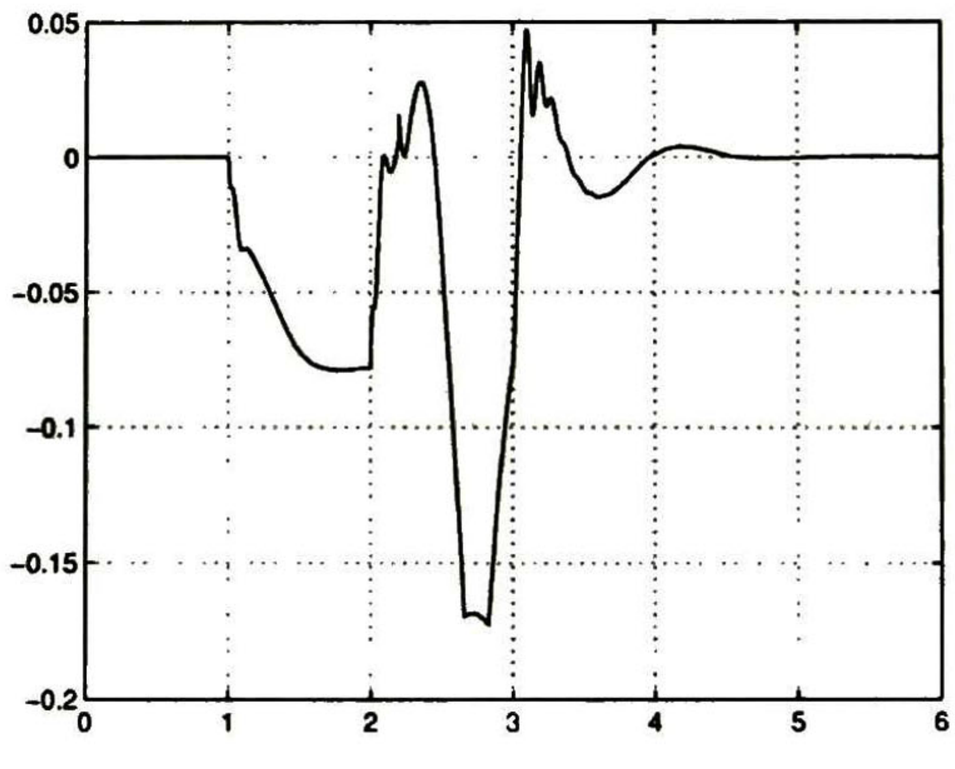

Figure 3.8: Active front steering angle δ_c [rad vs s].

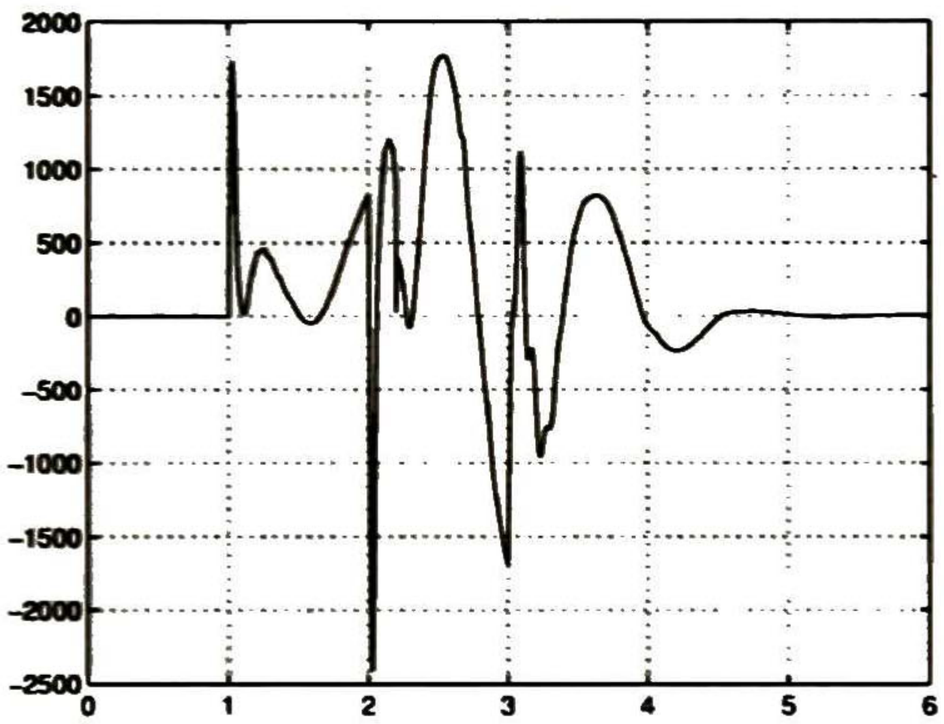

Figure 3.9: Yaw moment M_z [N m vs s].

Chapter 4

Dynamic Controller

In this chapter a dynamic controller is presented and the performances are shown using two standard maneuvers in CarSim.

4.1 Dynamic Controller Stability Proof

In this chapter we present the study of a dynamic controller. A controller is dynamic when at each time, the control law and the estimation of the observed variables are provided. For linear, time-invarying systems a dynamic controller is not necessary due to the *separation principle* which allows to design the controller and the observer as independent structures. Even if in several cases of non-linear systems the *separation principle* holds, in this case it does not and a global stability proof is required.

Let us assign the controller dynamics considering a copy of the system, i.e. one can consider a state observer

$$\begin{aligned}
\dot{\hat{v}}_x &= \hat{v}_y\omega_z + a_x - \frac{m_s}{m}h\omega_z\hat{\omega}_x + k_{o1}(v_x - \hat{v}_x) \\
\dot{\hat{v}}_y &= -\hat{v}_x\omega_z + \frac{J_x}{J_{x,e}}a_y - \frac{k_{x,e}}{J_{x,s}}\hat{\alpha}_x - \frac{b_x}{J_{x,s}}\hat{\omega}_x + (k_{o2} - \omega_z)(v_x - \hat{v}_x) \\
\dot{\hat{\alpha}}_x &= \hat{\omega}_x + k_{o3}(v_x - \hat{v}_x) \\
\dot{\hat{\omega}}_x &= -\frac{k_{x,e}}{J_{x,e}}\hat{\alpha}_x - \frac{b_x}{J_{x,e}}\hat{\omega}_x + \frac{m_s}{J_{x,e}}ha_y + k_{o4}(v_x - \hat{v}_x)
\end{aligned} \tag{4.1}$$

where $k_{o1}, \cdots, k_{o4}$ are positive gains. Therefore,

$$\begin{aligned}
\dot{e}_{v_x} &= -k_{o1} e_{v_x} + \omega_z e_{v_y} - \frac{m_s}{m} h \omega_z e_{\omega_x} \\
\dot{e}_{v_y} &= -k_{o2} e_{v_x} - \frac{k_{x,e}}{J_{x,s}} e_{\alpha_x} - \frac{b_x}{J_{x,s}} e_{\omega_x} \\
\dot{e}_{\alpha_x} &= -k_{o3} e_{v_x} + e_{\omega_x} \\
\dot{e}_{\omega_x} &= -k_{o4} e_{v_x} - \frac{k_{x,e}}{J_{x,e}} e_{\alpha_x} - \frac{b_x}{J_{x,e}} e_{\omega_x}
\end{aligned} \tag{4.2}$$

and deriving V_o,

$$\begin{aligned}
V_o(t, e) &= V_{o,1}(t, e_{v_x}, e_{v_y}) + V_{o,2}(e_{\alpha_x}, e_{\omega_x}) \\
V_{o,1}(t, e) &= \frac{1}{2}(\gamma_1 e_{v_x}^2 + e_{v_y}^2) - \kappa_1 \mathcal{S}_{\omega_z} e_{v_x} e_{v_y} \\
V_{o,2}(e_{\alpha_x}, e_{\omega_x}) &= \frac{1}{2} \begin{pmatrix} e_{\alpha_x} \\ e_{\omega_x} \end{pmatrix}^T P_2 \begin{pmatrix} e_{\alpha_x} \\ e_{\omega_x} \end{pmatrix}
\end{aligned}$$

one works out

$$\begin{aligned}
\dot{V}_o = &-(k_{o1}\gamma_1 - \gamma_2 k_{o2} \mathcal{S}_{\omega_z}) e_{v_x}^2 - \gamma_2 |\omega_z| e_{v_y}^2 - \left\| \begin{matrix} e_{\alpha_x} \\ e_{\omega_x} \end{matrix} \right\|_{Q_2}^2 + (\gamma_1 \omega_z - k_{o2} + k_{o1}\gamma_2 \mathcal{S}_{\omega_z}) e_{v_x} e_{v_y} \\
&- \left(\gamma_1 \frac{m_s}{m} h \omega_z - \gamma_2 \frac{b_x}{J_{x,s}} \mathcal{S}_{\omega_z} + p_{22} k_{o3} + p_{23} k_{o4} \right) e_{v_x} e_{\omega_x} + \left(\gamma_2 \frac{k_{x,e}}{J_{x,s}} \mathcal{S}_{\omega_z} - p_{21} k_{o3} - p_{22} k_{o4} \right) e_{v_x} e_{\alpha_x} \\
&- \frac{k_{x,e}}{J_{x,s}} e_{v_y} e_{\alpha_x} + \left(\gamma_2 \frac{m_s}{m} h |\omega_z| - \frac{b_x}{J_{x,s}} \right) e_{v_y} e_{\omega_x}
\end{aligned}$$

where $\dot{\mathcal{S}}_{\omega_z} = 2\delta_D(\omega_z)\dot{\omega}_z = 0$ under Assumption 1 ($|\omega_z| > 0$), with $\delta_D(\omega_z)$ the Dirac distribution, and

$$P_2 = P_2^T = \begin{pmatrix} p_{21} & p_{22} \\ p_{22} & p_{23} \end{pmatrix} > 0$$

has been determined as solution of the Lyapunov equation

$$P_2 A_2 + A_2^T P_2 = -Q_2, \qquad Q_2 = Q_2^T > 0, \qquad A_2 = \begin{pmatrix} 0 & 1 \\ -\frac{k_{x,e}}{J_{x,e}} & -\frac{b_x}{J_{x,e}} \end{pmatrix}$$

To simplify the expression of $\dot{V}_o$ we may choose

$$Q_2 = \begin{pmatrix} \lambda_1 & 0 \\ 0 & \lambda_2 \end{pmatrix} \tag{4.3}$$

$\lambda_1, \lambda_2 > 0$. The expression of $\dot{V}_o$ can be further simplified choosing the controller gains $k_{o1}, \cdots, k_{o4}$ such that

$$\begin{aligned}
&\gamma_1 k_{o1} - \gamma_2 k_{o2} \mathcal{S}_{\omega_z} = \frac{1}{2}\gamma_2 \omega_{z,\max} \\
&\gamma_1 \omega_z + \gamma_2 k_{o1} \mathcal{S}_{\omega_z} - k_{o2} = 0 \\
&\gamma_2 \frac{k_{x,e}}{J_{x,s}} \mathcal{S}_{\omega_z} - p_{21} k_{o3} - p_{22} k_{o4} = 0 \\
&\gamma_1 \frac{m_s}{m} h \omega_z - \gamma_2 \frac{b_x}{J_{x,s}} \mathcal{S}_{\omega_z} + p_{22} k_{o3} + p_{23} k_{o4} = 0
\end{aligned}$$

i.e.

$$\begin{pmatrix} k_{o1} \\ k_{o2} \end{pmatrix} = \frac{1}{\gamma_1 - \gamma_2^2} \begin{pmatrix} \frac{1}{2}\gamma_2 \omega_{z,\max} + \gamma_2 \gamma_1 |\omega_z| \\ \frac{1}{2}\gamma_2^2 \omega_{z,\max} \mathcal{S}_{\omega_z} + \gamma_1^2 \omega_z \end{pmatrix} \qquad \begin{pmatrix} k_{o3} \\ k_{o4} \end{pmatrix} = P_2^{-1} \begin{pmatrix} \gamma_2 \frac{k_{x,e}}{J_{x,s}} \mathcal{S}_{\omega_z} \\ -\gamma_1 \frac{m_s}{m} h \omega_z + \gamma_2 \frac{b_x}{J_{x,s}} \mathcal{S}_{\omega_z} \end{pmatrix} \tag{4.4}$$

so obtaining

$$\dot{V}_o \leq -\frac{1}{2}\gamma_2 \omega_{z,\max} e_{v_x}^2 - \gamma_2 \omega_{z,\max} e_{v_y}^2 - \lambda_1 e_{\alpha_x}^2 - \lambda_2 e_{\omega_x}^2 - \alpha_1 e_{v_y} e_{\alpha_x} + \alpha_2 e_{v_y} e_{\omega_x}$$

where it has been considered that $-|\omega_z| \leq -\omega_{z,\max}$ (Assumption 1), and

$$\alpha_1 = \frac{k_{x,e}}{J_{x,s}} > 0, \quad \alpha_2 = \gamma_2 \frac{m_s}{m} h |\omega_z| - \frac{b_x}{J_{x,s}}$$

The cross terms can be eliminated using the Young's inequality $\pm e_1 e_2 \leq e_1^2/\epsilon + \epsilon e_2^2$, for an $\epsilon > 1$, and with e_1, e_2 substituted by the error terms appearing in $\dot{V}_o$. Thanks to Assumption 1, one considers the following inequalities

$$\begin{aligned}
-\alpha_1 e_{v_y} e_{\alpha_x} &\leq \frac{\alpha_1}{\epsilon_1} e_{v_y}^2 + \alpha_1 \epsilon_1 e_{\alpha_x}^2 \\
\alpha_2 e_{v_y} e_{\omega_x} &\leq \frac{|\alpha_2|}{\epsilon_2} e_{v_y}^2 + |\alpha_2| \epsilon_2 e_{\omega_x}^2 \leq \frac{\alpha_{2,\max}}{\epsilon_2} e_{v_y}^2 + \alpha_{2,\max} \epsilon_2 e_{\omega_x}^2
\end{aligned}$$

where $\epsilon_j > 1$, $j = 1, 2$. Hence,

$$\dot{V}_o \leq -\frac{1}{2}\gamma_2 \omega_{z,\max} e_{v_x}^2 - \left(\gamma_2 \omega_{z,\max} - \frac{\alpha_1}{\epsilon_1} - \frac{\alpha_{2,\max}}{\epsilon_2}\right) e_{v_y}^2 - (\lambda_1 - \alpha_1 \epsilon_1) e_{\alpha_x}^2 - (\lambda_2 - \alpha_{2,\max} \epsilon_2) e_{\omega_x}^2.$$

Setting

$$\begin{aligned}\gamma_2 &= \frac{1}{\omega_{z,\max}}\left(2\lambda_o + \frac{\alpha_1}{\epsilon_1} + \frac{\alpha_{2,\max}}{\epsilon_2}\right)\\ \lambda_1 &= \lambda_o + \alpha_1\epsilon_1\\ \lambda_2 &= \lambda_o + \alpha_{2,\max}\epsilon_2\end{aligned} \tag{4.5}$$

$\lambda_o > 0$, one finally gets

$$\dot{V}_o \leq -\lambda_o(e_{v_x}^2 + e_{v_y}^2 + e_{\alpha_x}^2 + e_{\omega_x}^2) < 0. \tag{4.6}$$

Hence, the error system (4.2) has the origin exponentially stable, and the estimation errors tend exponentially to zero, with a time constant $\tau = 1/\lambda_o$. The second step in the controller design consists of the determination of control law. For, the following Lyapunov candidate is considered

$$V = V_s + V_o \tag{4.7}$$

with V_o as above, and

$$V_s = \frac{1}{2}z_{v_y}^2 + \frac{1}{2}z_{\omega_z}^2, \quad z_{v_y} = \hat{v}_y - v_{y,r},\ z_{\omega_z} = \omega_z - \omega_{z,r} \tag{4.8}$$

$z = \left(z_{v_y}, z_{\omega_z}\right)^T$ Using (2.3), (3.1) and reminding that:

$$a_x = \frac{\mu_x}{m}(F_{x,f} + F_{x,r}), \qquad a_y = \frac{\mu_y}{m}(F_{y,f} + F_{y,r})$$

one gets:

$$\begin{aligned}\dot{V}_s = z_{v_y}\Bigg[&- \hat{v}_x\omega_z + \frac{\mu_y}{m_e}(F_{y,f,d} + F_{y,r}) + \frac{\mu_y}{m_e}\Delta_c - \frac{k_{x,e}}{J_{x,s}}\hat{\alpha}_x - \frac{b_x}{J_{x,s}}\hat{\omega}_x + (k_{o2} - \omega_z)e_{v_x} - \dot{v}_{y,r}\Bigg]\\ &+ z_{\omega_z}\left[\frac{\mu_y}{J_z}(F_{y,f,d}l_f - F_{y,r}l_r) + \frac{\mu_y l_f}{J_z}\Delta_c + \frac{1}{J_z}M_z - \dot{\omega}_{z,r}\right].\end{aligned} \tag{4.9}$$

Considering that v_y, α_x, ω_x are not measured, for $\mu_y > 0$ the following controller can be designed

$$\begin{aligned}\Delta_c = &-k_{s1}\frac{m_e}{\mu_y}(\hat{v}_y - v_{y,r}) + \frac{m_e}{\mu_y}\dot{v}_{y,r} + \frac{m_e}{\mu_y}\hat{v}_x\omega_z - \hat{F}_{y,f,d} - \hat{F}_{y,r} + \frac{m_e}{\mu_y}\frac{k_{x,e}}{J_{x,s}}\hat{\alpha}_x + \frac{m_e}{\mu_y}\frac{b_x}{J_{x,s}}\hat{\omega}_x\\ &- \frac{m_e}{\mu_y}(k_{o2} - \omega_z)(v_x - \hat{v}_x)\\ M_z = &-k_{s2}J_z(\omega_z - \omega_{z,r}) + J_z\dot{\omega}_{z,r} - \mu_y(\hat{F}_{y,f,d}l_f - \hat{F}_{y,r}l_r) - \mu_y l_f\Delta_c\end{aligned} \tag{4.10}$$

where $k_{s1}, k_{s2} > 0$, and

$$\begin{aligned}\hat{F}_{y,f,d} &= D_{y,f}\sin\left(C_{y,f}\arctan B_{y,f}\hat{\alpha}_{f,d}\right)\\ \hat{F}_{y,r} &= D_{y,r}\sin\left(C_{y,r}\arctan B_{y,r}\hat{\alpha}_r\right)\end{aligned} \tag{4.11}$$

with $\hat{\alpha}_{f,d} = \delta_d - (\hat{v}_y + l_f\omega_z)/v_x$, $\hat{\alpha}_r = -(\hat{v}_y - l_r\omega_z)/v_x$. It is worth reminding that we do not consider a specific tire model in this work. Hence, (4.11) can be changed with any particular formula for the tire characteristic where the slip angles $\alpha_{f,d}, \alpha_r$ are substituted by the estimates $\hat{\alpha}_{f,d}, \hat{\alpha}_r$. With the control (4.10), equation (4.9) becomes

$$\dot{V}_s = -k_{s1}z_{v_y}^2 - k_{s2}z_{\omega_z}^2 + \phi^T \Delta z \tag{4.12}$$

where, since $v_y = e_{v_y} + \hat{v}_y$, the functions $\phi_f(\delta_d, e_{v_y}, \hat{v}_y, \omega_z) = F_{y,f,d} - \hat{F}_{y,f,d}$, $\phi_r(e_{v_y}, \hat{v}_y, \omega_z) = F_{y,r} - \hat{F}_{y,r}$, $\phi = \left(\phi_f, \phi_r\right)^T$ go to zero exponentially because e_{v_y} tends to zero exponentially, and where

$$\Delta = \begin{pmatrix} \frac{\mu_y}{m_e} & \frac{\mu_y l_f}{J_z} \\ \frac{\mu_y}{m_e} & -\frac{\mu_y l_r}{J_z} \end{pmatrix}$$

Therefore, considering (4.6) and (4.12), the derivative of (4.7) is such that

$$\dot{V} \leq -\lambda_{\mathrm{m}}\|x\|^2 + \Delta\,\|\phi\|\|x\|, \quad x = \begin{pmatrix} e \\ z \end{pmatrix} \tag{4.13}$$

$\lambda_{\mathrm{m}} = \min\{\lambda_o, k_{s1}k_{s2}\} > 0$.

Notice that ϕ is bounded, say $\|\phi(t)\| \leq c$, $\forall t \geq t_0$. Hence, one has that $\dot{V} \leq 0$ when $\|x\| \geq c\Delta/\lambda_{\mathrm{m}}$, namely $x(t)$ is bounded [61]. To prove the square integrability of $x(t)$, let us integrate both sides of (4.13)

$$\begin{aligned} V|_{t,x} - V|_{t_0,x_0} &\leq -\lambda_{\mathrm{m}} \int_{t_0}^{t} \|x(\tau)\|^2 d\tau + \Delta \int_{t_0}^{t} \|\phi(\tau)\|\|x(\tau)\| d\tau \\ &\leq -\lambda_{\mathrm{m}} \int_{t_0}^{t} \|x(\tau)\|^2 d\tau + \Delta \left[\int_{t_0}^{t} \|\phi(\tau)\|^2 d\tau\right]^{1/2} \left[\int_{t_0}^{t} \|x(\tau)\|^2 d\tau\right]^{1/2} \end{aligned}$$

where the Schwarz inequality [62] has been used and $x_0 = x(t_0)$. Considering the limit as t tends to infinity and denoting with $\|\cdot\|_2$ the $\mathcal{L}_2$–norm [61], one has

$$V|_{\infty,x} - V|_{t_0,x_0} \leq -\lambda_{\mathrm{m}}\|x\|_2^2 + \Delta\|\phi\|_2\|x\|_2. \tag{4.14}$$

Moreover, since $V|_{\infty,x} \geq 0$,

$$\lambda_{\mathrm{m}}\|x\|_2^2 - \Delta\|\phi\|_2\|x\|_2 \leq V|_{t_0,x_0} - V|_{\infty,x} \leq V|_{t_0,x_0}. \tag{4.15}$$

It has been noted that ϕ goes to zero exponentially, so that $\phi \in \mathcal{L}_2$. Observe also that $V \leq \alpha(\|x\|)$, with α a $\mathcal{K}_\infty$ function [61]. These facts and (4.15) imply that $x \in \mathcal{L}_2$, since

$$\|x\|_2 \leq \frac{1}{\sqrt{\lambda_{\mathrm{m}}}} \left[V|_{t_0,x_0} + \frac{\Delta^2}{4\lambda_{\mathrm{m}}}\|\phi\|_2^2\right]^{1/2} + \frac{\Delta}{2\lambda_{\mathrm{m}}}\|\phi\|_2.$$

The application of Barbalat's theorem allows concluding that $\lim_{t\to\infty} x = 0$, namely $\lim_{t\to\infty} z = 0$, $\lim_{t\to\infty} e = 0$, i.e. the controller (4.10), (3.1) fulfills the control objectives. We can conclude with the following statement.

Theorem 2 *Let us consider some bounded references $v_{y,r}, \omega_{z,r}$ with bounded derivatives $\dot{v}_{y,r}, \dot{\omega}_{z,r}$ Under Assumption 1, the controller* (4.10), (4.1), *with the gains $k_{s1}, k_{s2} > 0$ and* (4.4), (4.5), *ensures the global exponential convergence to zero of the estimation errors and of the tracking errors* (4.8), *with a time constant $1/\lambda_m$, for a $\lambda_m > 0$ fixed by the designer.* ◇

4.2 A First Test Maneuver: The Double Line Change

The DLC maneuver is a test procedure for a severe lane–change maneuver and object avoidance simulations, see Figure 4.1, and is described in the standard ISO/TR 3888

1. the vehicle enters into the first lane–section with a constant initial longitudinal velocity, and continues with a released throttle valve;
2. the steering wheel angle $\delta_{d,sw}$ is selected such that the vehicle completes the DLC maneuver without hitting the course boundaries;
3. braking action is not allowed;

In this test a constant tire–road friction coefficient, equal to $\mu_y = 0.9$, has been considered, with superimposed a random noise for a more realistic simulation (see Figure 4.2.b). A noise on the measured variables v_x (see Figure 4.4.b), ω_z (see Figure 4.3.b), a_x, a_y (see Figure 4.7), and $\delta_{d,sw}$ (see Figure 4.2.a) has been considered for the same reason.

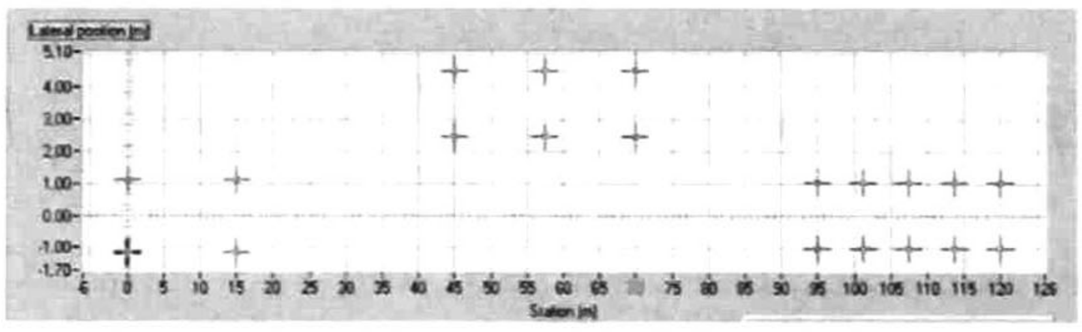

Figure 4.1: DLC maneuver

In Figure 4.2.a the imposed steering wheel angle $\delta_{d,sw}$ ensuring the path tracking is shown. The ratio between $\delta_{d,sw}$ and δ_d is $r_{sw} = 16.01$. By applying $\delta_d = \delta_{d,sw}/r_{sw}$ to the reference system (3.9), one generates the references $v_{y,r}, w_{z,r}$. A SUV vehicle with high center of gravity is considered, to amplify the effects of the roll dynamics. With the proposed controller (4.10),

(4.1), the references $v_{y,r}, w_{z,r}$ so generated are well tracked, as well as the desired DLC path. It is important to note that the tracking stability can not be ensured with the same controller that does not take into account the roll dynamics. In fact, if for the same maneuver one sets $\alpha_x \equiv 0$, $\omega_x \equiv 0$ in the controller (4.10), (4.1), namely if the roll dynamics are not taken into account in the controller design, the result is that the references are not tracked, see Figure 4.8.

The slip angle $\beta = v_y/v_x$ of the vehicle's center of gravity, the longitudinal velocity v_x, the lateral velocity v_y, and the roll angle α_x and rate ω_x have been measured from the simulated vehicle in order to compare them with the estimations $\hat{\beta} = \hat{v}_y/\hat{v}_x$, $\hat{v}_x$, $\hat{v}_y$, $\hat{\alpha}_x$, $\hat{\omega}_x$ obtained with the dynamic controller (4.10), (4.1). Figures 4.4, 4.3.a, and 4.5 show that these estimations follow very closely the vehicle's variables. Finally, in Figure 4.6 the AFS and RTV inputs are shown.

Notice the good tracking of both the estimated variables and the tracked references. Moreover, this dynamic controller shows good performances with respect to system parameter variations. In particular, it is robust with respect to variations of the tire–road friction coefficient, since the performance does not depend on this crucial parameter. The dynamic controller appears also to be robust with respect to the measurement noise.

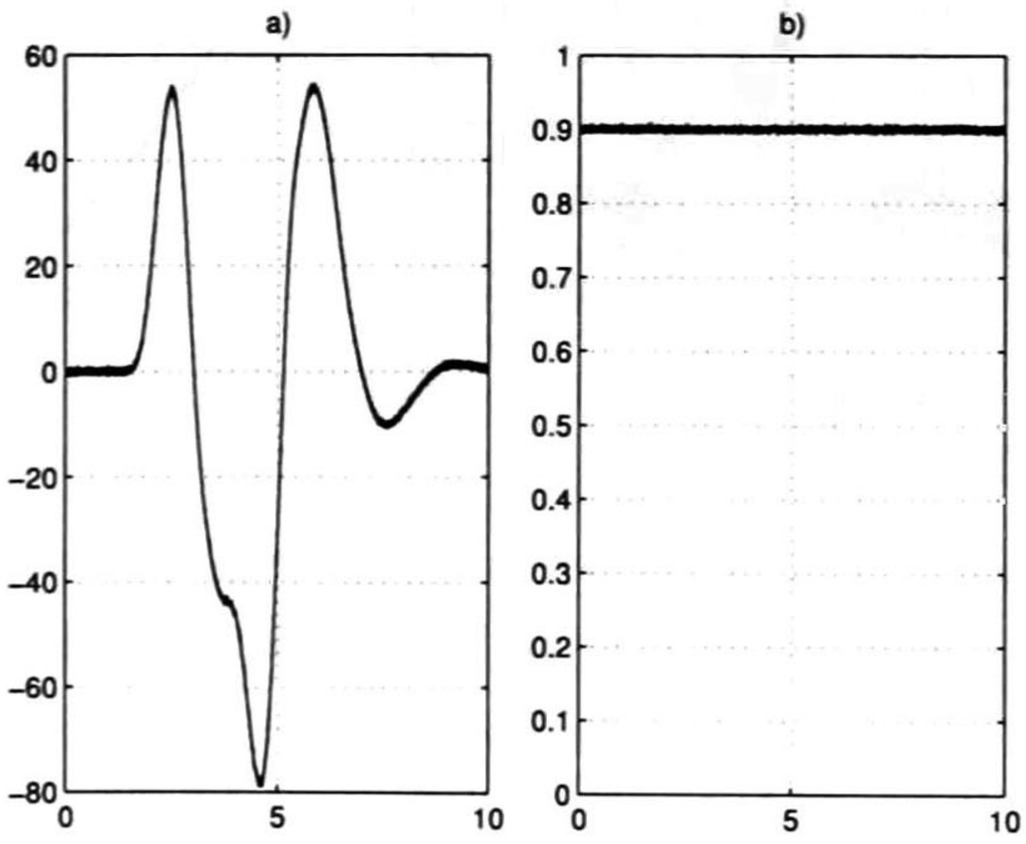

Figure 4.2: DLC maneuver: a) Steering wheel angle $\delta_{d,sw}$ applied during the DLC maneuver [deg vs s]; b) Tire–road friction coefficient μ_y [dimensionless vs s].

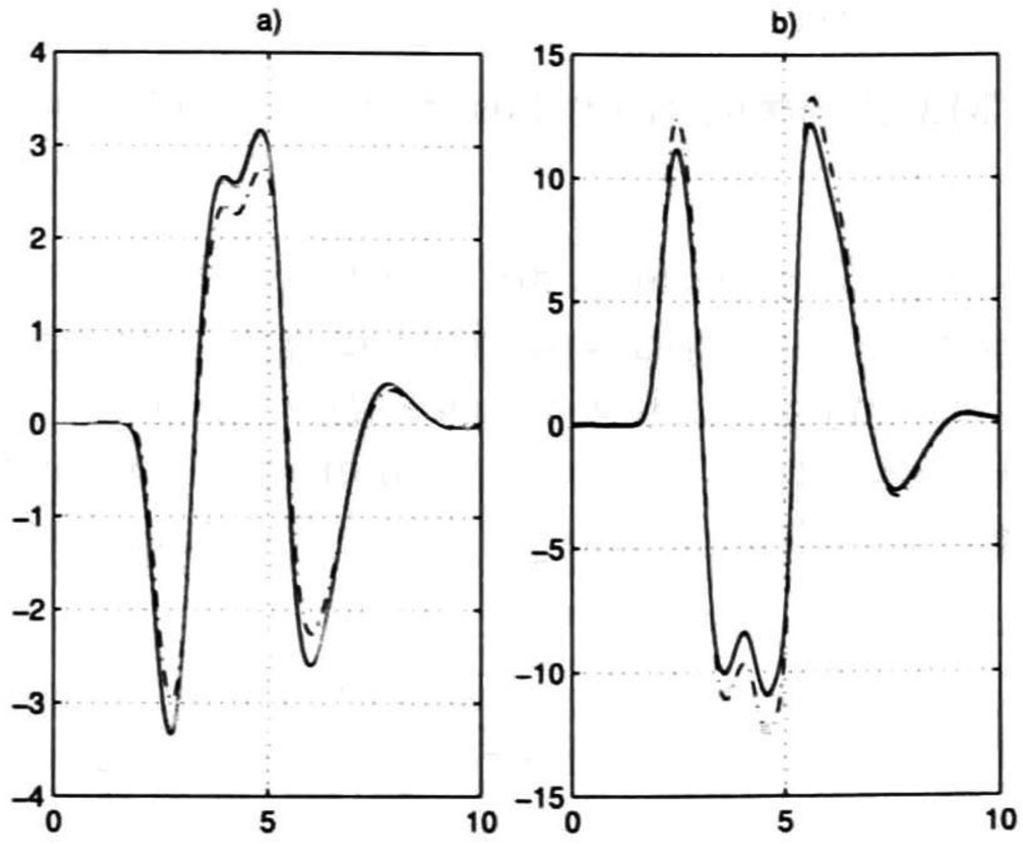

Figure 4.3: DLC maneuver: a) Lateral velocity v_y (solid), estimation $\hat{v}_y$ (gray), and reference $v_{y,r}$ (dotted) [km/h vs s]; b) Yaw rate ω_z (solid), and reference $\omega_{z,r}$ (dotted) [deg/s vs s].

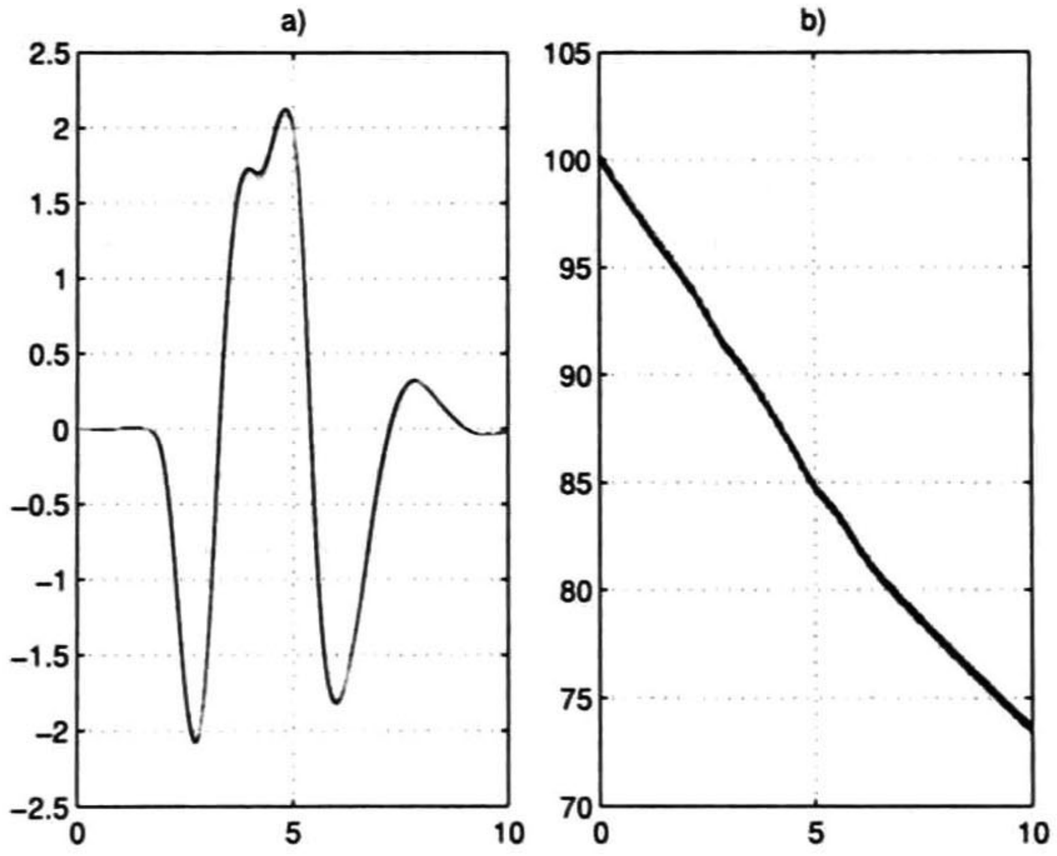

Figure 4.4: DLC maneuver: a) Slip angle $\beta = v_y/v_x$ of the vehicle's center of gravity (solid), and estimation $\hat{\beta} = \hat{v}_y/\hat{v}_x$ (gray) [deg vs s]; b) Longitudinal velocity v_x (solid), and estimation $\hat{v}_x$ (gray) [km/h vs s.

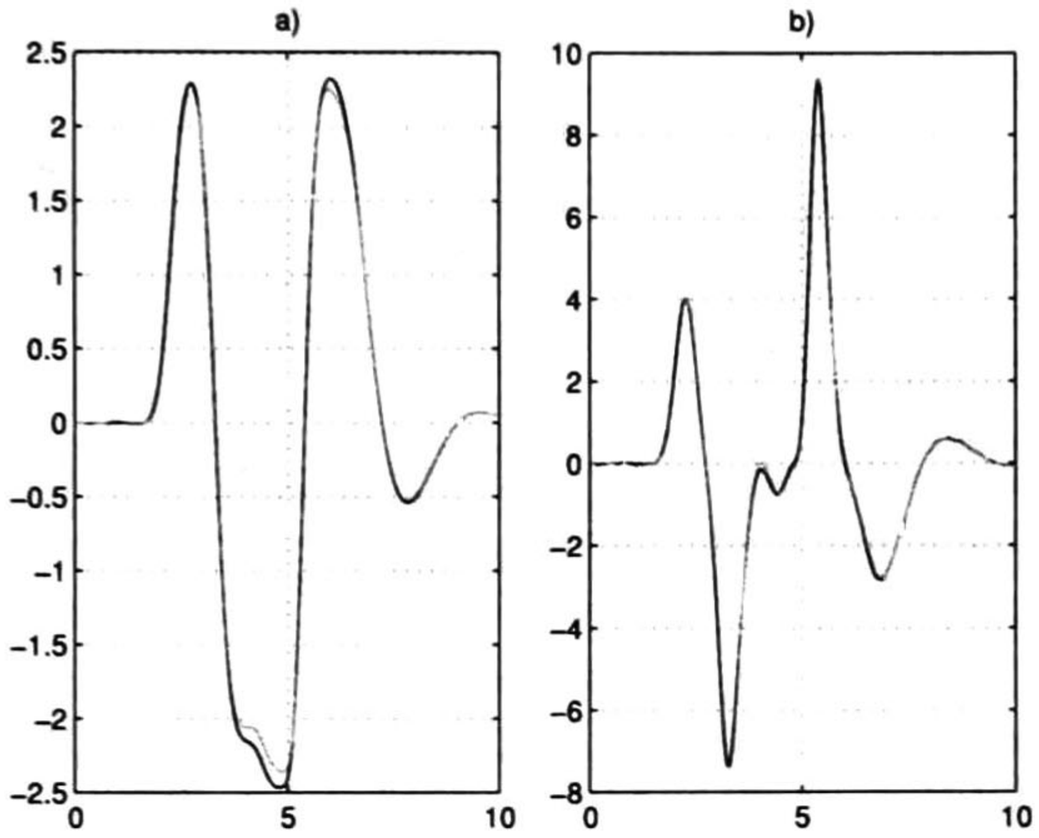

Figure 4.5: DLC maneuver: a) Roll position α_x (solid), and estimation $\hat{\alpha}_x$ (gray) [deg vs s]; b) Roll rate ω_x (solid), and estimation $\hat{\omega}_x$ (gray) [deg/s vs s].

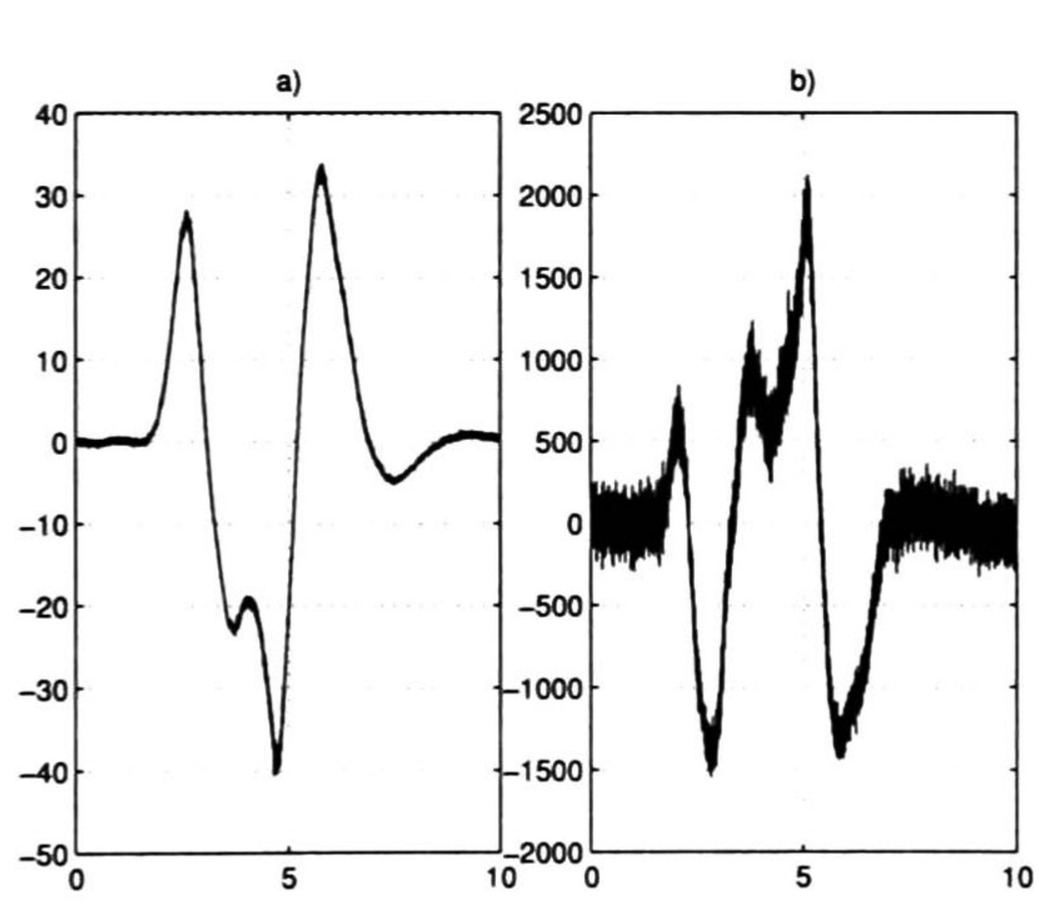

Figure 4.6: DLC maneuver: a) Active front steering δ_c [deg vs s]; b) Rear torque vectoring M_z [Nm vs s].

4.3 A Second Test Maneuver: The ATI 90–90

The ATI 90–90 maneuver is described in the standard ISO/TS 16949. The driver performs a step steer of $-90°$ at $t = 2$ s, and a step steer of $90°$ at $t = 2.6$ s, $\delta_d = 0$ at $t = 6$ s. This

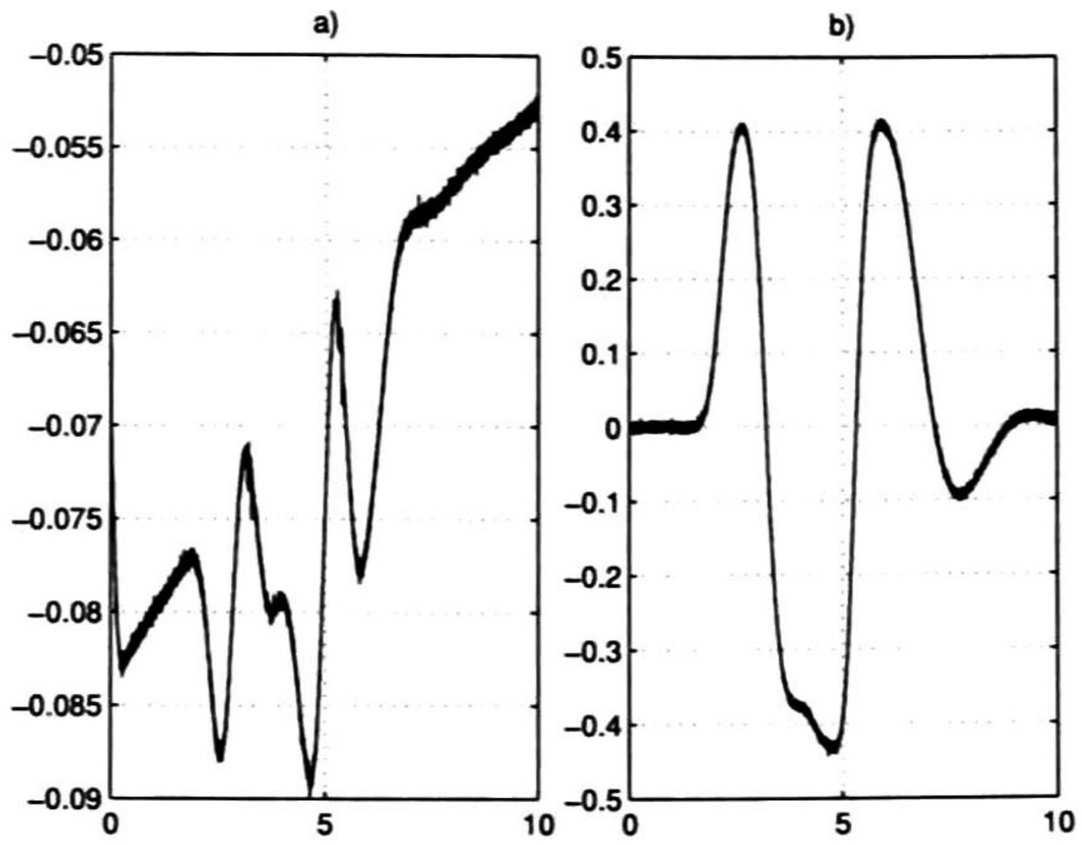

Figure 4.7: DLC maneuver: a) Measured longitudinal acceleration a_x [g's vs s]; b) Measured lateral acceleration a_y [g's vs s].

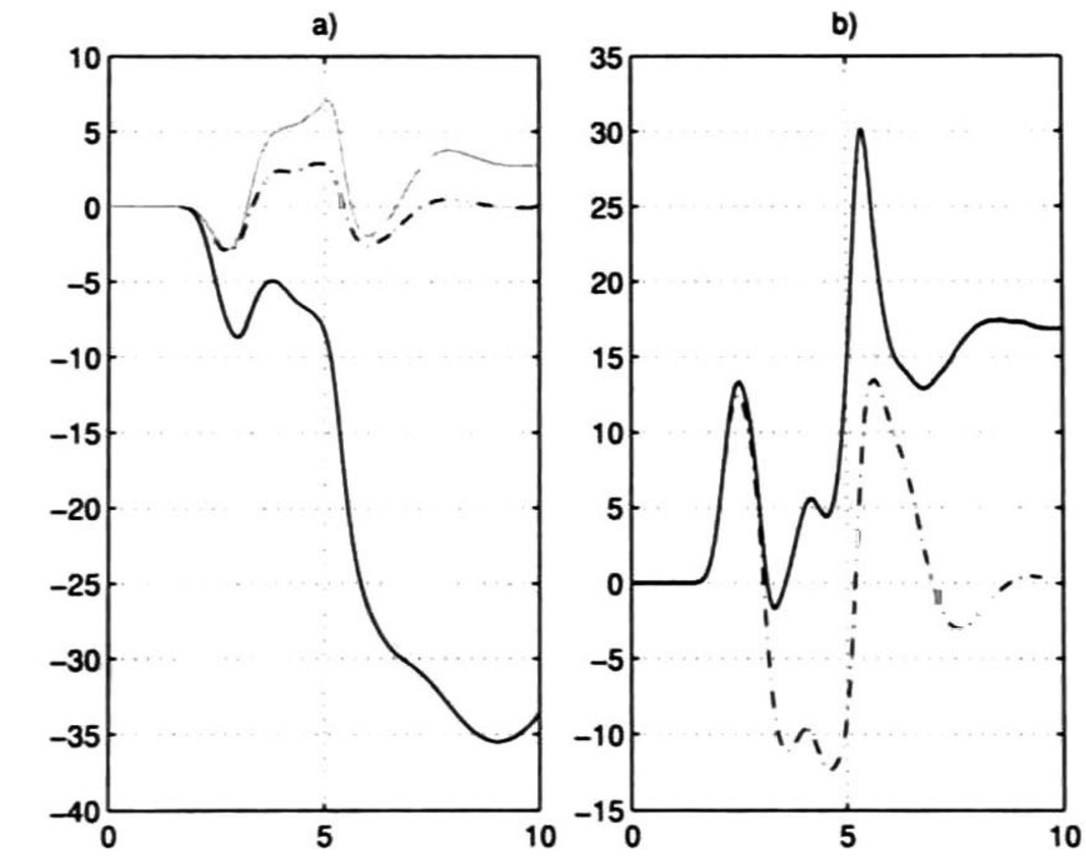

Figure 4.8: DLC maneuver: controller (4.10), (3.1) with $\alpha_x \equiv 0$, $\omega_x \equiv 0$; a) Lateral velocity v_y (solid), estimation $\hat{v}_y$ (gray), and reference $v_{y,r}$ (dotted) [km/h vs s]; b) Yaw rate ω_z (solid), and reference $\omega_{z,r}$ (dotted) [deg/s vs s].

is shown in Figure 4.9.a. A further source of difficulty is taken into account, considering an

abrupt change of the tire–road friction coefficient (see Figure 4.9.b)

$$\mu_y = \begin{cases} \mu_d & \text{for } t \in [0, 3.5) \text{ s} \\ \mu_w & \text{for } t \geq 3.5 \text{ s} \end{cases}$$

where $\mu_d = 0.9$, $\mu_w = 0.5$ correspond to dry, wet surfaces. A superimposed random noise is also considered, see Figure 4.2.b.

The obtained results are shown in Figures 4.10–4.14. The controller performance are good either in term of reference tracking (Figure 4.10), or estimation (Figures 4.10.a, 4.11, 4.12), in the presence of parameter variations and noise, in particular of the tire–road friction coefficient μ_y (Figure 4.9.b), and measurement noise on v_x (Figure 4.11.b), ω_z (Figure 4.10.b), a_x, a_y (Figure 4.14) and $\delta_{d,sw}$ (Figure 4.9.a). Finally, the AFS and RTV control inputs are shown in Figure 4.13.

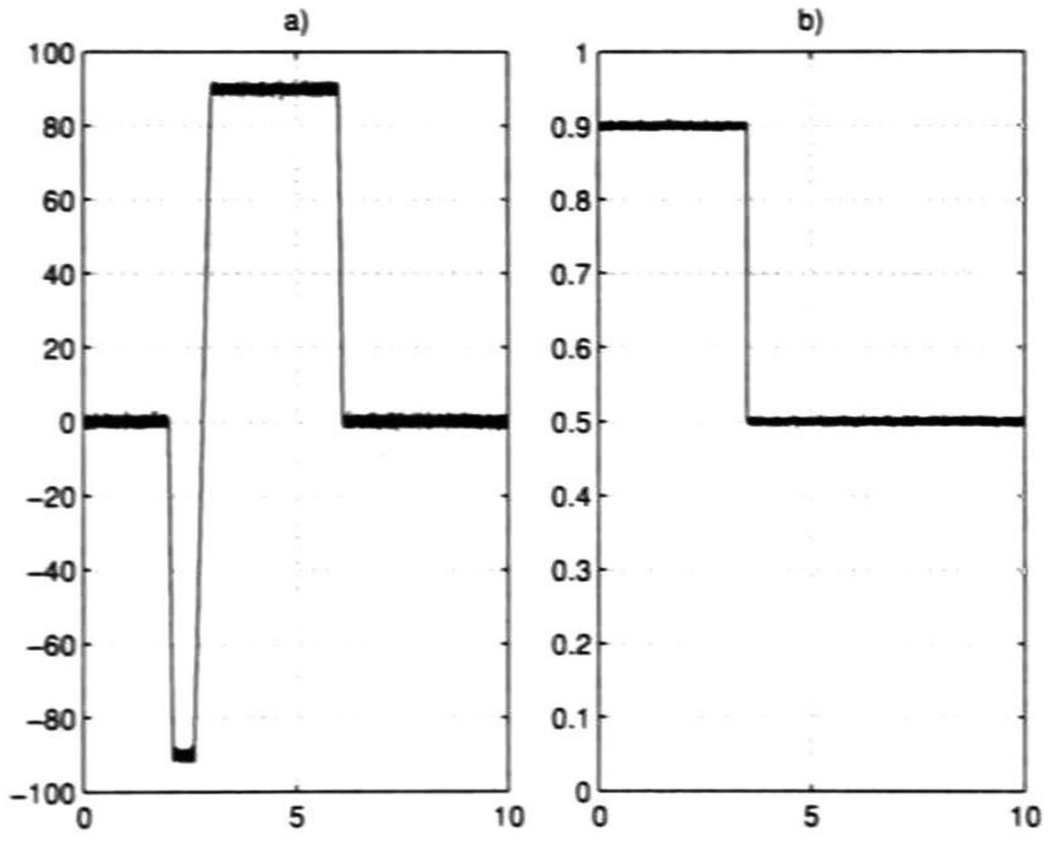

Figure 4.9: ATI 90–90 maneuver: a) Steering wheel angle $\delta_{d,sw}$ [deg vs s]; b) Tire–road friction coefficient μ_y [dimensionless vs s].

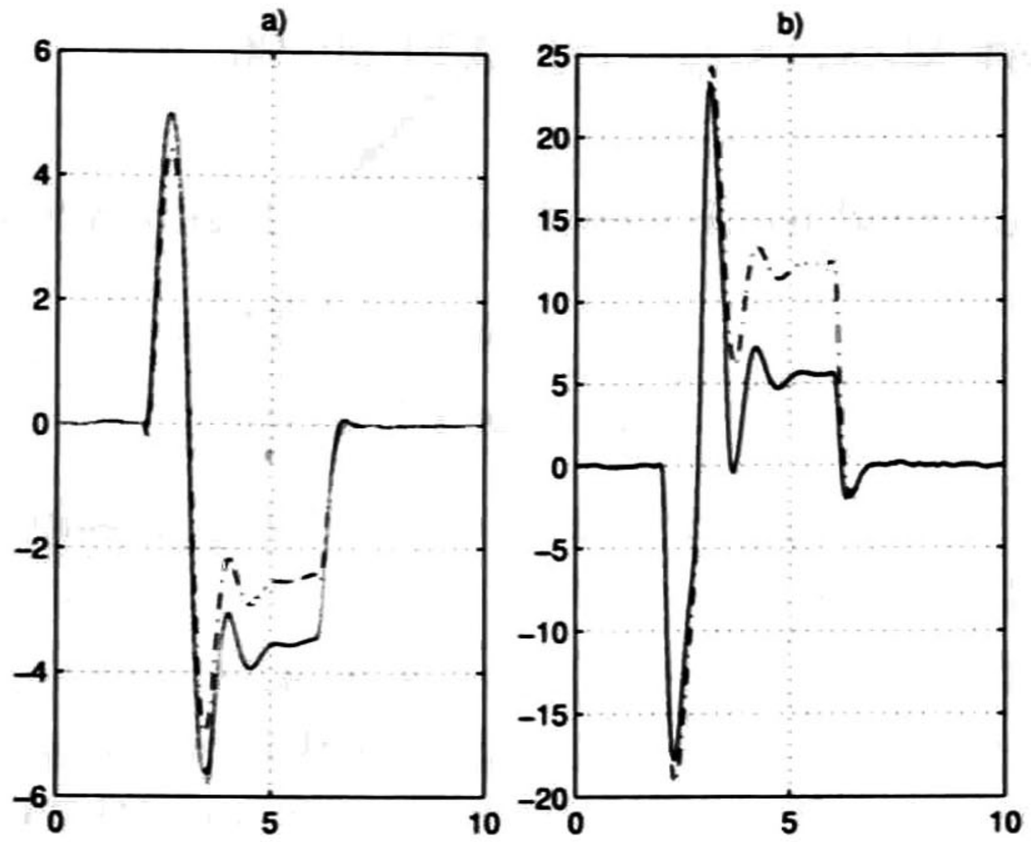

Figure 4.10: ATI 90–90 maneuver: a) Lateral velocity v_y (solid), estimation $\hat{v}_y$ (gray), and reference $v_{y,r}$ (dotted) [km/h vs s]; b) Yaw rate ω_z (solid), and reference $\omega_{z,r}$ (dotted) [deg/s vs s].

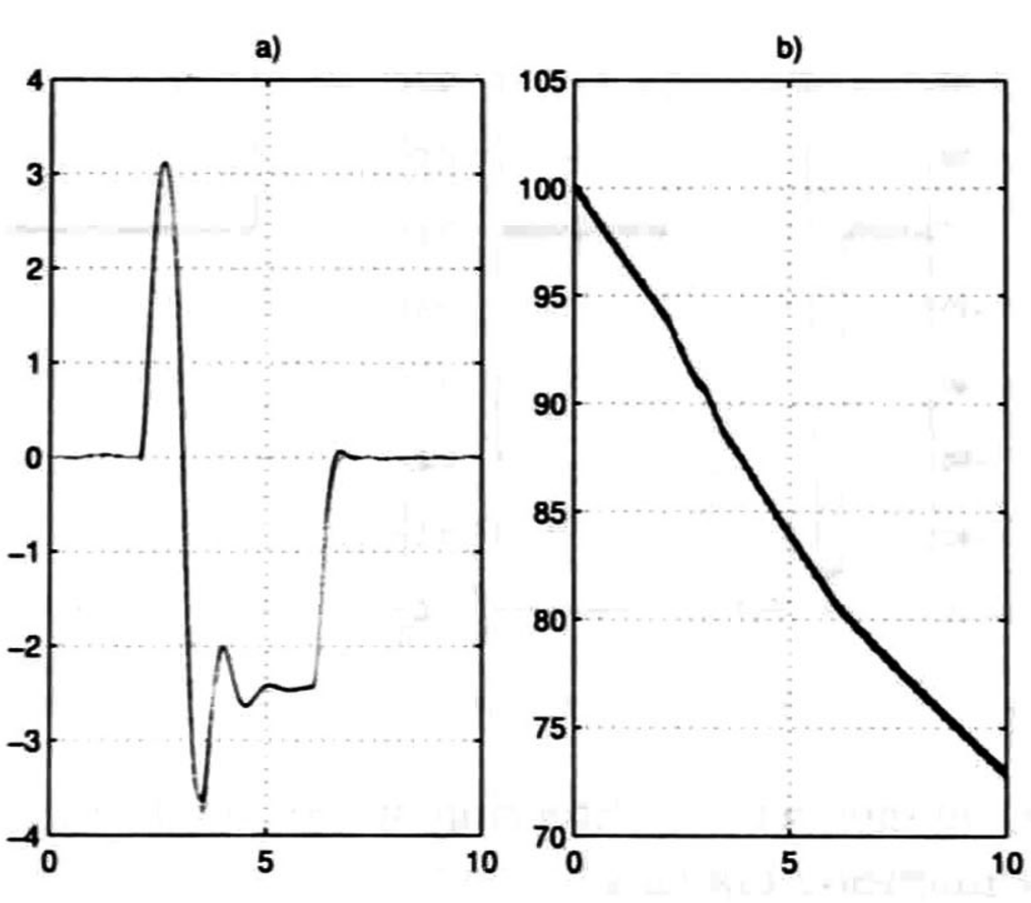

Figure 4.11: ATI 90–90 maneuver: a) Slip angle $\beta = v_y/v_x$ of the vehicle's center of gravity (solid), and estimation $\hat{\beta} = \hat{v}_y/\hat{v}_x$ (gray) [deg vs s]; b) Longitudinal velocity v_x (solid), and estimation $\hat{v}_x$ (gray) [km/h vs s].

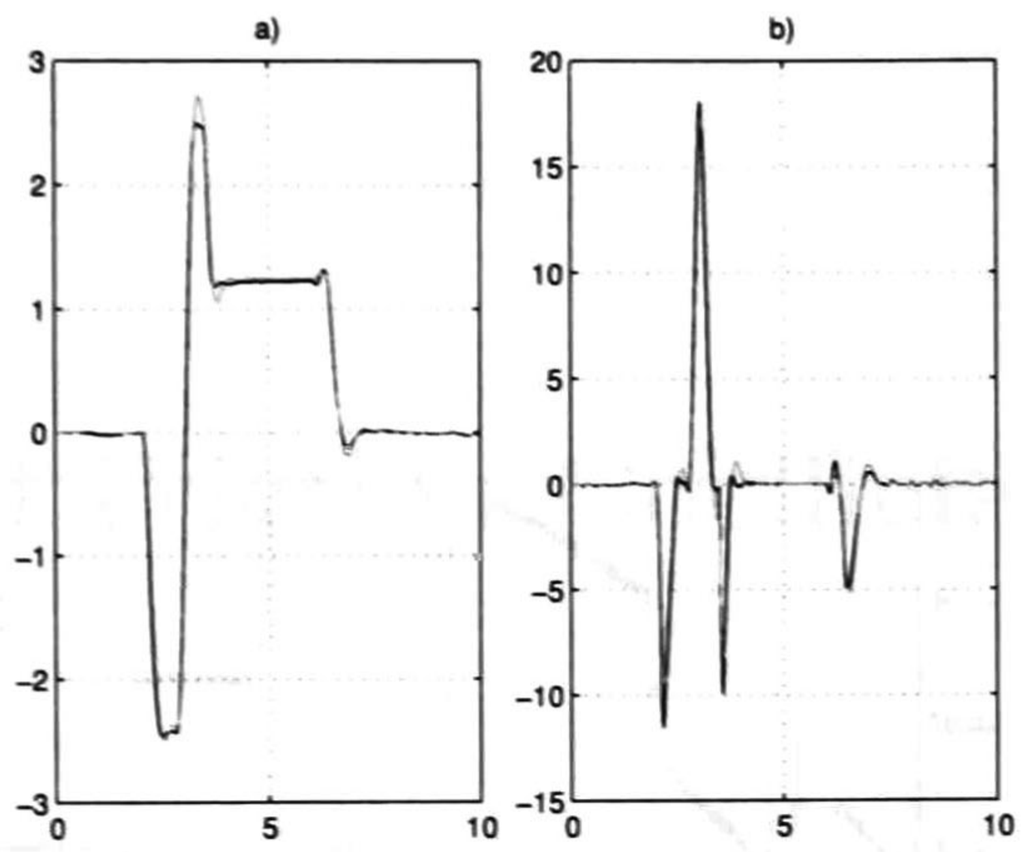

Figure 4.12: ATI 90–90 maneuver: a) Roll position α_x (solid), and estimation $\hat{\alpha}_x$ (gray) [deg vs s]; b) Roll rate ω_x (solid), and estimation $\hat{\omega}_x$ (gray) [deg/s vs s].

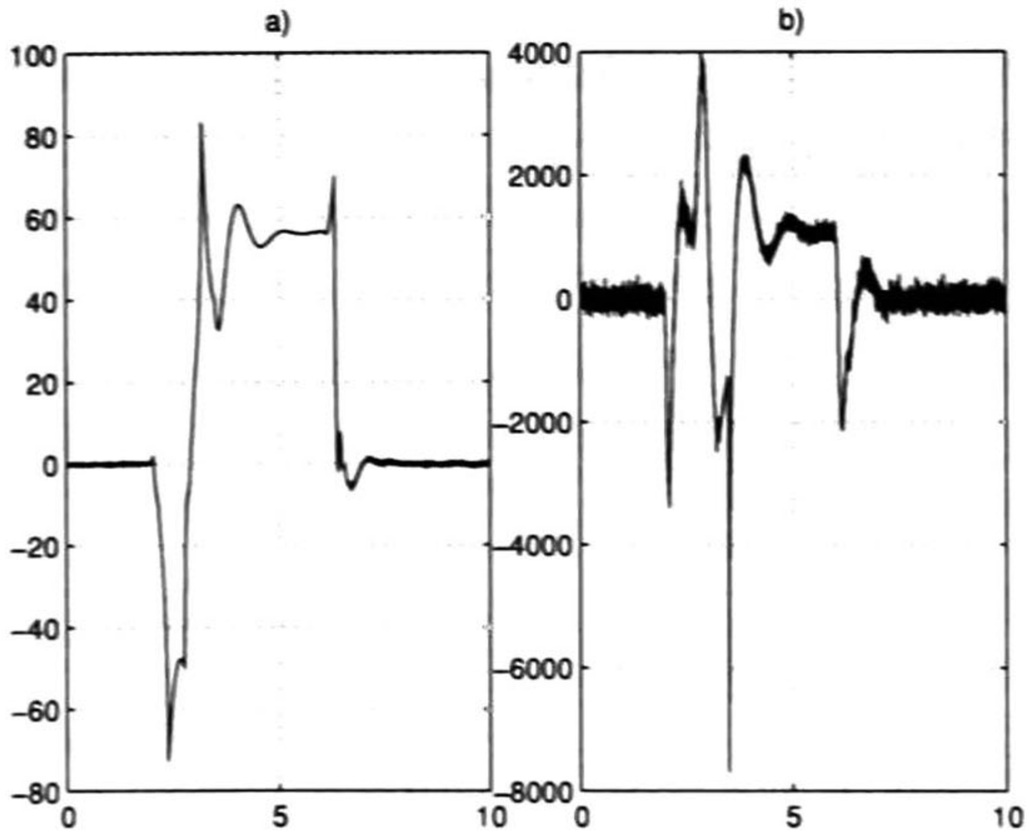

Figure 4.13: ATI 90–90 maneuver: a) Active front steering δ_c (solid) [deg vs s]; b) Rear torque vectoring M_z (solid) [Nm vs s].

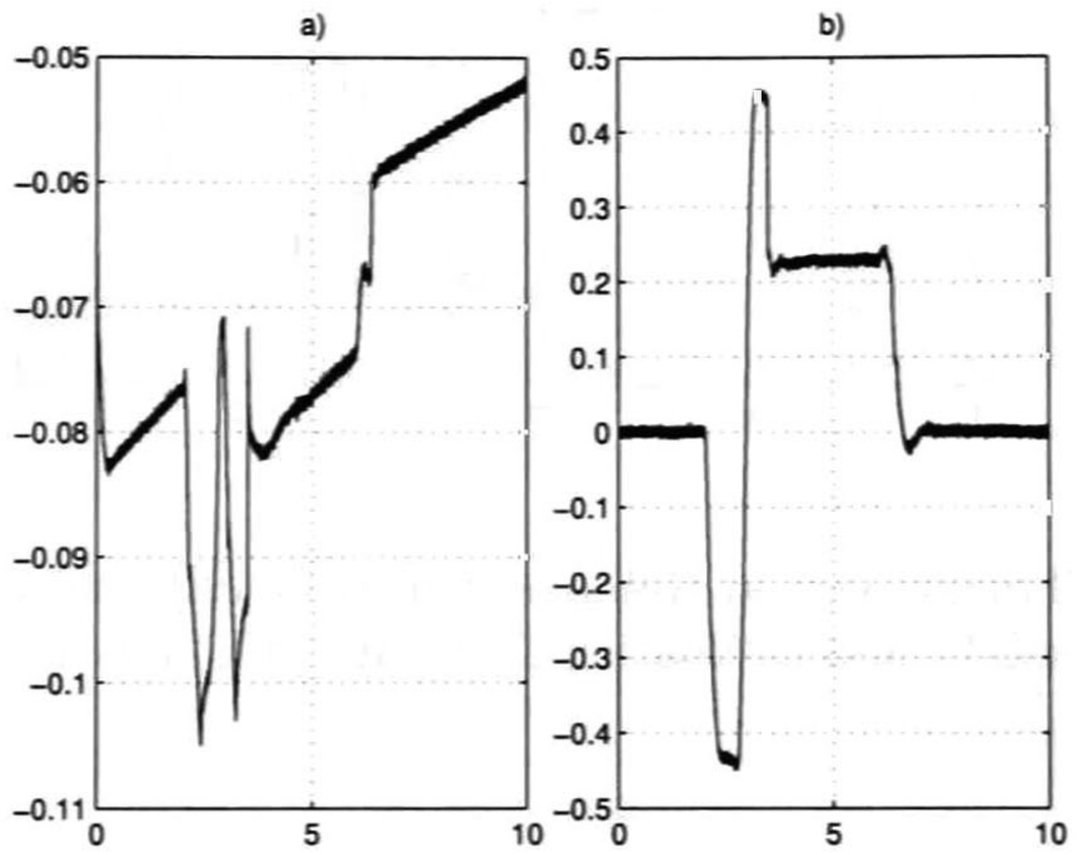

Figure 4.14: ATI 90–90 maneuver: a) Measured longitudinal acceleration a_x [g's vs s]; b) Measured lateral acceleration a_y [g's vs s].

Chapter 5

Tyre Road Friction Coefficient Estimation

In this chapter a tyre road friction coefficient estimation technique is presented. This approach is based on tyre carcass deflection. A curve fitting method is applied to estimate tyre lateral force and tyre self aligning moment. Performances are tested using CarSim.

5.1 Introduction

Estimation of tyre forces and friction potential could improve the performance of the active safety systems that have rapidly become common equipment in all vehicle categories. In practice, almost all the forces and moments acting on a vehicle are generated by the tyres. In addition, tyre characteristics dominate the vehicle response. These are naturally reasons why many involved in developing active safety systems are interested in tyre sensors.

Tyre sensors can be used for various purposes and a number of different technologies are being studied. To clarify this, tyre sensors can be divided into groups depending on function and technology. The different functions for the tyre sensors could be:

- estimation of friction potential;
- estimation of tyre forces (used friction);
- estimation of wheel speed, slip ratio and slip angle;
- tyre pressure monitoring;
- recognition of tyre wearing, imbalance etc., and
- recognition of worn suspension components (mostly heavy vehicles).

Even though intensive research is being conducted in some of these areas, only tyre pressure monitoring systems are available on the market. If tyre forces and friction potential are the main interest, the following technologies could come into question:

- measuring forces and moments from suspension parts
- measuring deflection of wheel
- measuring tyre deflections with sensor in suspension
- sensor in tyre

It is possible to measure tyre forces and moments from suspension parts. Furthermore, the relation of lateral force and aligning moment can be used to estimate friction potential and slip angle. However, some lateral force is needed for estimation.

As well as the suspension parts, the rim can be used for force and moment estimation. The important difference is that the wireless data transmission is needed from the rotating rim and this makes the setup more expensive and complicated. It is also questionable whether it can produce any information in addition to that gained from a measurement setup in the suspension. A tyre carcass is deflected under vertical, lateral and longitudinal forces; there are several approaches to measuring such deflections. The Continental Side Wall Torsion (SWT) sensor seemed really promising when it was first presented. However, due to the fact that has not appeared in production, it is possible that, even if the tyre forces could be accurately measured, the ABS/ESP system would not be of sufficient benefit to justify the costs of such system.

The type of tyre sensor that measures tyre tread deformation is probably the most interesting. Darmstadt Technical University has studied this area carefully since 1988. Atyre tread deformation sensor can yield information on the coefficient of friction, on tyre forces (X, Y, Z), the risk of hydroplaning, tyre temperature and tyre pressure.

Bridgestone has been developing both acceleration and strain tyre sensors. They call their concept 'Contact area information sensing' (CAIS). The strain sensor is used to calculate the lateral force, wheel load, camber angle and slip angle. The acceleration sensor is for road condition characterisation. The most interesting part, the friction estimation algorithm, is based on the phenomenon of the movement of the tread block being larger on a low friction surface. Thus, the strain monitoring of the tyre might be key to the friction potential estimation.

The APOLLO project (2002/2005) developed the "3 in 1" intelligent tyre. This consists of three different types of sensors in the same tyre to make the comparison of sensors as effective as possible.

The acceleration sensor and strain sensor showed potential, but the durability problems made these approaches less attractive. Meanwhile, an optical sensor that can measure carcass deflections was simple and practical and indicated potential for tyre force estimation. If the optical sensor could measure the aligning moment of the tyre as well, it would provide an opportunity for friction potential estimation. Another possibility for friction potential estimation is to detect influence of stress distribution along the contact patch from measured carcass deflections. This would offer friction potential estimation from free rolling tyre. In addition, aquaplaning detection and tyre pressure monitoring are obvious and realistic functions for optical tyre sensors.

Recent statistics show that a large number of traffic accidents occur due to a loss of control on vehicle by the driver. This is mainly due to a loss of friction between tyre and road. Many of these accidents could be avoided by introducing an estimation of loss of tire/road friction. Friction which is a parameter of tire/road interaction, mainly depends on the state of the road (dry, wet, snow, ice) and is closely related to the efforts at the tyre level.

5.2 Four Wheels Vehicle Motion

To continue with the analysis of the problem, a new approach is necessary: the bicycle mathematic model must be extended to a four wheels mathematic model.

The dynamics of a ground vehicle can be described by the so–called Four Wheel Vehicle Motion model (FWVM)[55][56][66]

$$\begin{aligned} m(\dot{v}_x - v_y\omega_z) &= ma_x - m_s h\omega_z\dot{\alpha}_x \\ m(\dot{v}_y + v_x\omega_z) &= ma_y + m_s h\ddot{\alpha}_x \\ J_z\dot{\omega}_z &= \mu_y(F_{y,f}l_f - F_{y,r}l_r) + J_{zx}\ddot{\alpha}_x \end{aligned} \tag{5.1}$$

where m, J_z are the total vehicle mass and inertia with respect to the perpendicular axis, l_f, l_r are the distances from the vehicle center of gravity ($C.G.$) to the front and rear tires, a_x, a_y are the longitudinal and lateral accelerations, v_x, v_y are the longitudinal and lateral velocities of the $C.G.$, ω_z is the yaw rate, α_x is the roll angle, m_s is the so–called sprung mass, h is the distance between the center of gravity and the roll axis, and J_{xz} is the inertia product with respect to the longitudinal and yaw axes with δ the steering wheel angle(see Figure 5.1).

In (5.1), the vehicle roll acceleration can be expressed as follows[56][57][58]

$$\begin{aligned} J_x\ddot{\alpha}_x = &-b_x\dot{\alpha}_x - k_x\alpha_x + m_s gh\sin\alpha_x \\ &+ m_s h(\dot{v}_y + \omega_z v_x)\cos\alpha_x + J_{xz}\dot{\omega}_z \end{aligned} \tag{5.2}$$

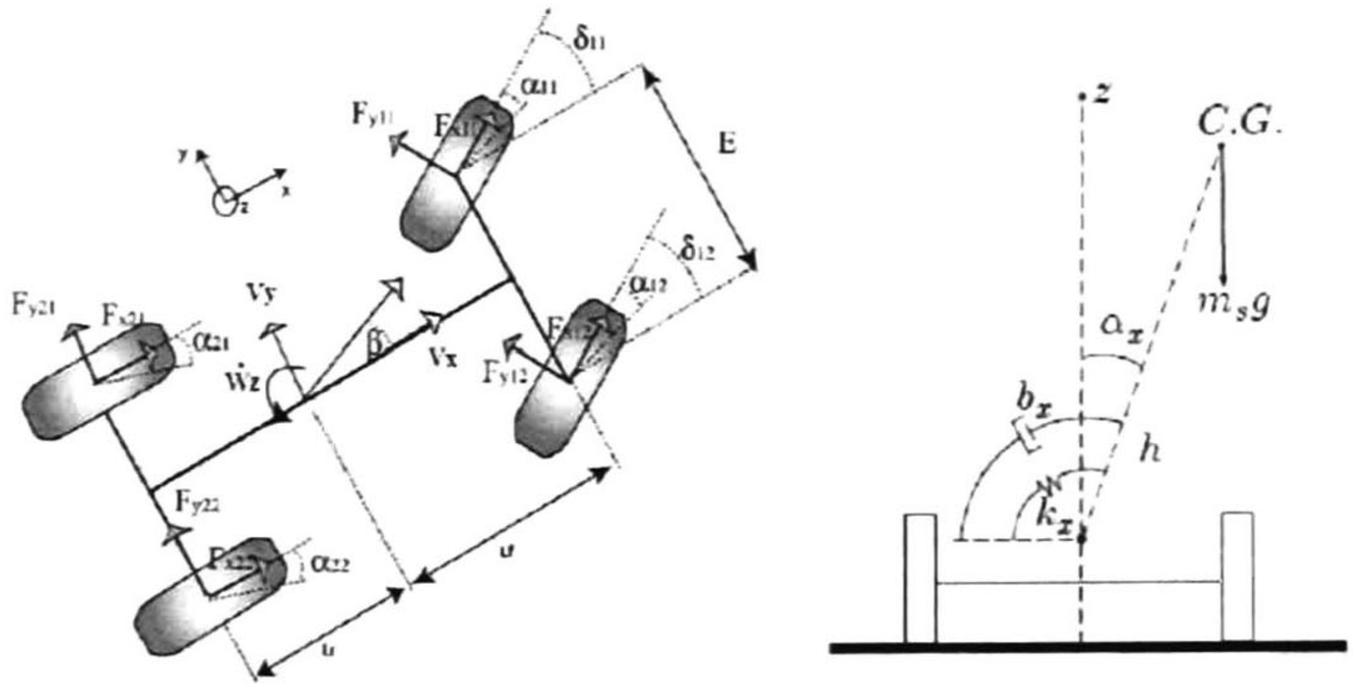

Figure 5.1: Four Wheels Vehicle Model with Roll Dynamic

where $J_x = J_x^G + m_s h^2$ is the vehicle moment of inertia with respect to the longitudinal axis, J_x^G is the vehicle moment of inertia with respect to the longitudinal axis passing for the $C.G.$, g is the weight acceleration, and b_x, k_x are the suspension roll damping and stiffness (see Figure 5.1).

Considering small angles α_x, and considering that $J_{xz} \simeq 0$, from (5.1) and (5.2), we obtain the system dynamics

$$\begin{aligned}
\dot{v}_x &= v_y \omega_z + a_x - \frac{m_s}{m} h \omega_z \omega_x \\
\dot{v}_y &= -v_x \omega_z + \frac{J_x}{J_{x,e}} a_y - \frac{k_{x,e}}{J_{x,s}} \alpha_x - \frac{b_x}{J_{x,s}} \omega_x \\
\dot{\omega}_z &= \frac{\mu_y}{J_z}(F_{y,f} l_f - F_{y,r} l_r) + \frac{1}{J_z} M_z \\
\dot{\alpha}_x &= \omega_x \\
\dot{\omega}_x &= -\frac{k_{x,e}}{J_{x,e}} \alpha_x - \frac{b_x}{J_{x,e}} \omega_x + \frac{m_s}{J_{x,e}} h a_y
\end{aligned} \tag{5.3}$$

with

$$J_{x,e} = J_x - \frac{m_s^2}{m} h^2, \quad J_{x,s} = \frac{m J_{x,e}}{m_s h}, \quad k_{x,e} = k_x - m_s g h.$$

Moreover, $F_{y,f}$, $F_{y,r}$ are the lateral forces of the front and rear axes, which are defined as the following [66]:

$$\begin{aligned}
F_{y,f} &= F_{y,11} \cos\delta + F_{y,12} \cos\delta + F_{x,1} \sin\delta \\
F_{y,r} &= F_{y,21} + F_{y,22}
\end{aligned} \tag{5.4}$$

with $F_{x,1}$, the front axle longitudinal force.
The tyre slip angles are defined according to the (FWVM) model [66]:

$$\begin{aligned}
\alpha_{11} &= \delta - \arctan\left[\frac{v_x\beta + l_f\omega_z}{v_x - E\omega_z/2}\right] \\
\alpha_{12} &= \delta - \arctan\left[\frac{v_x\beta + l_f\omega_z}{v_x + E\omega_z/2}\right] \\
\alpha_{21} &= -\arctan\left[\frac{v_x\beta - l_f\omega_z}{v_x - E\omega_z/2}\right] \\
\alpha_{22} &= -\arctan\left[\frac{v_x\beta - l_f\omega_z}{v_x + E\omega_z/2}\right]
\end{aligned} \tag{5.5}$$

where $\beta = v_x/v_y$ is the vehicle body sideslip angle.

This model describes the vehicle dynamics under the following assumptions

1. Pitch dynamic is neglected.
2. The system is rigid.
3. The suspension is passive.
4. The steering wheel angle $\delta_{11} = \delta_{12} = \delta$.
5. The front and rear track widhs (E) are assumed to be equal.
6. Camber angle is null.

Note that the longitudinal and lateral accelerations a_x, a_y in (2.3), which can be expressed in terms of the front/rear longitudinal and lateral tire forces

$$\begin{aligned}
a_x &= \frac{\mu_x}{m}\Big(- F_{y,11}\sin\delta - F_{y,12}\sin\delta + F_{x,1}\cos\delta\Big) \\
a_y &= \frac{\mu_y}{m}\Big(F_{y,11}\cos\delta + F_{y,12}\cos\delta + (F_{y,21} + F_{y,22}) \\
&\quad + F_{x,1}\sin\delta\Big)
\end{aligned} \tag{5.6}$$

are measured by accelerometers, usually present aboard of a modern automobile. Here, μ_x is the longitudinal tyre-road friction coefficient.

5.3 Tyre-Road Friction Coefficient Estimation using CarSim

The interaction of a tyre with the ground is defined by a longitudinal force (F_X), a lateral force (F_Y), a vertical force (F_Z), and an aligning moment (M_Z). The forces F_X, F_Y, F_Z and the moment M_Z are applied to the wheels and reacted by the ground in the center of tyre contact (CTC). The effects of overturning moment (M_X), which are small for most maneuvers, are not included in this models.

The mass of the vehicle contributes the major portion of the total normal forces on the tyres. The lateral and longitudinal forces acting on the vehicle redistribute the normal forces between the tyres. Anyway, the instantaneous vertical tyre force can be calculated by knowing the vertical compression of the tyre σ_z and its vertical spring rate C_z as the following:

$$F_z = \sigma_z C_z \tag{5.7}$$

where σ_z is defined as the spatial relationship between the wheel center (WC) and the center of tyre contact (CTC).
On the other hand, the lateral and longitudinal tyre deflection (y_b, x_b) can be calculated by subtracting the lateral and longitudinal position of the (WC) to the lateral and longitudinal position of the (CTC) obtaining the same result given by an optical sensor as in [28], [29], [30], [31] and [32] as shown in Fig. 5.2

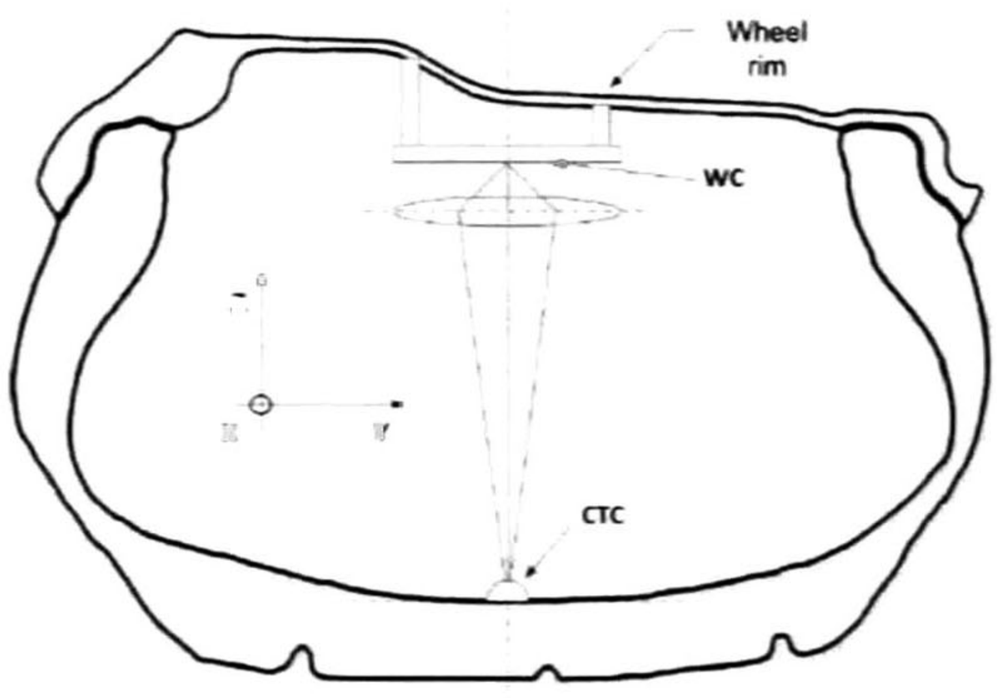

Figure 5.2: Tyre Lateral Deflection.

The lateral deflection profile of the tyre's equatorial line, y_b is assumed to be a parabolic function of the contact patch position, x_b:

$$y_b = \frac{F_y}{2C_{bend}} x_b^2 + \frac{M_z}{C_{yaw}} x_b + \frac{F_y}{C_{lat}} \tag{5.8}$$

By applying the curve fitting technic to x_b, y_b in (5.8) one can find the estimation of the lateral force F_y and the aligning moment M_z for a given $C_{bend}, C_{yaw}, C_{lat}$ representing the tyre bend, yaw and shift stiffness.

This technique describes the tyre lateral deflection under the following assumptions:

1. The tyre deflection profile measured inside the contact patch is assumed to be a continuous function of the time.

2. During the driving maneuver, the tyre is in full adhesion condition.

Therefore, the tyre-road friction coefficient is estimated through a tyre brush model in equations (5.9) which correlates the tyre-road friction coefficient μ_y, the tyre slip angle α and the sliding tyre slip angle α_{sl} with the lateral force F_y. The sliding tyre slip angle represents the limit tyre slip angle before the tyre starts sliding. The friction coefficient μ_y is estimated by solving the nonlinear equations as in [33]

$$\begin{aligned}
F_y &= 3\mu_y F_z \frac{\tan(\alpha)}{\tan(\alpha_{sl})}\Big(1 - \Big|\frac{\tan(\alpha)}{\tan(\alpha_{sl})}\Big| + \frac{1}{3}\frac{\tan^2(\alpha)}{\tan^2(\alpha_{sl})}\Big) \\
M_z &= -\mu F_z a \frac{\tan(\alpha)}{\tan(\alpha_{sl})}\Big[1 - 3\Big|\frac{\tan(\alpha)}{\tan(\alpha_{sl})}\Big| + 3\Big(\frac{\tan(\alpha)}{\tan(\alpha_{sl})}\Big)^2 - \Big|\frac{\tan^2(\alpha)}{\tan^2(\alpha_{sl})}\Big|^3\Big] \\
\mu_y &= \frac{2C_{py}a^2}{3F_z}\tan(\alpha_{sl})
\end{aligned} \tag{5.9}$$

where C_{py} is a given lateral stiffness of a tyre tread element, F_z is the normal force and a is the half length of the tyre-road contact patch calculated as in [33]:

$$a = \sqrt{2R(\Delta R) - (\Delta R)^2} \tag{5.10}$$

where R is the wheel radius and ΔR is the maximum value of the measured vertical tyre deflection.

5.4 Simulation Results

In this section the behavior of the proposed nonlinear observer is shown for an interesting case, in which the vehicle performs a circular maneuver. The driver performs a constant steer

of 23° During the imposed maneuver, the tire–road friction coefficient is supposed to vary from $\mu_y = 0.9$ (dry surface) to $\mu_y = 0.5$ (wet surface) at $t = 4$ s and the tyre deflection is only measured to the front-left wheel with $R = 0.16$m.

The initial longitudinal velocity is $v_x(0) = 28$ m/s (about 100 km/h) and the vehicle moves in a constant target speed. The initial values of the observer variables are

$$\hat{v}_x(0) = v_x, \quad \hat{v}_y(0) = 0, \quad \hat{\alpha}_x(0) = 0, \quad \hat{\omega}_x(0) = 0$$

and the nominal vehicle parameters, used in the observer (3.1), are given in Table 5.1.

Variable	*Value*	*Unit*
m_0	1200	kg
$m_{s,0}$	1000	kg
h_0	0.32	m
$J_{z,0}$	990	$kg\ m^2$
$b_{x,0}$	10000	$Nm\ rad/s$
$k_{x,0}$	114000	$Nm\ rad$
$J_{x,0}$	280	$kg\ m^2$

Table 5.1: Nominal parameters used in the observer.

To show that the proposed controller is robust with respect to parameter variations, we have considered the parameters given in Table 5.2 for the vehicle dynamics (2.3).

Variable	*Value*	*Unit*
m	1260	kg
m_s	1020	kg
h	0.32	m
J_z	996	$kg\ m^2$
b_x	10000	$Nm\ rad/s$
k_x	114000	$Nm\ rad$
J_x	288	$kg\ m^2$
l_f	1.165	m
l_r	1.165	m

Table 5.2: Real parameters used in the observer.

The obtained results are shown in Figure 5.3, with $k_{o1}, \cdots, k_{o4}$ in (3.1) set considering $\gamma_1 = 100$, $\kappa_1 = 9$ in (4.4), and $\lambda_1 = 1$, $\lambda_2 = 1000$ in (3.5). Notice the good tracking

performance of the observer. Moreover, this nonlinear observer shows good performances with respect to system parameter variations. In particular, it is robust with respect variations of the tire–road friction coefficient, since the performance does not depend relevantly on this crucial parameter. In Figure 5.4 the measured longitudinal and lateral accelerations, vertical tyre force and contact patch are presented. Notice that a random sensor noise has been considered. Finally in Figure 5.5 the estimation of the sideslip angle (β), tyre slip angle (α_{11}), tyre lateral force ($F_{y,11}$) and tyre-road friction coefficient (μ_y) are shown for $C_{lat} = 185$ kN/m, $C_{bend} = 10$ kNm, $C_{p,y} = 170$kN/m. Notice the good behavior of the estimations.

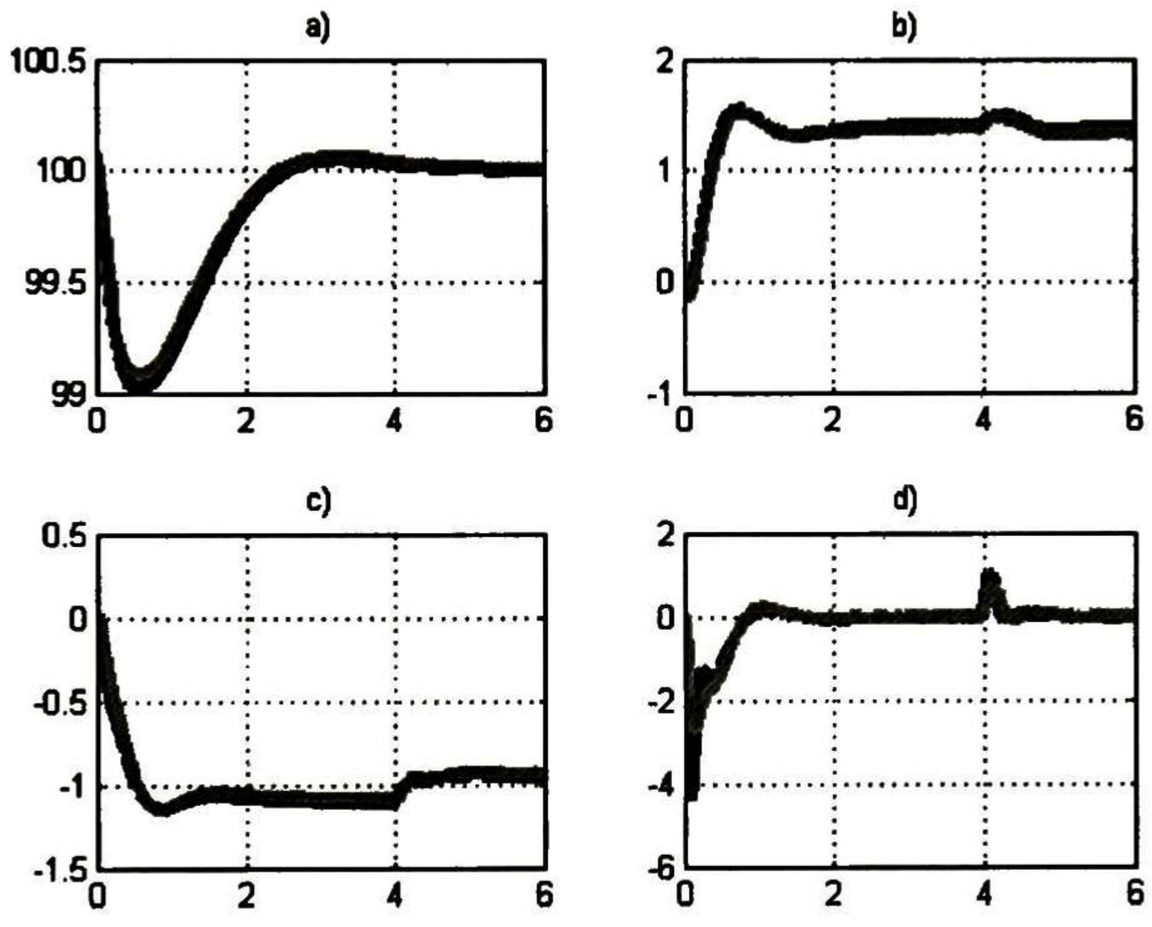

Figure 5.3: a) Real longitudinal velocity v_x (black) and estimation $\hat{v}_x$ (gray) [km/h vs s]; b) real lateral velocity v_y (black) and estimation $\hat{v}_y$ (gray) [km/h vs s]; c) real roll position α_x (black) and estimation $\hat{\alpha}_x$ (gray) [deg vs s]; d) real roll rate w_x (black) and estimation $\hat{w}_x$ (gray) [deg/s vs s].

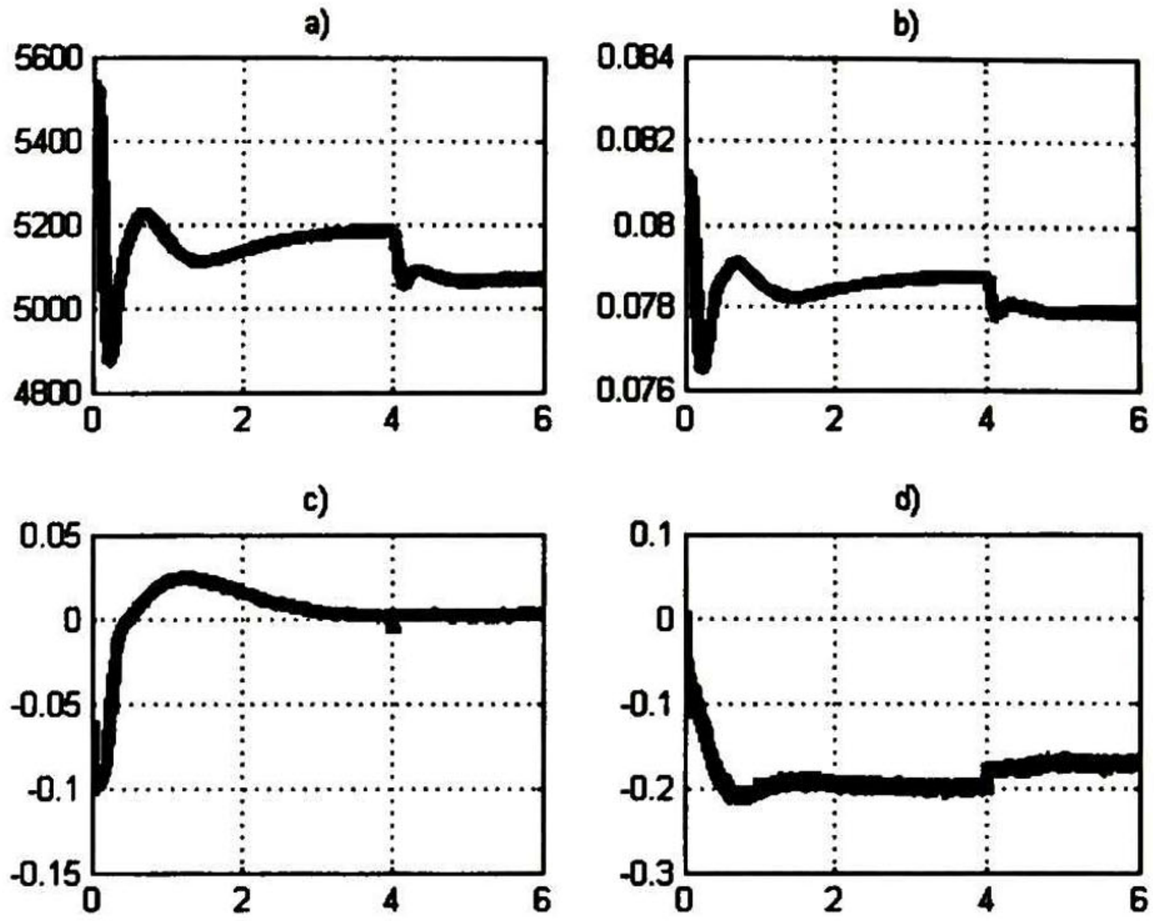

Figure 5.4: a) Vertical tyre force $F_{z,11}$ [N vs s]; b) contact patch length a [m vs s]; c) measured longitudinal acceleration a_x [g's vs s]; d) measured lateral acceleration a_y [g's vs s].

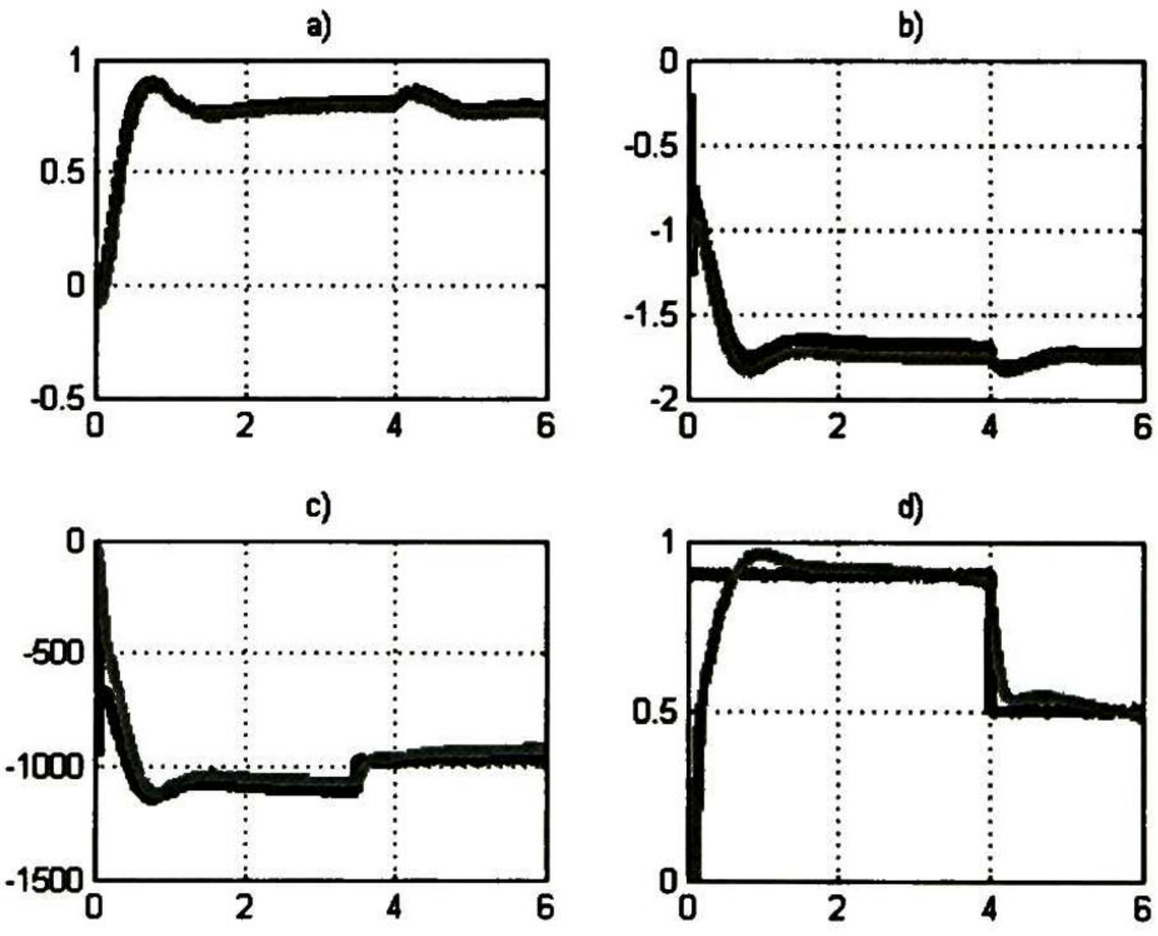

Figure 5.5: a) Real sideslip angle β (black) and estimation $\hat{\beta}$ (gray) [deg vs s]; b) real tyre slip angle α_{11} (black) and estimation $\hat{\alpha}_{11}$ (gray) [deg vs s]; c) real tyre lateral force $F_{y,11}$ (black) and estimation $\hat{F}_{y,11}$ (gray) [N vs s]; d) real tyre-road friction coefficient μ_y (black) and estimation $\hat{\mu}_y$ (gray) [adimensional vs s].

Chapter 6

CarSim Simulator

In this chapter we present a brief information about the CarSim simulation. Then the technical configuration of each part is discussed. A long list of imagines describe accurately the configuration in both works.

6.1 What is CarSim?

CarSim is a commercial software package that predicts the performance of vehicles in response to driver controls (steering, throttle, brakes, clutch, and shifting) in a given environment (road geometry, coefficients of friction, wind). CarSim is produced and distributed by an American company, Mechanical Simulation Corporation, using technology that originated at The University of Michigan Transportation Research Institute (UMTRI) in Ann Arbor, Michigan.

The software is used by over 30 automotive manufacturers (General Motors, Toyota, Honda, Ford, etc.), over 60 suppliers, and over 150 research labs and universities. The math models simulate physical tests to allow engineers to view results that are similar to test results, but which can be obtained repeatably, safely, and much quicker than is possible with physical testing. The simulation models are often used to evaluate vehicle designs that have not yet been built. Results are visualized via animation, plotted for analysis, or exported to other software for analysis using the same methods that are applied to physical test data.

The math models replicate system-level behavior with high fidelity. They contain the major effects that determine how the tire contacts the road, and how forces from the tire/road interface are transferred through the suspension to the chassis. However, they do not have details of linkage connections or structure compliance. The models have been validated repeatedly by manufacturers for reproducing overall vehicle motions needed to evaluate handling, directional and roll stability, braking, and acceleration. On the other hand, they do

not include component details needed to determine durability, fatigue, or high-frequency vibrations.

The math models are generated with a symbolic multibody code generator called VehicleSim Lisp (originally named AutoSim) that was developed by one of the company founders at UMTRI. The machine-generated code is highly optimized to achieve fast computation, such that the math models run much faster than real time. Starting in 1998, real-time versions of CarSim have been available for testing hardware in the loop (HIL). The math models are used directly in over 350 driving simulators to provide physics models that have been validated over most conditions of interest.

The main applications of the CarSim software are: Test engineers simulate hundreds of tests ahead of time to identify problems or clear designs that show no problems. Developers of advanced controls (brakes, stability, traction, etc.) test their simulated control designs with the simulated vehicle. In these applications, CarSim simulates the basic vehicle dynamic behavior as a plug-in to controller design software such as Simulink (from Mathworks), LabVIEW (from National Instruments), or custom code (MATLAB, Visual Basic, C/C++, etc.) Car manufacturers and suppliers test actual controller hardware using real-time HIL systems. Researchers and others use the CarSim math models in driving simulators, ranging from low-cost systems using game controller up to full-scale large motion simulators such as the Toyota simulator.

6.2 Why CarSim?

The CarSim math models are built on decades of research in characterizing vehicles and reproducing their behavior with mathematical models. CarSim simulates the dynamic behavior of passenger cars, racecars, light trucks, and utility vehicles. CarSim animates simulated tests and outputs over 800 calculated variables to plot and analyze, or export to other software such as MATLAB, Excel, and optimization tools. It is:

Accurate The CarSim math models are built on decades of research in characterizing vehicles and reproducing their behavior with mathematical models. Validation testing continues as new features are added. OEM users consistently find close agreement between CarSim predictions and actual test results.

Extensible The CarSim math models cover the complete vehicle system and its inputs from the driver, ground, and aerodynamics. The models are extensible using built-in VehicleSim commands, MATLAB/Simulink from the Mathworks, LabVIEW from National Instruments, and custom programs written in Visual Basic, C, MATLAB, and other languages. Use these options to add advanced controllers or extend the detail in subsystem or component models such as tires, brakes, powertrain, etc.

Fast CarSim combines a complete vehicle math model with high computational speed. The software development team at Mechanical Simulation uses the VehicleSim Lisp symbolic multibody program to generate the equations for the vehicle math models. Besides providing correct nonlinear equations for fairly complicated models, the machine-generated equations are highly optimized to provide fast computation. CarSim models typically run more than ten times faster than real time on a 3 GHz PC, so you always get results quickly. CarSim easily supports real-time (RT) testing with hardware in the loop (HIL) using systems from most RT suppliers. This speed also helps with software that requires many repetitions (optimization, design-of-experiments, etc.).

Cost Effective, Stable, Reliable CarSim has all the tools you need to predict vehicle dynamics behavior in one integrated package, with the capability of working with other software to extend its capabilities even further. It combines the accuracy and validation resulting from decades of research in vehicle dynamics with the ease-of-use associated with modern video games and Internet browsers.

CarSim includes everything needed to simulate vehicle tests and view the results, yet it is priced at a fraction of the cost of other commercial vehicle dynamics software.

6.3 CarSim Configuration for Active Control Testing

In order to validate performances of the active control, we have used a D-Class SUV vehicle with high center of gravity (CG) as shown in Figure 6.1

Figure 6.1: D-Class SUV vehicle

This vehicle offers a good simulation condition due to its high center of gravity. In fact, we could show the difference between a control which makes use of the roll dynamic and a controller which does not take in to account the roll dynamic. The high center of gravity (around $1m$) produces a so stimulated roll dynamic.

The maneuver we have chosen for the test is called the Double Lane Change (DLC) which is used in case of object avoidance and similar trajectories. The DLC maneuver is shown in Figure 6.2

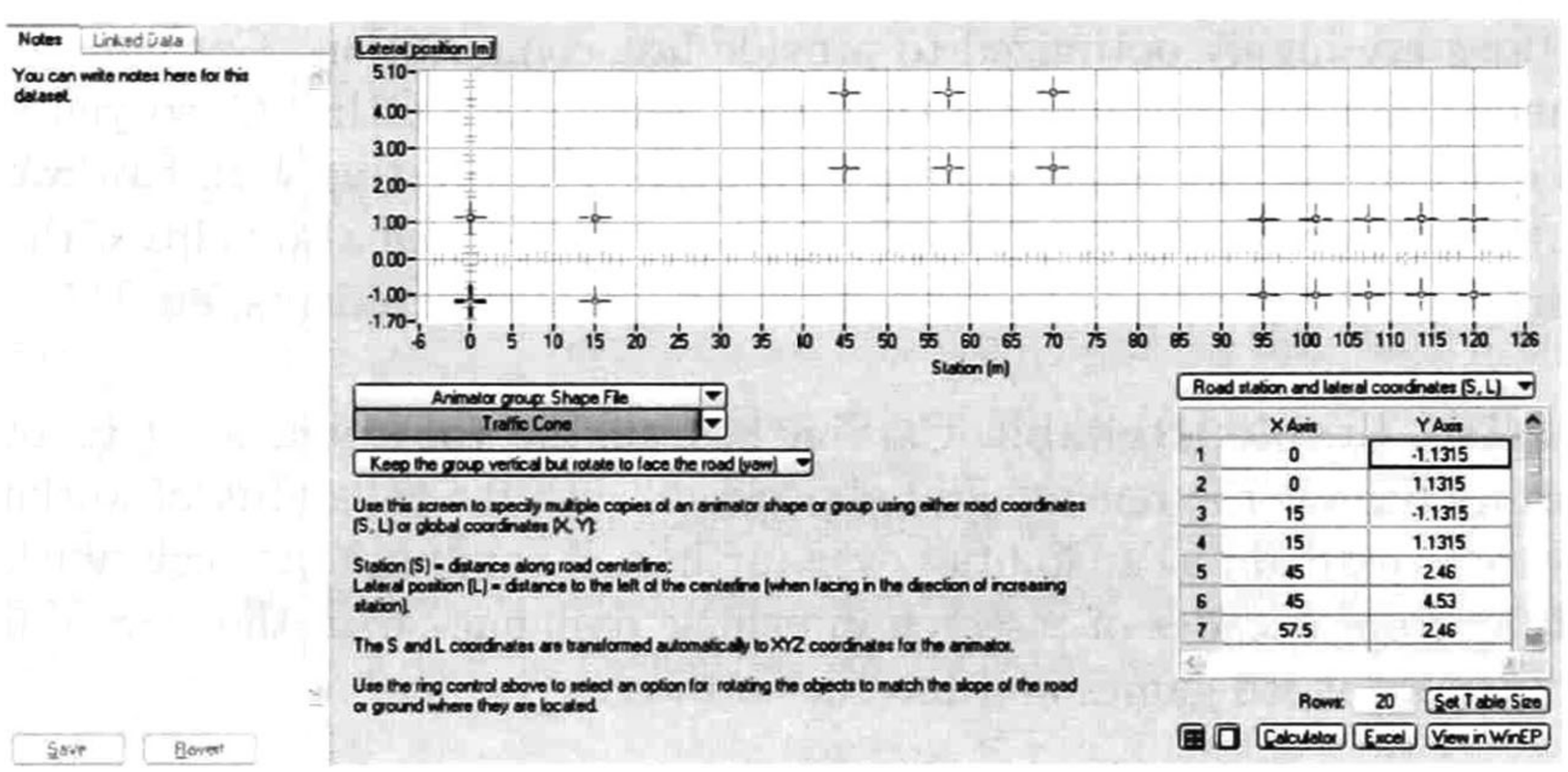

Figure 6.2: Double Lane Change Maneuver in CarSim.

As shown in the picture, this maneuver is protected by the standard ISO 3888 which guarantees the unique conditions for the maneuver execution.

Clearly, all the other dynamics that we have not considered in our mathematic model must be studied. First of all we have minimized the Camber Change, Toe, Movement, Caster Change as shown in Figure 6.3.

This strategy allows us to take into account a simplified model of the vehicle.

On the other hand, the Pacejka Tyre parameters must be defined. CarSim offers a realistic condition and we decided to derive our study from the realistic situation. Then we have applied the same wheel at same side as front-rear and right-left. The wheels used in this simulation are the 255/75 R16 and its react with the ground producing the Dynamics of lateral force, longitudinal force and yaw moment as in Figure 6.4.

Then in Figure 6.5 one can observe how the CarSim simulator deal the longitudinal tyre dynamic: the graphic represent Newton vs K (Absolute Slip Rate) in case of differents loads conditions.

Then in Figure 6.6 we present the tyre lateral graphic. This one represent Newton vs Degree that means Newton vs tyre slip angle. As we said, the linearity of the wave guarantees

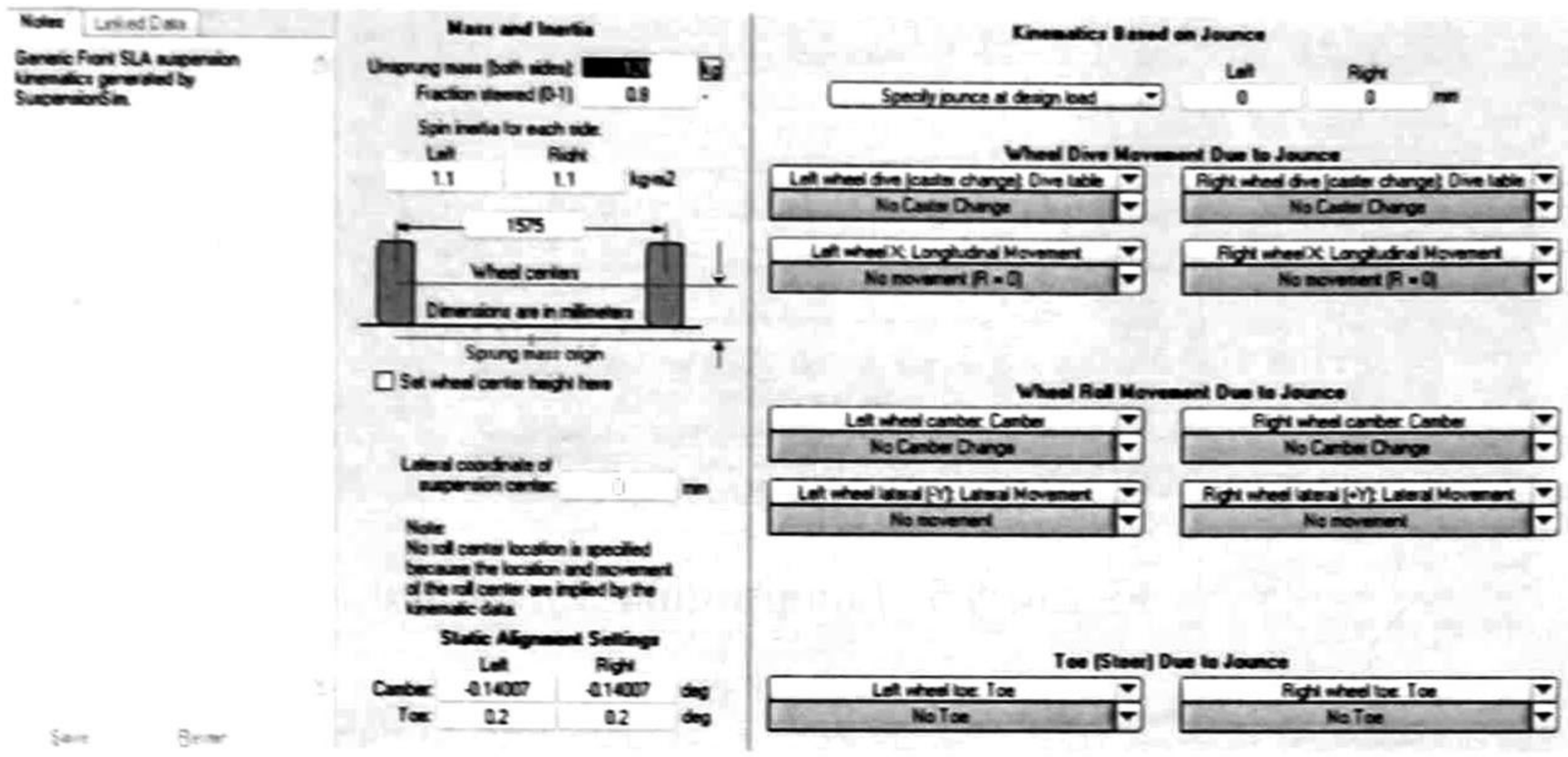

Figure 6.3: Non-modeled Dynamics in CarSim

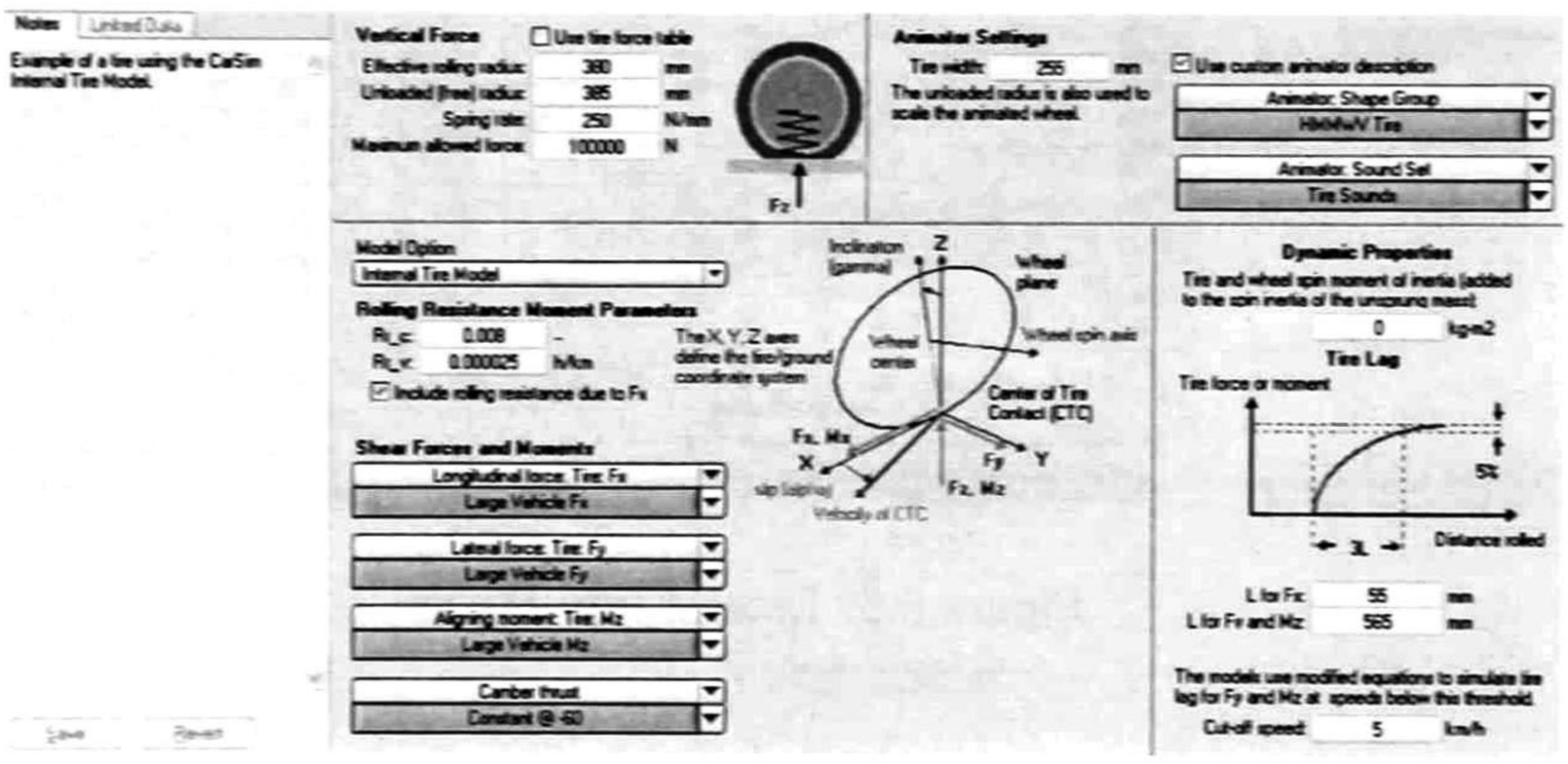

Figure 6.4: Wheel used in the simulation: 255/75 R16

a good stability of the vehicle while the non-linear part means a skid condition which is dangerous for the driver. The graphic moves on five trajectory depending on the vehicle vertical load.

Finally, the self aligning moment is present in Figure 6.7

Now it is necessary to introduce a little discussion. In Figure 6.8 all the geometric parameters of the vehicle must be declared.

As the reader can appreciate, the height of the body-vehicle center of gravity (CG) is established at 0.8 m while in our Simulink model is 0.63 m. This choice must be explained: as presented in [65], the roll dynamic is created by the unsprung mass which moves depending on the distance of the CG with respect to the roll axle as shown in Figure 6.9. This axle

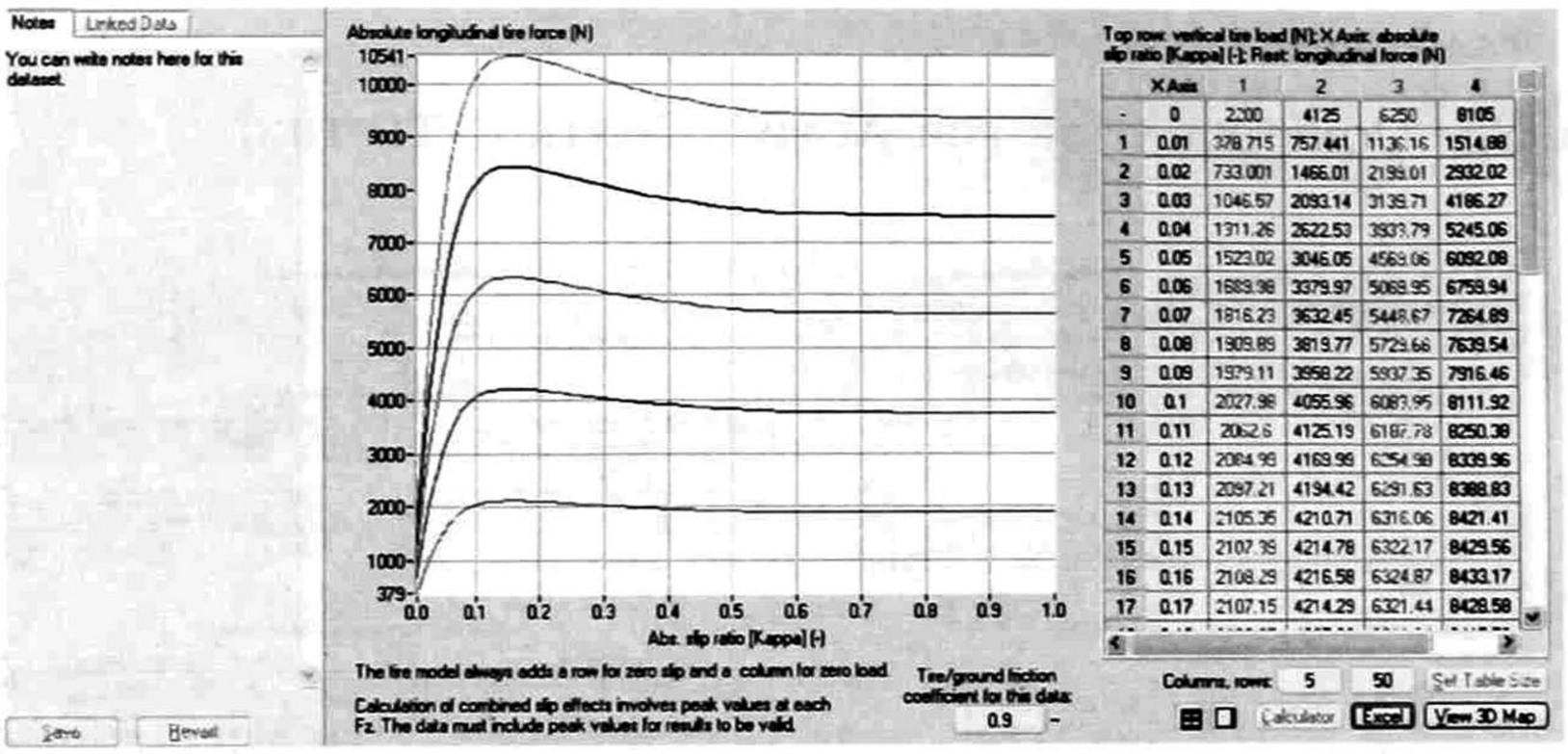

Figure 6.5: Longitudinal tyre force.

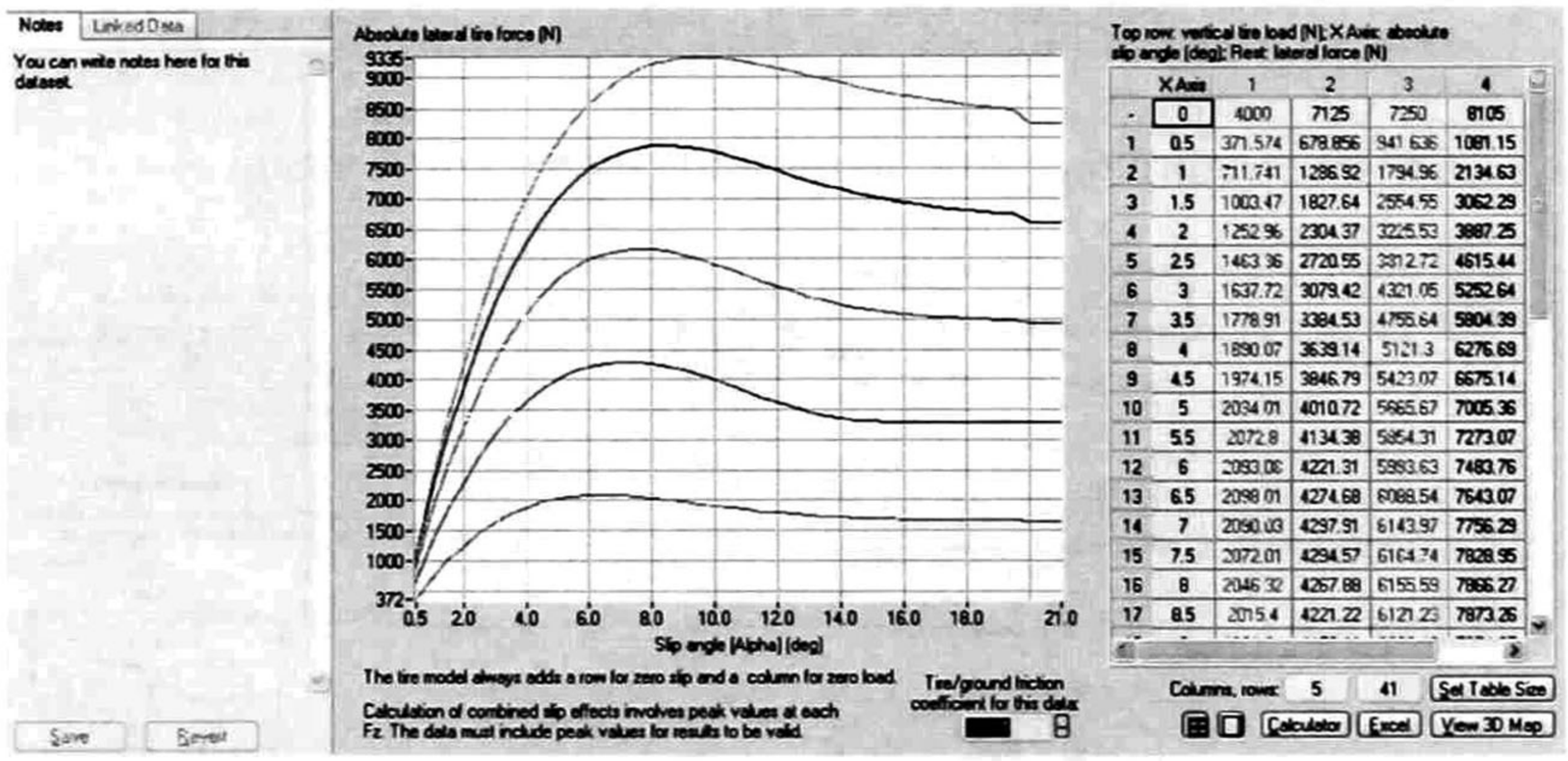

Figure 6.6: Lateral tyre Force.

is identified by plotting a line passing through the front roll center and the rear roll center. Tho determine these points is possible to consult some specific software. Another possibility is to identify the height in which the roll dynamic in null and in which a little less height produce a negative roll. This point is situated exactly at the measure of the roll axle.

On the other hand, the CarSim input variables must be selected. As shown in Figure 6.10 we take in first position the steering angle, then the second control low that is the rear torque vectoring and then eight parameters indicating the road friction condition with respect of the lateral and longitudinal direction.

At the end, a brief comment on the suspensions in CarSim. The passive suspension is defined as spring and dumping compression dynamics. In most cases the relation between

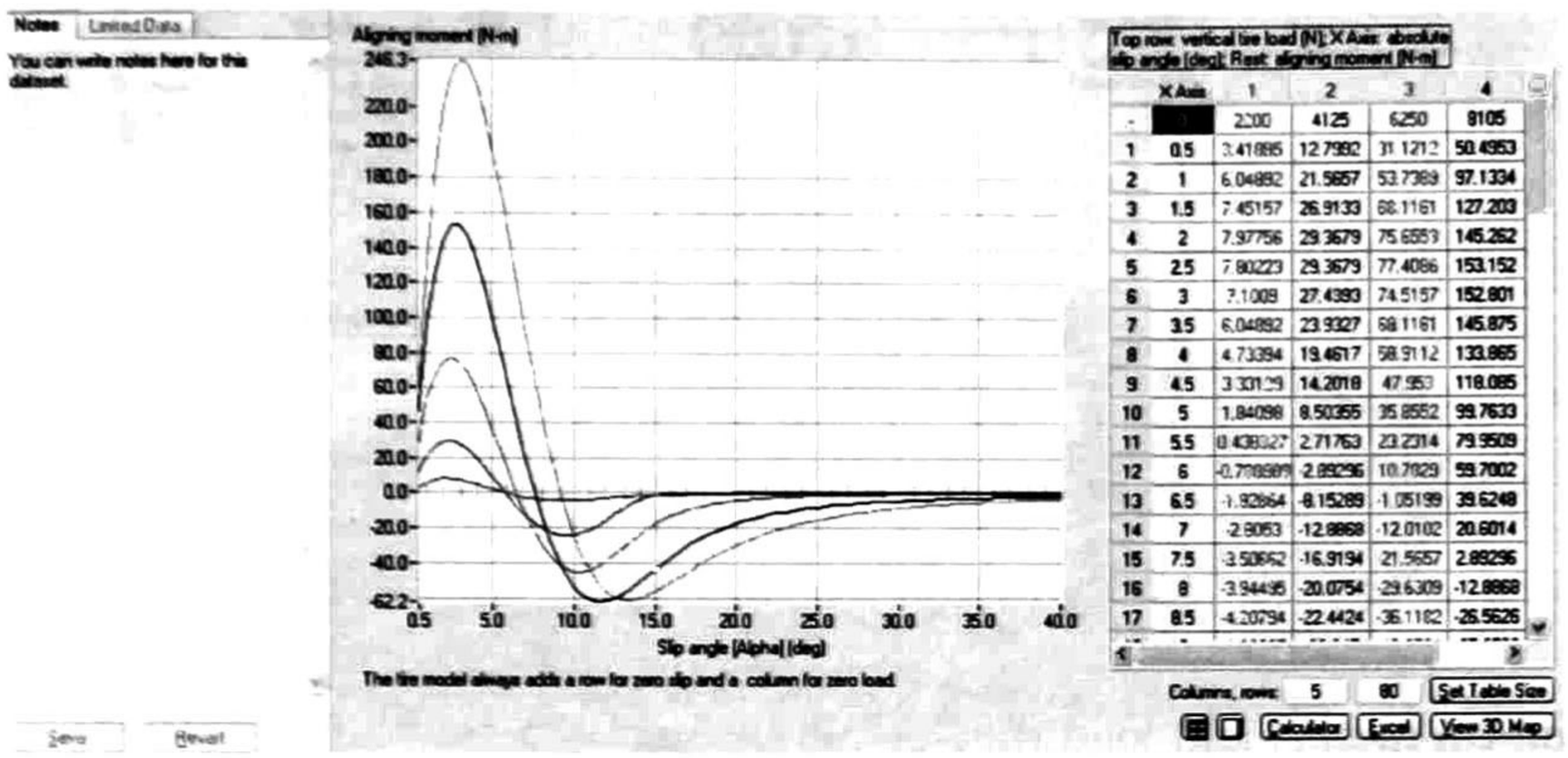

Figure 6.7: Tyre self aligning moment.

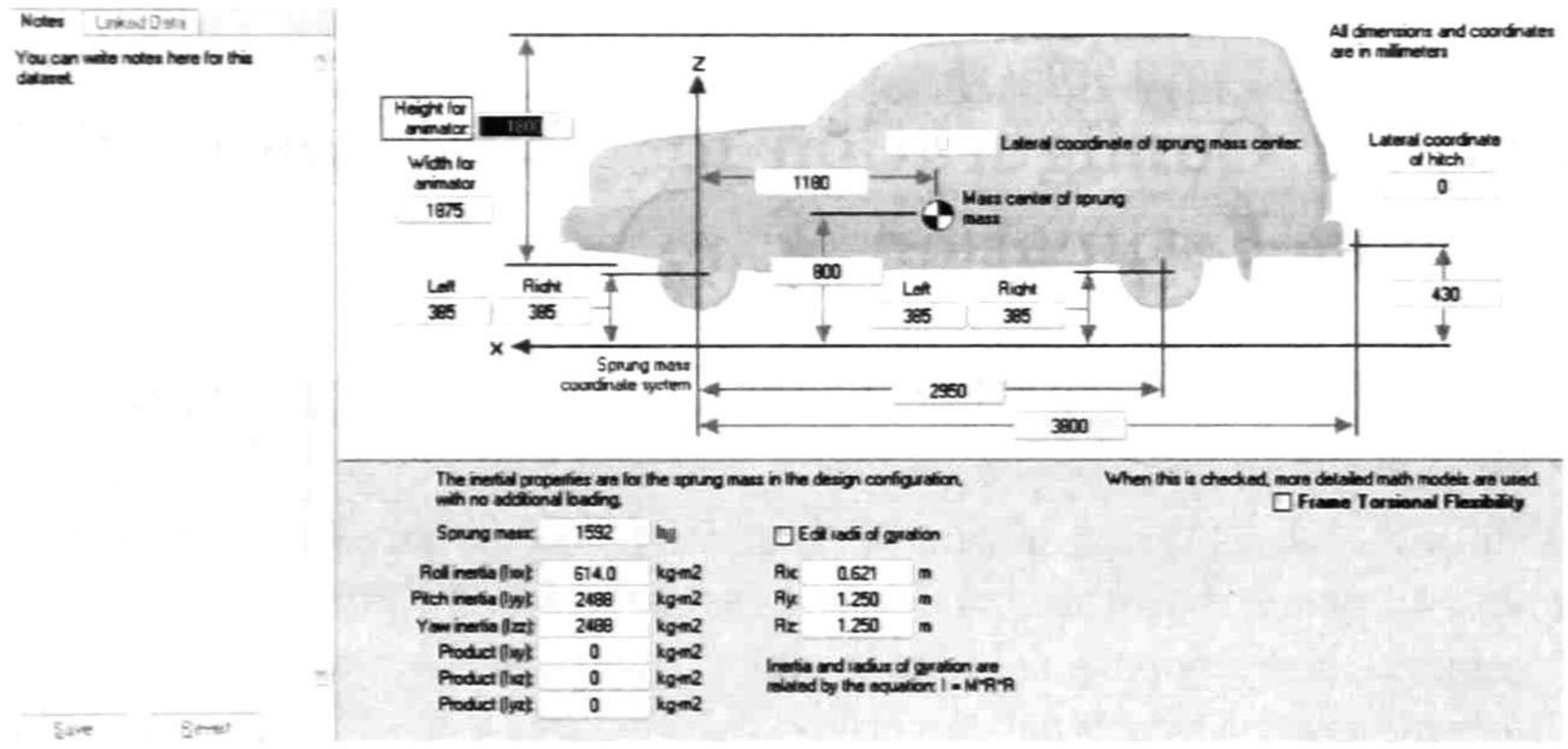

Figure 6.8: Vehicle parameters.

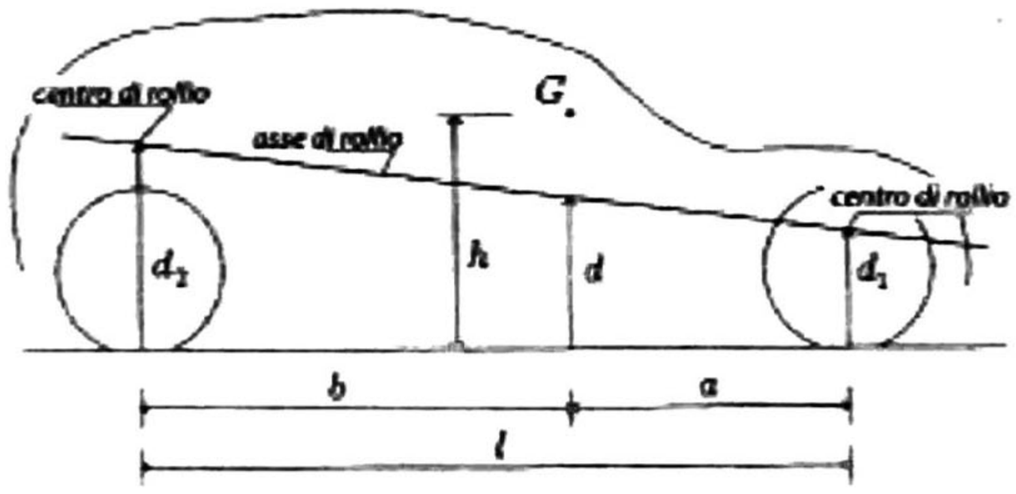

Figure 6.9: Roll axle.

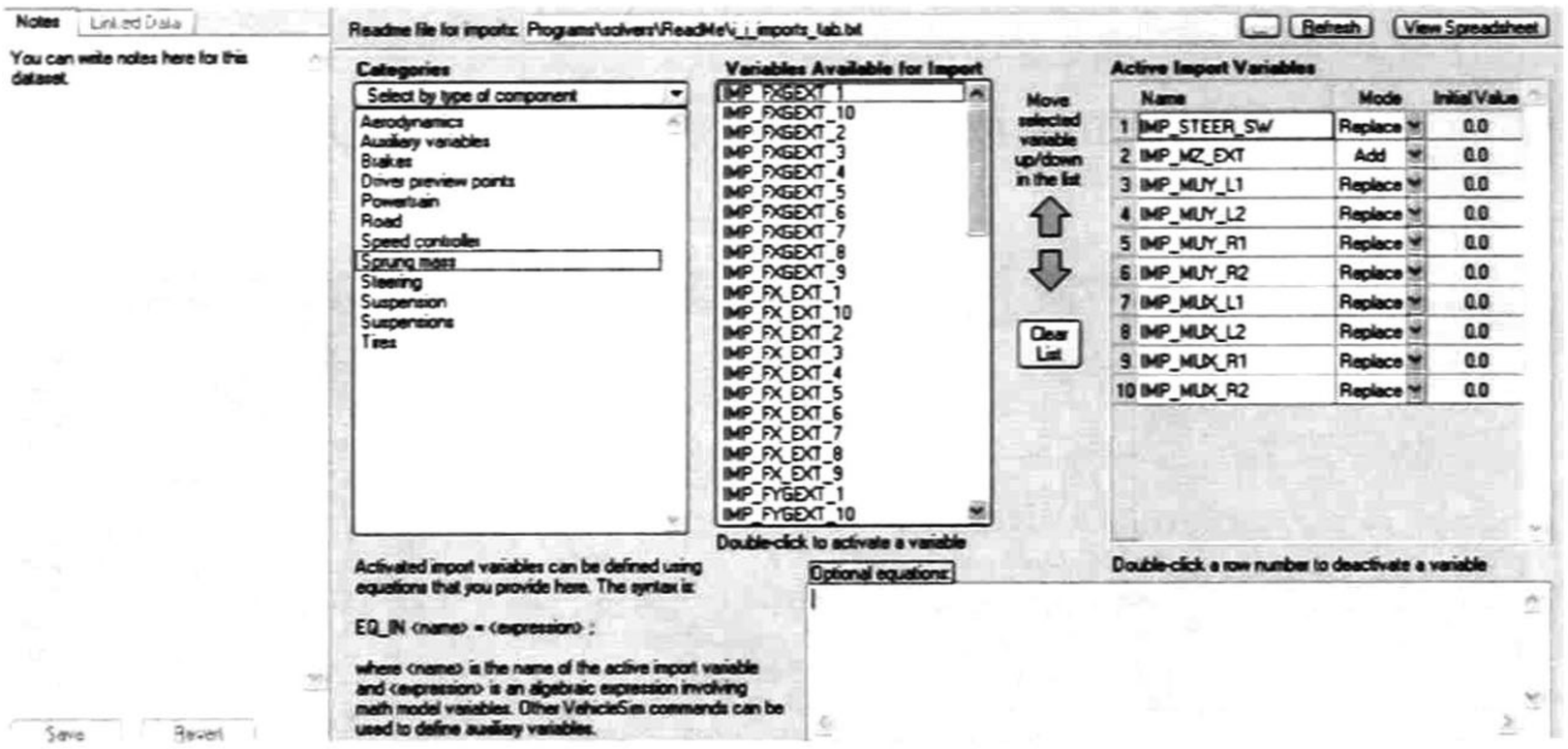

Figure 6.10: CarSim input variables.

compression (in meter) and load (in Newton) is a non-linear relation. In this application has been necessary to create a linear condition. This method is help full in order to identify the stiffness and dumping coefficient.

6.4 CarSim Configuration for Tyre-Road Friction Coefficient Estimation

For the Tyre road friction coefficient estimation, we decided to select a B-Class Sport Car as shown in Figure 6.11.

All the characteristics discussed below remaining the same. The maneuver is a constant steering vehicle in order to obtain a vehicle moving in circular trajectory. This technique has been used to guarantee a constant lateral velocity, vertical load and slip angle as required for the friction coefficient estimation.

Finally, in Figure 6.12 and Figure 6.13 a graphic lay-out is presented.

Figure 6.11: Selected vehicle for friction estimation.

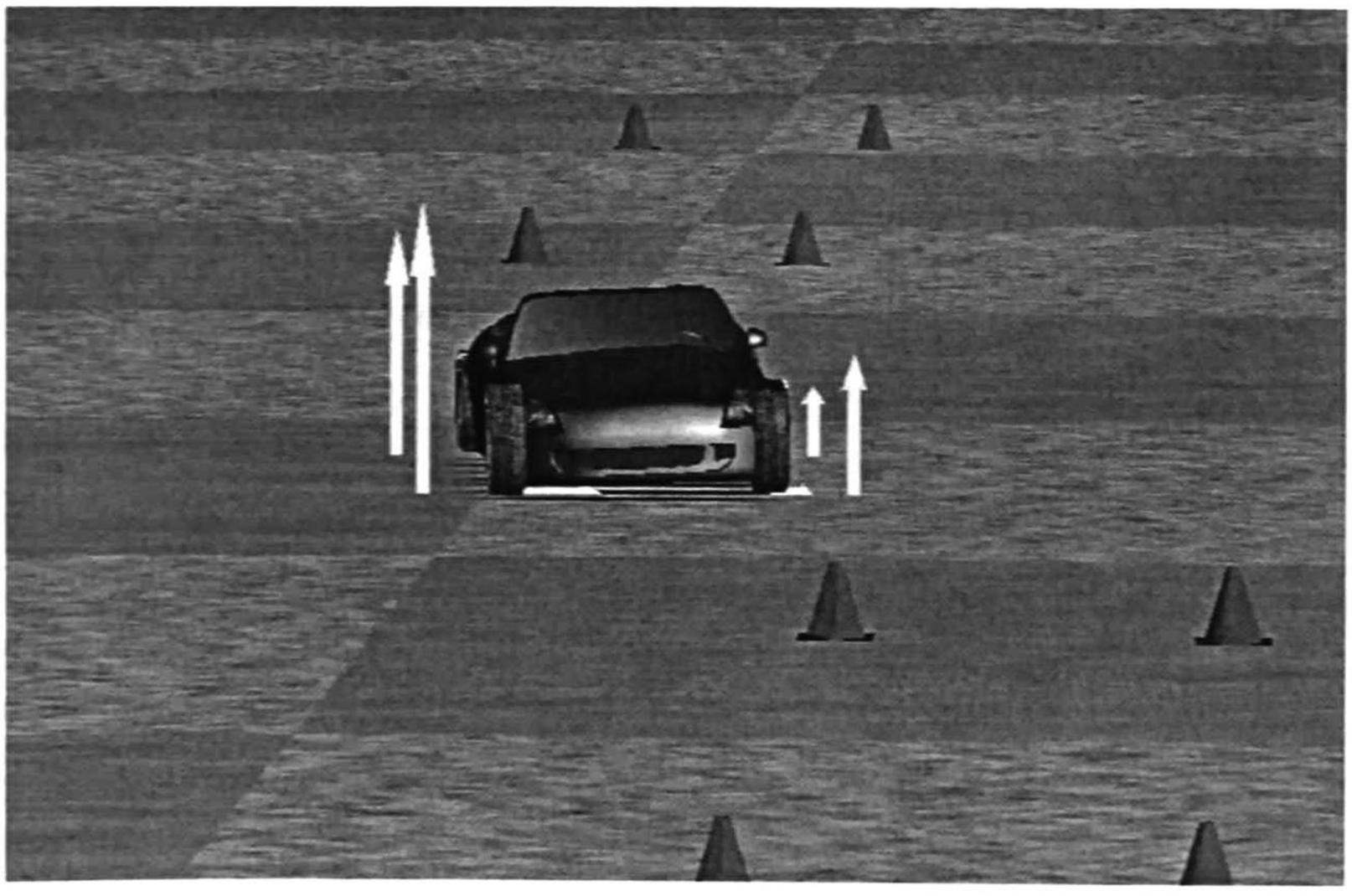

Figure 6.12: CarSim realtime simulation with Sport car.

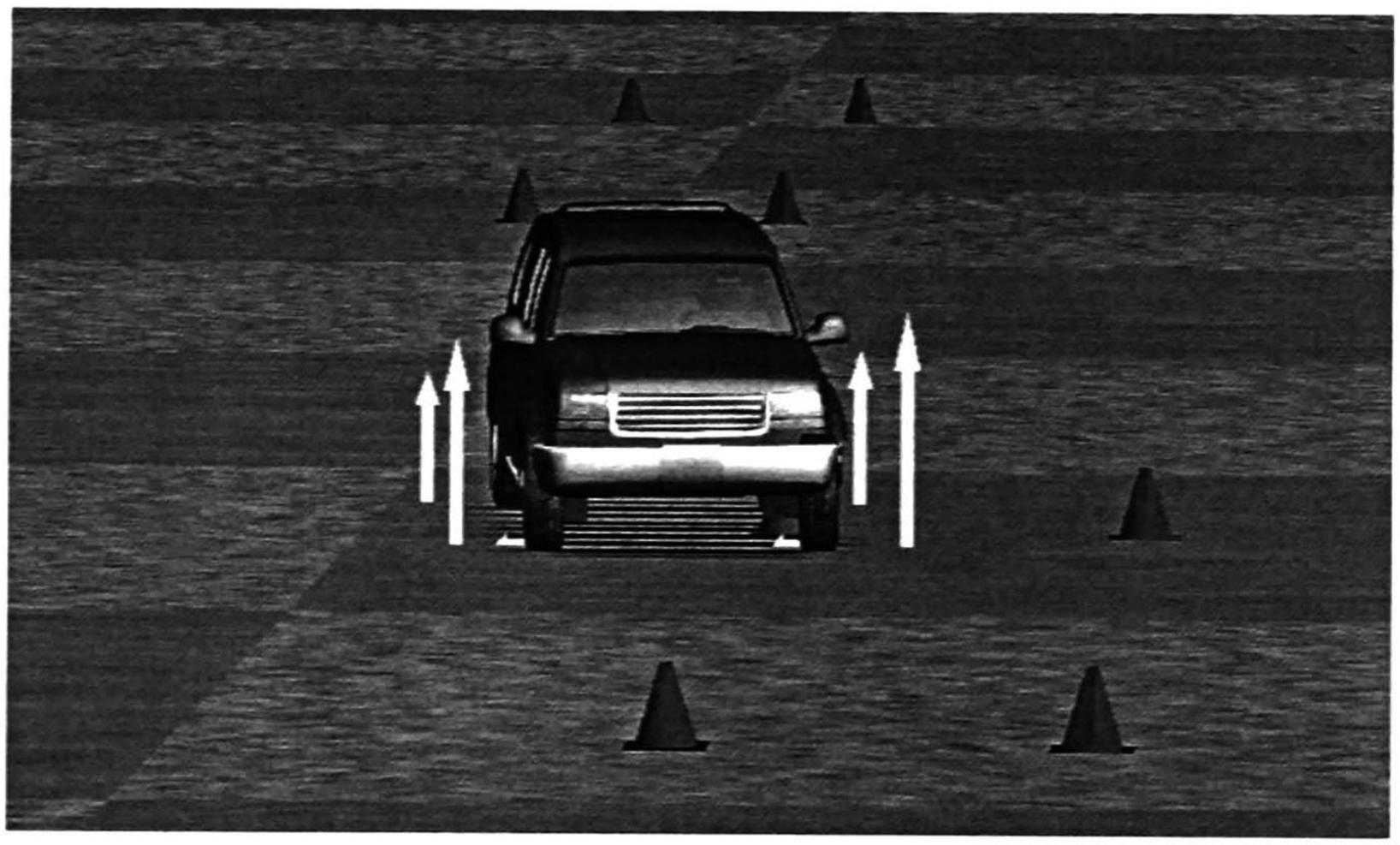

Figure 6.13: CarSim realtime simulation with SUV car.

Chapter 7

Conclusions

In this chapter several conclusions and future works are presented.

7.1 Conclusions

We have presented a non-linear observer for a ground vehicle. The error dynamic is a time-varying system. To show the asymptotic stability of the origin we have proposed a time-varying Lyapunov candidate function. The stability proof offers a clear image of the observer behavior. We have also concluded that the non-linear observer is exponentially stable. On the other hand, we have studied a controller able to guarantee safer driving conditions. This technique is based on an ideal function of the lateral Pacejka trajectory in which the non linearity is substituted by a linear function.

The two control laws are applied to the CarSim for the tracking of the reference of the lateral velocity and yaw rate.

The simulation has shown a good performance of both the observer and the controller.

To avoid the problem coming from the separation principle, we have demonstrated the global stability creating a dynamic controller. Two standard maneuvers have been used to prove the good behavior of the controller.

In order to plot a more realistic car condition, we have configured the car simulator CarSim depending on our necessity. Actually a D-Class SUV vehicle with high center of gravity has been utilized to prove the importance of the roll dynamic.

On the other hand, the study moved to the tyre friction coefficient estimation. This parameter permit us to improve the quality of the dynamic controller by applying an estimated tyre-road friction coefficient to the reference system.

The estimation is based on tyre carcass deflection measured with CarSim and making use of the brush mathematic model. Lateral tyre force and self aligning tyre moment are estimated with a curve fitting technique.

A constant maneuver with a B-Class Sport Car provided all the desired results.

7.2 Future Works

Depending on the obtained results, the design of other non-linear observer with different nature as sliding mode observer and high order neuronal network observer are planned. This may permit us to compare advantages and disadvantages of each observer.

Moreover, the tyre optical sensor can not offer continuous measurements. For this reason, next step is to discretize the observer.

Another interesting topic is the Vehicle to Vehicle communication (V2V) and vehicle to Infrastructure (V2I). This seems to be the most demanded topic from automotive companies.

Bibliography

[1] J. Ackermann, D. Odenthal, and T. Bünte, Advantages of Active Steering for Vehicle, *Proceedings of the* 32^{nd} *International Symposium on Automotive Technology and Automation*, pp. 263–270, 1999.

[2] D. Bianchi, A. Borri, G. Burgio, M. D. Di Benedetto, and S. Di Gennaro, Adaptive Integrated Vehicle Control using Active Front Steering and Rear Torque Vectoring, *International Journal of Vehicle Autonomous Systems*, Special Issue on: "Autonomous and Semi–Autonomous Control for Safe Driving of Ground Vehicles", Vol. 8, No. 2/3/4, pp. 85–105, 2010.

[3] F. Borrelli, P. Falcone, T. Keviczky, J. Asgari, and D. Hrovat, MPC–Based Approach to Active Steering for Autonomous Vehicle Systems, *International Journal of Vehicle Autonomous Systems*, Vol. 3, pp. 265–291, 2005.

[4] J. Cao, H. Liu, P. Li, and D. J. Brown, State of the Art in Vehicle Active Suspension Adaptive Control Systems Based on Intelligent Methodologies, *IEEE Transactions on Intelligent Transportation Systems*, Vol. 9, No. 3, pp. 392–405, 2008.

[5] P. Falcone, F. Borrelli, J. Asgari, H. E. Tseng, and D. Hrovat, Predictive Active Steering Control for Autonomous Vehicle Systems, *IEEE Transactions on Control Systems Technology*, Vol. 15, No. 3, pp. 566–580, 2007.

[6] M. Lindner, and T. Tille, Design of Highly Integrated Mechatronic Gear Selector Levers for Automotive Shift–by–Wire Systems, *IEEE/ASME Transactions on Mechatronics*, Vol. 15 , No. 6, pp. 961–968, 2010.

[7] S. Mammer and D. Koenig, Vehicle Handeling Improvement by Active Steering, *Vehicle System Dynamics*, Vol. 38, No. 3, pp. 211–242, 2002.

[8] C. Acosta–Lua, B. Castillo–Toledo and S. Di Gennaro and A. Toro, Nonlinear Robust Regulation of Ground Vehicle Motion, *Proceedings of the* 46^{th} *IEEE Conference on Decision and Control*, pp. 3871–3876, 2007.

[9] C. Acosta–Lua, B. Castillo–Toledo and S. Di Gennaro, Nonlinear Output Robust Regulation of Ground Vehicle in Presence of Disturbances and Parameter Uncertainties, *Proceedings of the* 17^{th} *IFAC World Congress*, pp. 141–146,, 2008.

[10] J. Sou, J. Y. Joeng, K. I. Lee and K. Yi, Vehicle Stability Control System for Enhancing Steerabilty, Lateral Stability, and Roll Stability, *International Journal of Automotive Technology*, Vol. 9, No. 5, 571–576, 2008.

[11] J. Farrelly and P. Wellstead, Estimation of Vehicle Lateral Velocity, *Proceedings of the 1996 IEEE International Conference on Control Applications*, pp. 552–557, 1996.

[12] Y. Fukada, Slip-angle estimation for stability control, *Vehicle Systems Dynamics*, Vol. 32, pp. 375–388, 1999.

[13] T. L. Lam, H. Qian, and Y. Xu, Omnidirectional Steering Interface and Control for a Four-Wheel Independent Steering Vehicle, *IEEE/ASME Transactions on Mechatronics*, Vol. 15, No. 3, pp. 329–338, 2010.

[14] A. Goodarzi, and E. Esmailzadeh, Design of a VDC System for All–Wheel Independent Drive Vehicles, *IEEE/ASME Transactions on Mechatronics*, Vol. 12 , No. 6, pp. 632–639, 2007.

[15] B. Allotta, L. Pugi, F. Bartolini, Design and Experimental Results of an Active Suspension System for a High–Speed Pantograph, *IEEE/ASME Transactions on Mechatronics*, Vol. 13, No. 5, pp. 548–557, 2008.

[16] G. Baffet, A. Charara, and G. Dherbomez, An Observer of Tire–Road Forces and Friction for Active Security Vehicle Systems, *IEEE/ASME Transactions on Mechatronics*, Vol. 12 , No. 6, pp. 651–661, 2007.

[17] S. C. Baslamisli, I. Polat, and I. E. Kose, Gain Scheduled Active Steering Control Based on a Parametric Bicycle Model, *IEEE Intelligent Vehicles Symposium*, pp. 1168–1173, 2007.

[18] R. Karbalaei, A. Ghaffari, R. Kazemi, and S. H. Tabatabaei, Design of an Integrated AFS/DYC Based on Fuzzy Logic Control, *IEEE International Conference on Volume Vehicular Electronics and Safety*, pp. 1–6, 2007.

[19] APOLLO Final Report, Intelligent Tyre for Accident–Free Traffic, *IST-2001–34372*, Deliverable 22/23, 2005.

[20] S.C. Ergen, A. Sangiovanni–Vincentelli, X. Sun, R. Tebano, S. Alalusi, G. Audisio, and M. Sabatini, The Tire as an Intelligent Sensor, *IEEE Transactions on Computer–Aided Design of Integrated Circuits and Systems*, Vol. 28, No. 7, pp. 941–955, 2009.

[21] H.–G. Xu, M. Yang, C.–X. Wang, and R.–Q. Yang, Magnetic Sensing System Design for Intelligent Vehicle Guidance, *IEEE/ASME Transactions on Mechatronics*, Vol. 15, No. 4, pp. 652–656, 2010.

[22] G. Baffet, A. Charara, and G. Dherbomez, An Observer of Tire–Road Forces and Friction for Active Security Vehicle Systems, *IEEE/ASME Transactions on Mechatronics*, Vol. 12, No. 6, pp. 651–661, 2007.

[23] A.Y. Ungoren, H. Peng and H. Tseng, A Study on Lateral Speed Estimation Methods, *International Journal on Vehicle Autonomous Systems*, Vol. 2, pp. 126–144, 2004.

[24] P. J. Venhovens, and K. Naab, Vehicle Dynamics Estimation using Kalman Filters, *Vehicle System Dynamics*, Vol. 32, pp. 171–184. 1999.

[25] U. Kiencke and A. Daiss, Observation of Lateral Vehicle Dynamics, *Control Engineering Practice*, Vol. 5, No. 8, pp. 1145–1150, 1997.

[26] U. Kiencke and L. Nielsen, *Automotive Control Systems*, Springer, Berlin, 2000.

[27] M. Hiemer, A. VonVietinghoff, U. Kiencke and T. Matsunaga, Determination of Vehicle Body Slip Angle with Non–Linear Observer Strategies, *Proceedings of the SAE World Congress*, Paper No. 2005–01–0400, 2005.

[28] A. J. Tuononen, Optical position to measure tyre carcass deflectioin, *Vehicle System Dynamics*, volume 46, no 6, pages 471–481, 2008.

[29] A. J. Tuononen, and L. Hartikainen., Optical position detection to measure tyre carcass deflection in aquaplaning, *International Journal of Vehicle System Modelling and Testing*, volume 3, no 3, pages 189–197, 2008.

[30] A. J. Tuononen, On-board estimation of dinamic tyre forces from optical measured tyre carcass deflection, *Journal of Heavy Vehicle Systems*, volume 16, no 3, pages 362–378, 2009.

[31] A. J. Tuononen, and M. J. Matilainen., Real time estimation of aquaplaning with an optical tyre sensor, *Journal of Automobile Engineering*, volume 223, no D10, pages 1263–1272, 2009.

[32] A. J. Tuononen, Vehicle lateral state estimation based on measured tyre forces, *Sensors*, volume 9, no 11, pages 8761–8775, 2009.

[33] G. Erdogan, L. Alexander, and R. Rajamani., Estimation of tyre-road friction coefficient using a novel wireless piezoelectric tire sensors, *IEEE Sensors Journal*, volume 11, no 2, pages 267–279, 2011.

[34] G. Baffet, J. Stephant and A. Charara, Lateral Vehicle–Dynamic Observers: Simulations and Experiments, *International Journal of Vehicle Autonomous Systems*, Vol. 5, No. 3–4, pp. 184–203, 2007.

[35] J. Stephant, A. Charara and D. Meizel, Evaluation of Sliding Mode Observer for Vehicle Sideslip Angle, *Control Engineering Practice*, vol. 15, pp. 803–812, 2007.

[36] L. R. Ray, Nonlinear State and Tire Force Estimation for Advanced Vehicle Control, *IEEE Transactions on Control Systems Technology*, Vol. 3, No. 1, pp. 117–124, 1995.

[37] A. Suissa, Z. Zomotor and F. Bttiger, Method for Determining Variables Characterizing Vehicle Handling, *Patent US 5557520*, 1996.

[38] M. C. Best, T. J. Gordon and P. J. Dixon, An Extended Adaptive Kalman Filter for Real–Time State Estimation of Vehicle Handling Dynamics, *Vehicle System Dynamics: International Journal of Vehicle Mechanics and Mobility*, Vol. 34, No. 1, pp. 57–75. 2000.

[39] J. Lu and T.A. Brown, Vehicle Side Slip Angle Estimation Using Dynamic Blending and Considering Vehicle Attitude Information, *Patent US 6671595*, 2003.

[40] A. Hac and M. D. Simpson, Estimation of Vehicle Side Slip Angle and Yaw Rate, *Proceedings of SAE 2000 World Congress*, Detroit, MI, USA, 2000.

[41] Sangoh Han and Kunsoo Huh, Monitoring System Design for Lateral Vehicle Motion, *IEEE Transactions on Vehicular Technology*, Vol. 60, No. 4, pp. 1394–1403, 2011.

[42] H. Ohara, and T. Murakami, A Stability Control by Active Angle Control of Front–Wheel in a Vehicle System, *IEEE Transactions on Industrial Electronics*, Vol. 55, No. 3, pp. 1277–1285, 2008.

[43] J. Tjonnas, and T.A. Johansen, Stabilization of Automotive Vehicles Using Active Steering and Adaptive Brake Control Allocation, *IEEE Transactions on Control Systems Technology*, Vol. 18, No. 3, pp. 545–558, 2010.

[44] N. Hamzah, Y.M. Sam, H. Selamat, M.K. Aripin, and M.F. Ismail, Yaw Stability Improvement for Four–Wheel Active Steering Vehicle using Sliding Mode Control, *2012 IEEE 8th International Colloquium on Signal Processing and its Applications (CSPA)*, pp. 127–132, 2012.

[45] Li Gang, Zong Chang–fu, Zheng Hong–yu, Hong Wei, Vehicle Active Front Steering and Yaw Moment Integrated Control, *2011 International Conference on Transportation, Mechanical, and Electrical Engineering (TMEE)*, Changchun, China, pp. 787–790, 2009.

[46] S. Di Cairano, H.E. Tseng, D. Bernardini, ans A. Bemporad, Vehicle Yaw Stability Control by Coordinated Active Front Steering and Differential Braking in the Tire Sideslip Angles Domain, *IEEE Transactions on Control Systems Technology*, Vol. 21, No. 4, pp. 1236–1248, 2013.

[47] D. Rubin, and S. Arogeti, Vehicle Yaw Stability Control Using Rear Active Differential via Sliding Mode Control Methods, *2013 21st Mediterranean Conference on Control & Automation (MED)*, Platanias–Chania, Crete, Greece, pp. 317–322, 2013.

[48] D. Bianchi, A. Borri, B. Castillo–Toledo, M.D. Di Benedetto, and S. Di Gennaro, Active Control of Vehicle Attitude with Roll Dynamics, *Proceedings of the 18th IFAC World Congress*, Milan, Italy, August 28–September 2, pp. 7174–7179, 2011.

[49] D. Bianchi, A. Borri, B. Castillo–Toledo, M. D. Di Benedetto and S. Di Gennaro, Smart Management of Actuator Saturation in Integrated Vehicle Control, *Proceedings of the 50th IEEE Conference on Decision and Control*, Orlando, FL, USA, pp. 2529–2534, 2011.

[50] J. Guo, P. Hu, L. Li and R. Wang, Design of Automatic Steering Controller for Trajectory Tracking of Unmanned Vehicles Using Genetic Algorithms, *IEEE Transactions on Vehicular Technology*, Vol. 61, No. 7, pp. 2913–2924, 2012.

[51] M. Alirezaei, M. Corno, D. Katzourakis and A. Ghaffari, A Robust Steering Assistance System for Road Departure Avoidance, *IEEE Transactions on Vehicular Technology*, Vol. 61, No. 5, pp. 1953–1960, 2012.

[52] Wanki Cho, Jaewoong Choi, Chongkap Kim and Seibum Choi, Unified Chassis Control for the Improvement of Agility, Maneuverability, and Lateral Stability *IEEE Transactions on Vehicular Technology*, Vol. 61, No. 3, pp. 1008–1020, 2012.

[53] D. Tuan, Z. Man, C. Zhang, H. Wang and F. Tay, Robust Sliding Mode based Learning Control for Steer–by–Wire Systems in Modern Vehicles, *IEEE Transactions on Vehicular Technology*, Vol. PP, No. 99, pp. 1, 2013.

[54] Y. Xu, M. Ahmadian and R. Sun, Improving Vehicle Lateral Stability based on Variable Stiffness and Damping Suspension System via MR Damper, *IEEE Transactions on Vehicular Technology*, Vol. PP, No. 99, pp. 1, 2013.

[55] G. J. Heydinger, W. R. Garrott, J. P. Chrstos, and D. A. Guenther, A Methodology for Validating Vehicle Dynamics Simulations, *Society of Automotive Engineers*, Paper 900128, 1990.

[56] J. Wong, *Theory of Ground Vehicles*, New York, Wiley, 1978.

[57] S. Mammar, V. B. Baghdassarian, and L. Nouveliere, Speed Scheduled Vehicle Lateral Control, *Proceedings of the 1999 IEEE/IEEJ/JSAI International Conference on Intelligent Transportation Systems*, (Cat. No.99TH8383), pp. 80–85, 1999.

[58] H. B. Pacejka, *Tyre and Vehicle Dynamics*, Elsevier Butterworth–Hein, 2005.

[59] C. Canudas de Wit, P. Tsiotras, E. Velenis, M. Basset, and G. Gissinger, Dynamic Friction Models for Road/Tire Longitudinal Interaction, *Vehicle System Dynamics*, Vol. 39, No. 3, pp. 189–226, 2003.

[60] J. Li, Y. Zhang, and J. Yi, A Hybrid Physical–Dynamic Tire/Road Friction Model, *Journal of Dynamic Systems, Measurement, and Control*, Vol. 135, No. 1, pp. 1–11, 2013.

[61] H. K. Khalil, *Nonlinear Systems*, Prentice Hall, Upper Saddle River, New Jersey, USA, 1996.

[62] R. F. Curtain, and A. J. Pritchard, *Functional Analysis in Modern Applied Mathematics*, Academic Press, New York, NY, 1977.

[63] Y. Hori, Future Vehicle Driven by Electricity and Control–Research on Four–Wheel–Motored "UOT Electric March II", *IEEE Transactions on Industrial Electronics*, Vol. 51, No. 5, pp. 954–962, 2004.

[64] A. Y. Ungoren, and H. Peng, Evaluation of Vehicle Dynamic Control for Rollover Prevention, *International Journal of Automotive Technology*, Vol. 5, No. 2, pp. 115–122, 2004.

[65] M. Guiggiani, Dinamica del Veicolo, *Città Studi*, 2007.

[66] M. Doumiati, A. C. Victorino, A. Charara, and D. Lechner, On-board real-time estimation of vehicle lateral tire-road forces and sideslip angle, *IEEE/ASME Transaction on Mechatronics*, Vol. 16, No. 4, pp. 601–614, 2011.

[67] A.N. Atassi and H.K. Khalil, A Separation Principle for the Control of a Class of Nonlinear Systems, *IEEE Transactions on Automatic Control*, Vol. 46, No. 5, pp. 742–746, May 2011.

[68] M. Doumiati, A.C. Victorino and A. Charrara, Onboard Real Time Estimation of Vehicle Lateral Tire Road Forces and Sideslip Angle, *IEEE/ASME Transactions on Mechatronics*, Vol. 16, No. 4, pp. 601–6096, August 2011.

Appendix A

Theory Background

A.1 Luenberger Observer

Many sophisticated analytical procedures for control design are based on the assumption that the full state vector is available for measurement. These procedures specify the current input value as a function of the current value of the state vector-that is, the control is a static function of the state. Mathematically, of course, there is very good reason for this kind of control specification. The system evolves according to its state vector equations, and thus intelligent control, influencing future behavior, should be based on the current value of the state. The complete flexibility in specification of the characteristic polynomial assumes that all state variables can be measured. In many systems of practical importance, however, the entire state vector is not avail- able for measurement. In many physical systems, for example, measurements require the use of costly measurement devices and it may be unreasonable to measure all state variables. In large social or economic systems, measurements may require extensive surveys or complex record-keeping procedures. And, in some systems, certain components of the state vector correspond to inaccessible internal variables, which cannot be measured. In all these situations, control strategies must be based on the values of a subset of the state variables. When faced with this rather common difficulty, there are two avenues of approach. The first is to look directly for new procedures that require fewer measurements-either restricting the choice of static feedback functions or developing more complex (dynamic) feedback processing procedures. The second (simpler) approach is to construct an approximation to the full state vector on the basis of available measurements. Any of the earlier static control procedures can then be implemented using this approximate state in place of the actual state. In this way the relatively simple and effective control procedures, which assume that the state is available, are applicable to more general situations. We recall that a system is completely observable if by observation of the system outputs the value of the initial state can be deduced within a finite time period. In our earlier

discussion of observability, the required calculation was treated rather indirectly. Within the present context, however, it is apparent that such calculations become a matter of practical significance. Effective control can be dependent on the results. It is shown in this section that the state (or an approximation to it) can be conveniently computed by a device known as an observer. The observer is itself a non-linear dynamic system. Its input values are the values of measured outputs from the original system, and its state vector generates missing information about the state of the original system. The observer can be regarded as a dynamic device that, when connected to the available system outputs, generates the entire state.

The most obvious approach to estimating the state of a known system:

$$\dot{x(t)} = Ax(t) + Bu(t) \tag{A.1}$$

is to create a copy:

$$\dot{z(t)} = Az(t) + Bu(t) \tag{A.2}$$

whose state provides an estimate $z(t)$ of the original system's state $x(t)$. (One knows the input $u(t)$, so we can apply it to the copy as well as to the original system.) The simplicity of this method has a downside, however. If the initial state of the copy matches that of the original system exactly, i.e. $z(0) = x(0)$, the copy will provide the exact value of the state of the initial system. However, if the initial states do not match exactly, the error evolves according to

$$\dot{e(t)} = \Big[\dot{z(t)} - \dot{x(t)}\Big] = A\Big[z(t) - x(t)\Big] = Ae(t) \tag{A.3}$$

If the matrix A is Hurwitz (has all eigenvalues in the left half plane) then the error will decay to zero. On the other hand, if any eigenvalue of A has positive real part, a nonzero error initial error will lead the error to tend to infinity. Clearly, one needs a somewhat more sophisticated approach to observer design. We will consider the more general situation in which a fully-observable, linear, time-invariant system has state $x(t)$ of length n, input $u(t)$, and output $y(t)$ of length p with state and output equations:

$$\begin{aligned} \dot{x(t)} &= Ax(t) + Bu(t) \\ y(t) &= Cx(t) \end{aligned} \tag{A.4}$$

The more general case in which the output also depends on the input, $y(t) = Cx(t) + Du(t)$, can be addressed in the same manner as outlined here. We address the simpler case for readability. The output $y(t)$ gives us information about the state of the system, even if somewhat indirectly. In particular, we can augment the trivial observer above by incorporating a term depending on the difference between the observed and expected output. We obtain, for some $n \times p$ matrix L, the following structure:

$$\dot{z(t)} = Az(t) + L\Big[y(t) - Cz(t)\Big] + Bu(t) \tag{A.5}$$

It is clear that unless $p = n$, the observer gain matrix L is needed in order to obtain a term of the correct dimension. We expect that the choice of the observer gain matrix will also affect the dynamic behavior of the state estimate and thus the state error. Our observer has a slightly more complicated structure in that it has two input vectors, $u(t)$ and $y(t)$, but we hope to obtain better dynamic response. Substituting for the output vector, we obtain the differential equation describing the observer error:

$$\dot{e(t)} = \dot{z(t)} - \dot{x(t)} = \Big[A - LC\Big][z(t) - x(t)\Big] = \Big[A - LC\Big]e(t) \tag{A.6}$$

Now, one has an observer whose dynamical behavior can be adjusted by adjusting the observer gain L. In particular, the initial observer state need not match the initial system state, so long as the observer gain is chosen such that all eigenvalues of the matrix $A - LC$ are in the left half plane. Even better, we can adjust the rate at which the observer error goes to zero by adjusting the values of the observer gain to adjust the locations of these eigenvalues.

A.2 Lyapunov Stability

In order to understand the non-linear observer stability proof, one needs to remark the followings:

Consider a dynamical system which satisfies:

$$\begin{aligned} \dot{x} &= f(t, x) \\ x(t_0) &= x_0 \end{aligned} \tag{A.7}$$

Where we assume that $f(t, x)$ satisfies the standard conditions for the existence and uniqueness of solutions. Such conditions are, for instance, that $f(t, x)$ is Lipschitz continuous with respect to x, uniformly in t, and piecewise continuous in t. A point x^* of R^n is an equilibrium point of (A.7) if $f(t, x^*) = 0$. Intuitively and somewhat crudely speaking, we say an equilibrium point is locally stable if all solutions which start near x^* (meaning that the initial conditions are in a neighborhood of x^*) remain near x^* for all time. The equilibrium point x^* is said to be locally asymptotically stable if x^* is locally stable and, furthermore, all solutions starting near x^* tend towards x^* We say somewhat crude because the time-varying nature of equation (A.7) introduces all kinds of additional subtleties. Nonetheless, it is intuitive that a pendulum has a locally stable equilibrium point when the pendulum is hanging straight down and an unstable equilibrium point when it is pointing straight up. If the pendulum is damped, the stable equilibrium point is locally asymptotically stable. By shifting the origin of the system, we may assume that the equilibrium point of interest occurs at $x^* = 0$. If multiple equilibrium points exist, we will need to study the stability of each by

appropriately shifting the origin.

Stability in the sense of Lyapunov
The equilibrium point $x^* = 0$ of (A.7) is stable (in the sense of Lyapunov) at $t = t_0$ if for any $\epsilon > 0$ there exists a $\delta(t_0, \epsilon) > 0$ such that $\|x(t_0)\| < \delta \Rightarrow \|x(t)\| < \epsilon, \forall t \geqq t_0$

Lyapunov stability is a very mild requirement on equilibrium points. In particular, it does not require that trajectories starting close to the origin tend to the origin asymptotically. Also, stability is defined at a time instant t0. Uniform stability is a concept which guarantees that the equilibrium point is not losing stability. We insist that for a uniformly stable equilibrium point x^*, δ not be a function of t_0, so that equation (A.7) may hold for all t_0. Asymptotic stability is made precise in the following definition:

Asymptotic stability
An equilibrium point $x^* = 0$ of (A.7) is asymptotically stable at $t = t_0$ if

1. $x^* = 0$ is stable, and
2. $x^* = 0$ is locally attractive; i.e., there exists $\delta(t_0)$ such that $\|x(t_0)\| < \delta \Rightarrow$

$$\lim_{t \to \infty} x(t) = 0.$$

As in the previous definition, asymptotic stability is defined at t_0.

Uniform asymptotic stability requires:

1. $x^* = 0$ is uniformly stable, and
2. $x^* = 0$ is uniformly locally attractive; i.e., there exists δ independent

of t_0 for which equation (A.7) holds. Further, it is required that the convergence in equation (A.7) is uniform.

Exponential stability:
The equilibrium point $x* = 0$ is an exponentially stable equilibrium point of (A.7) if there exist constants $m, \alpha > 0$ and $\epsilon > 0$ such that

$$\|x(t)\| \leq m\|x(t_0)\|e^{-\alpha(t-t_0)}$$

for all $\|x(t_0)\| \leq \epsilon$ and $t \geq t_0$.
The largest constant α which may be utilized is called the rate of convergence.

Exponential stability is a strong form of stability; in particular, it implies uniform, asymptotic stability. Exponential convergence is important in applications because it can be shown to be robust to perturbations and is essential for the consideration of more advanced control algorithms, such as adaptive ones. A system is globally exponentially stable if the bound holds for all x_0.

The direct method of Lyapunov

Lyapunov's direct method (also called the second method of Lyapunov) allows us to determine the stability of a system without explicitly integrating the differential equation (A.7). The method is a generalization of the idea that if there is some measure of energy in a system, then we can study the rate of change of the energy of the system to ascertain stability. To make this precise, we need to define exactly what one means by a measure of energy. Let B_ϵ be a ball of size ϵ around the origin, $B_\epsilon = \{x \in R^n : \|x\| < \epsilon\}$.

Locally positive definite functions (lpdf)

A continuous function $V : R^n \times R^+ \rightarrow R$ is a locally positive definite function if for some $\epsilon > 0$ and some continuous, strictly increasing function $\alpha : R^+ \rightarrow R$,

$$V(0,t) = 0 \qquad V(x,t) \geq \alpha(\|x\|) \qquad \forall x \in B_\epsilon, \forall t \geq t_0.$$

A locally positive definite function is locally like an energy function. Functions which are globally like energy functions are called positive definite functions:

Positive definite functions (pdf)

A continuous function $V : R^n \times R^+ \rightarrow R$ is a positive definite function if it satisfies the conditions of lpdf and, additionally, $\alpha(p) \rightarrow \infty$ as $p \rightarrow \infty$.
To bound the energy function from above, we define decrescence as follows:

Decrescent functions

A continuous function $V : R^n \times R^+ \rightarrow R$ is decrescent if for some $\epsilon > 0$ and some continuous, strictly increasing function $\beta : R^+ \rightarrow R$,

$$V(x,t) \leq \beta(\|x\|) \qquad \forall x \in \beta_\epsilon, \forall t \geq 0.$$

Using these definitions, the following theorem allows us to determine stability for a system by studying an appropriate energy function. Roughly, this theorem states that when $V(x,t)$ is a locally positive definite function and $\dot{V}(x,t) \leq 0$ then we can conclude stability of the equilibrium point. The time derivative of V is taken along the trajectories of the system:

$$\dot{V} = \frac{\partial V}{\partial t} + \frac{\partial V}{\partial x} f$$

Theorem 3 *Let $V(x,t)$ be a non-negative function with derivative $\dot{V}$ along the trajectories of the system.*

1. *If $V(x,t)$ is locally positive definite and $V(x,t) \leq 0$ locally in x and for all t, then the origin of the system is locally stable (in the sense of Lyapunov).*

2. *If $V(x,t)$ is locally positive definite and decrescent, and $\dot{V}(x,t) \leq 0$ locally in x and for all t, then the origin of the system is uniformly locally stable (in the sense of Lyapunov).*

3. *If $V(x,t)$ is locally positive definite and decrescent, and $-\dot{V}(x,t) \leq 0$ is locally positive definite, then the origin of the system is uniformly locally asymptotically stable.*

4. *If $V(x,t)$ is positive definite and decrescent, and $-\dot{V}(x,t) \leq 0$ is positive definite, then the origin of the system is globally uniformly asymptotically stable.*

The conditions in the theorem are summarized in Table A.1 Theorem 1 gives sufficient conditions for the stability of the origin of a system. It does not, however, give a prescription for determining the Lyapunov function $V(x,t)$. Since the theorem only gives sufficient conditions, the search for a Lyapunov function establishing stability of an equilibrium point could be arduous. However, it is a remarkable fact that the converse of Theorem 1 also exists: if an equilibrium point is stable, then there exists a function $V(x,t)$ satisfying the conditions of the theorem. However, the utility of this and other converse theorems is limited by the lack of a computable technique for generating Lyapunov functions. Theorem 1 also stops short of giving explicit rates of convergence of solutions to the equilibrium. It may be modified to do so in the case of exponentially stable equilibria.

Exponential stability theorem $x^* = 0$ is an exponentially stable equilibrium point of $\dot{x} = f(t,x)$ if and only if there exists an $\epsilon > 0$ and a function $V(x,t)$ which satisfies:

$$\alpha_1 \|x\|^2 \leq V(x,t) \leq \alpha 2 \|x\|^2$$

$$\dot{V} \leq -\alpha 3 \|x\|^2$$

$$\|\frac{\partial V}{\partial x}(t,x)\| \leq \alpha 4 \|x\|$$

for some positive constants $\alpha 1, \alpha 2, \alpha 3, \alpha 4$, and $\|x\| \leq \epsilon$.

Condition on V(t,x)	Condition on -$\dot{V}(t,x)$	Conclusion
lpdf	≥ 0 *locally*	*Stable*
lpdf, decrescent	≥ 0 *locally*	*Uniformly Stable*
lpdf, decrescent	*lpdf*	*Unif. asympt. stable*
lpdf, decrescent	*pdf*	*Glob. unif. asympt. stable*

Table A.1: Summary of the basic theorem of Lyapunov.

A.3 Separation Principle

The separation principle always holds in case of stabilizable, detectable, time-invariant linear systems. According to the system:

$$\begin{aligned} \dot{x} &= Ax + Bu \\ y &= Cx \end{aligned} \tag{A.8}$$

one can find two different matrixes K, L such that $A - BK$ and $A - LC$ are Hurwitz. Then $u = -Kx$ stabilizes the system and the observer with the gains L generates a state estimation $\hat{x}$which asymptotically reconstructs x. The separation principle allows one replacing the unavailable x by the available $\hat{x}$ for control: $u = -K\hat{x}$.

Definition:

For the design parameters K and L,the linear system

$$\begin{aligned} \dot{x} &= A\hat{x} + Bu + L(y - \hat{y}) \\ \hat{y} &= C\hat{x} \\ u &= -K\hat{x} \end{aligned} \tag{A.9}$$

is called observer-based output-feedback controller.

Theorem 4 *The interconnection of the observer-based output- feedback controller with* (A.8) *leads to the closed-loop system*

$$\begin{aligned} \dot{\hat{x}} &= Ax - BK\hat{x} \\ \dot{\hat{x}} &= (a - LC - BK)\hat{x} + LCx \end{aligned} \tag{A.10}$$

This is asymptotically stable iff $A - BK$ and $A - LC$ are Hurwitz.

In case of non-linear, time-variant systems the Separation Principle does not hold. Only in particulars cases the separation principle can be used; one of those is given in [67] where a high gain observer and an input to state stability proof is required.

Appendix B

Publication List

Submitted Papers

- R. Cespi, C. Acosta-Lua, B. Castillo-Toledo and S. Di Gennaro. *Non-linear Observed Based Active Control of Ground Vehicle with Non-Negligible Roll Dynamic.* IJCAS International Journal of Control, Automation, and Systems, May 2014.

- C. Acosta-Lua, B. Castillo-Toledo, R. Cespi, and S. Di Gennaro. *Integrated Active Dynamic Control of Ground Vehicle with Non-Negligible Roll Dynamic.* IEEE Transactions on Intelligent Transportation Systems, January 2014.

- R. Cespi, C. Acosta-Lua, B. Castillo-Toledo and S. Di Gennaro. *Tyre-Road Friction Coefficient Estimation Based On Tyre Carcass Deflection..* AMCA Conferencia Latinoamericana de Control Automàtico, Cancùn, Quintana Roo, April 2014.

CENTRO DE INVESTIGACIÓN Y DE ESTUDIOS AVANZADOS DEL I.P.N.
UNIDAD GUADALAJARA

El Jurado designado por la Unidad Guadalajara del Centro de Investigación y de Estudios Avanzados del Instituto Politécnico Nacional aprobó la tesis

Control activo de vehículos

del (la) C.

Riccardo CESPI -

el día 15 de Agosto de 2014.

Dr. Bernardino Castillo Toledo
Investigador CINVESTAV 3C
CINVESTAV Unidad Guadalajara

Dr. Alexander Georgievich Loukianov
Investigador CINVESTAV 3C
CINVESTAV Unidad Guadalajara

Dr. Antonio Ramírez Treviño
Investigador CINVESTAV 3A
CINVESTAV Unidad Guadalajara

Dr. Cuauhtémoc Acosta Lúa
Profesor de tiempo completo
Centro Universitario de la Cienega